Doctoral Dissertation (Shinshu University)

Development of Fibrous Bioactive Glass-based Composites for Bone Tissue Engineering Applications

September 2012

Chunxia Gao

Acknowledgments

Foremost, I would like to express my deepest gratitude to my supervisors, Professor Koji Abe and Associate Professor Akira Teramoto for their valuable guidance, support and encouragement in my academic research work.

My deep and special thanks go to Prof. Mohamed N. Rahaman in the Department of Materials Science and Engineering, Missouri University of Science and Technology, Missouri, USA. His strong insight in science and technology has inspired me into this most exciting interdisciplinary field, the development of novel bioglass-based biomaterials for treating bone defects. I have learned so much from him not only intellectually but also spiritually. I really appreciate the time, training and caring that he invested in me throughout my three months overseas studying in his Lab, all of which made this dissertation possible.

I would like to extend my appreciations to Professor Yadong Li from my Almamater Soochow University. He kindly helped me a lot even after I came to Shinshu University, Japan. Also I would like to extend my special thanks to Mr. Ueno Takeo, technician of the Materials and Chemical Engineering for his various technical supports throughout the duration of my research. My sincere gratitude goes to Dr. Xuxu Bao and Yuan Li for their kind help in the study and life in Shinshu University, Japan. My thanks go to all the friends in Abe Lab for the help and moral support. I would like to thank the friends in Missouri University of Science and Technology. Thanks for the kind help from Dr. Xin Liu, Dr. Hailuo Fu and Dr. Yifei Gu.

I dedicate my greatest thanks to my beloved family, my parents and sister. My family encourages me to move forward and makes my life meaningful and colourful. Without their

encouragement, I could not have pursued my dream and fulfilled my passion for discovery and innovation in science and technology. I would like to thank my fiance, Qiang Gao, as my best friend in life has provided the most important mental support for my graduate studies. Without his love, support and motivation, I could not overcome all the difficulties I encountered at Japan. Last, I sincerely appreciate the Global COE Program by the Ministry of Education, Culture, Sports, Science and Technology, Japan for the sponsorship of my PhD studies as well as the research financial support.

Table of Contents

Abstract

Self-repair of bone tissue depends on the defect size and host source of osteoprogenitors. Whereas minor injuries heal spontaneously, critical size defects will not completely repair by this self-regeneration process. Moreover, the defects caused by trauma, tumors and infections will compromise the host source of osteoprogenitors for bone repair is not practical. Therefore, bone replacement procedures using autografts, allograft tissue and synthetic materials have been proposed. However, limited source and immunological rejection restrict the administration of autograft and allograft tissue replacement. Scaffold-based tissue engineering can provide an alternative approach to the use of autogeneic and allogeneic sources to meet the increasing need for implants to repair and regenerate bone. In general, the scaffold should be biocompatible, bioactive, mechanical properties comparable to the bone to be replaced, and a porous architecture to support bone ingrowth and integration.

A porous architecture that mimics the extracellular matrix (ECM) is desirable; in addition, the scaffolds should have the ability to serve as a temporary support structure to allow cells to synthesize new tissue and to degrade upon neogenesis of tissue. The bone ECM consists of an organic–inorganic nanocomposite, in which type I collagen fibrils and nanocrystalline hydroxyapatite (HA)-like particles are intimately combined. Biomaterials in the form of nanoparticles, nanofibers, and nanocomposites have been receiving increasing attention for bone repair applications in an attempt to mimic the physical structure of the inorganic HA-like phase of bone. In addition, biomaterials have been developed to mimic the collagen fibrils using

processing techniques such as electrospinning, phase separation, and self-assembly. The use of electrospinning has been receiving considerable interest as a scaffold fabrication technique because of its ability to create scaffolds with a fibrous architecture that mimics the ECM. In addition, electrospinning can be used to process a wide range of materials, does not rely on expensive equipment, and has low operating costs.

In this study, one of the most important objectives is to design and develop an appropriate organic/inorganic hybrid with highly tailorable properties which can achieved through careful control of their nanoscale interactions. Combining tough biodegradable polymer with brittle bioactive glass (BG) can produce composite with improved mechanical properties. Two different biodegradable polymers contain synthetic poly(vinyl alcohol) (PVA) and natural gelatin have been introduced into the silicate-based BG system by the sol-gel process. To mimic the structure of the nature bone, electrospinning techniques have been employed to fabricate the fibrous scaffolds.

Chapter 3 described a novel hierarchical nanofibrous BG mats using polymer/Pluronic F127 as co-templates by electrospinning. Compared with other BG, these mesoporous BG nanofibers exhibited a larger specific surface area and pore volume, which enhanced the deposition rate of a HAp layer in stimulated body fluid (SBF). Although the unique nanoscale mesoporous structure can greatly improve the bioactivity, their brittleness is still a defect which limited their further applications in bone tissue engineering. An effective strategy is to introduce a polymer to improve their toughness.

Chapter 4 described a facile method for creating a fibrous composite scaffold that would

combine the bioactivity of BG desirable structure and properties of a nanofibrous biodegradable polymer. Our approach was to deposit a sol–gel derived BG coating on cross-linked electrospun PVA fibers. PVA was selected as a model polymer because it can be electrospun from aqueous solutions, in addition to its acceptable biomechanical properties, biocompatibility, and chemical stability. The results showed that a sol–gel method provided a facile process for coating electrospun PVA fibers (diameter = 286 ± 14 nm) with a layer of BG. The BG coating resulted in mineralization of the fiber surface within 3 days in a SBF. When compared to PVA scaffolds (no BG coating), the bioglass-coated PVA scaffolds showed a higher elastic modulus, no difference in tensile strength, and a reduction in elongation to failure. Immersion of the bioglass-coated PVA scaffolds in SBF for 5 days resulted in an increase in the elastic modulus and elongation to failure when compared to the as-fabricated PVA scaffolds. *In vitro*, the bioglass-coated PVA scaffolds showed a better capacity to support the proliferation of osteogenic MC3T3-E1 cells, alkaline phosphatase activity, and mineralization when compared to the uncoated PVA scaffolds. Although these bioglass-coated PVA fibrous scaffolds showed excellent bioactivity and good tensile mechanical, a drawback with this bioglass-coated PVA scaffolds is that the constituent phases have different dissolution rate which can often be unpredicate, leading to unhomogenous depredate.

Therefore, chapter 5 described a homogeneous solution, composed of gelatin, the BG precursor, and 3-glycidoxyproyl-trimethoxysilane (GPTMS) as a coupling agent, was used in the electrospinning process to enhance the mixing of the gelatin and BG phases and to covalently link the gelatin and BG at the nanoscale level. A process that combined sol–gel and

electrospinning techniques was used to prepare gelatin–BG hybrid scaffolds with a fibrous architecture that mimicked the ECM. The scaffolds consisted of an amorphous homogenous phase consisting of gelatin covalently bonded to a siloxane network. Immersion of the scaffolds in the SBF resulted in the formation of HA-like crystals on the surface of the fibers within 12 hours, showing the excellent bioactivity of the scaffolds. The external surface of the scaffolds was almost completely covered with an HA-like layer within 5 days. The gelatin–bioglass hybrid scaffolds supported the proliferation of osteoblastic MC3T3-E1 cells, alkaline phosphatase activity, and mineralization during *in vitro* culture, showing their biocompatibility. When compared to electrospun gelatin scaffolds with the same nanofibrous architecture, the gelatin–bioglass hybrid scaffolds showed approximately an order of magnitude increase in tensile strength (from 0.5 ± 0.2 MPa to 4.3 ± 1.2 MPa) and a large improvement in the elongation to failure (from 63 ± 2 % to 168 ± 14 %).

CHAPTER 1 Introduction and Objectives

1.1 Background

The increasing in life expectancy has led to a rapidly aging population and, consequently, to a higher incidence of bone diseases such as osteoporosis as well as bone fractures [1]. Therefore, developing and providing the next generation of advanced materials suitable for bone tissue repair is a compelling challenging.

Current surgical procedures for bone repair include transplantation of naturally derived tissue graft or a synthetically derived biomaterial [2]. The most common reconstructive graft is the autograft, which involves harvesting of the patient's tissue from a donor site and transplantation to the damaged or deficient recipient site [3]. Alternatives are allografts which transplant from another patient and xenografts which transplant from a different species [4]. There are some limitations to these techniques, such as autografts have limited availability and may result in morbidity and mortality as a consequence of the invasive surgical procedures required for harvesting; allografts carry the risk of disease transmission, bone resorption, and rejection; and xenografts are available, however, immunological sequelae, disease transmission, and problematic outcomes are concerns [5, 6].

These limitations of grafts have prompted the development and use of synthetic materials as bone substitutes. Tissue response to a synthetic material depends on the physicochemical and biomechanical properties of that material [7]. Materials with high mechanical properties such as Titanium-Alumium-Vanadium Alloy (Ti-6Al-4V) and Cobalt-Chromium-Nickel Alloy

(Co-Cr-Ni) as well as Alummium Oxide (Al_2O_3) and Zirconium Oxide (Zr_2O_3) ceramic are used for load-bearing applications such as artificial joints [8, 9]. Bioactive ceramics are characterized as having surface composition similar to the mineral phase of bone [10]. Therefore, bioactive ceramics such as hydroxyapatite (HAp) and bioactive glass (bioglass) may stimulate osteoblast cell function [11-13]. However, synthetically derived biomaterials lack three of the most critical characteristics of living tissues: (Ⅰ) ability to self-repair, that is, remodel; (Ⅱ) ability to induce and maintain angiogenesis; and (Ⅲ) ability to self-modulate in response to the dynamics of mechanical loading [14,15]. Consequently, the paradigm for novel bone implants has shifted from bone replacement to tissue regeneration. Recent advances in the field of biomaterials have emphasized regeneration rather than tissue substitution by replacement [16, 17]. The aim of regeneration therapies is to restore diseased or damaged tissue to its original state of form and function, thus reducing the need for transplantation, substitution, and replacement [18]. Moreover, the end result of the regenerative process is the production of functional complex anatomical tissue units without scar formation [19].

Materials used in regenerative therapies are often designed to act as either templates or scaffolds since tissue growth in three dimensions and to predictably biodegrade in synchrony with the regeneration tissues, leaving the body to remodel the new tissue to its original contour and form [20]. Strategies to achieve this complex outcome may use porous, bioactive resorbable materials as scaffolds to guide, promote, and stimulate differentiation of cells and tissues [21]. A variety of biomaterials, including synthetic polymers, ceramics, and natural polymers are being used to fabricated synthetic scaffolds that acts as guide and stimulus for three-dimensional tissue

growth[22, 23]. Among these biomaterials, bioglass has been considered as one of the most promising materials for it has the potential to bond to bone by the formation of HAp-like layer on the surface of scaffolds and can stimulate new bone growth even away from the glass-bone interface [24]. Although silicate based 45S5 bioglass(46.1% SiO_2, 24.4% Na_2O, 26.9% CaO, and 2.6%P_2O_5, in mol%) has been in clinical use since 1985 and has been used in over a million operations as Perioglas (dental) and NovaBone (orthopaedics) particulates, its commercial use have been limited owing to processing limitations[25-27]. In order to produce a scaffold from glass powder, a sintering processing is required, which means the glass must be raised above its glass transition temperature (Tg), however, the 45S5 glass begins to crystallize as soon as it Tg is surpassed, creating a glass-ceramic that can lead to a reduction in bioactivity and unpredictable biodegradation behavior [28]. New compositions have been developed to increase the sintering window, but this has so far led to a reduction in bioactivity [29]. Therefore, sol-gel derived glass scaffolds were developed with a view to increase the degradation rate, owing to the high inherent surface area and allow glass to be bioactive with higher silica content with few compositional components [30, 31]. Although sol-gel derived bioglasses have many advantages, such as excellent bioactivity, good compressive strengths and osteoconductivity, they are brittle [32]. Producing a composite of bioglass in a degradable polymer matrix is the obvious way to introduce toughness in a glass [33-35]. A problem for conventional composites is that the inactive phase would mask the bioactive phase, so that only those parts protruding from the surface would be in contact with the host bone and provide islands of attachment sites for progenitor cells [36]. Another problem is the likelihood of differing degradation rates of two

phases in a conventional composite [37]. An alternative strategy is the synthesis of hybrids where the degradable polymer is introduced into the sol stage of the sol-gel process, so that the polymer chains interlock between the nanoparticles of silica while they coalesce. Importantly, the silica network is still continuous in three dimensions [38].

Meanwhile, bone tissue engineering strategy may involve harvesting of osteogenic cells from the patient. The cells are expanded in culture and seeded on a scaffold that acts as template and stimulus for tissue growth in three-dimensions [39]. The osteogenic cells express a collagen-enriched extracellular matrix that calcifies and morphologically assumes the shape of woven [40]. Then this tissue-engineered construct can be implanted into the tissue. However, implantable biomaterials currently in use do not adequately fulfill the performance criteria for scaffolds in regeneration medicine. Consequently, there is a compelling need to design and develop a new materials platform that fulfills the stringent criteria necessary for regenerative therapeutic medicine.

1.2 Objectives

Objectives of this study mainly including: (1) Determination of potential uses and limitations of nanofibrous bioglass as a 3D scaffold for culture and mechanical stimulation of MC3T3-E1 cells; (2) Due to the brittleness of nanofibrous bioglass, a synthetic polymer could be introduced into the bioglass system. A facile method has been developed for creating a fibrous composite scaffold that would combine the bioactivity of bioglass with attractive structural characteristics of nanofibrous biodegradable polymer, and the effect of the BG coating on the mechanical response of the PVA nanofibers and their ability to support the proliferation and function of

osteogenic MC3T3-E1 cells were evaluated to the potential application for bone regeneration. (3) To overcome the defects of conventional composites, hybrid scaffolds with a fibrous microstructure were prepared by a combined sol–gel and electrospinning technique and evaluated *in vitro* using osteogenic MC3T3-E1 cells.

1.3 Research approach

1.3.1 Sol-gel process

The sol-gel process, which is mainly based on inorganic polymerization reactions, is a chemical synthesis method initially used for the preparation of inorganic materials such as bioglasses and ceramics [41-43]. Sol-gel derived glasses have many advantages compared with their melt-quench derivatives. Typically, sol-gel derived bioglasses are synthesized by the hydrolysis of alkoxide precursors to form a sol, which is a colloidal silica solution [44]. The sol then undergoes polycondensation to form a silica network (gel). The gel then treated to form a glass.

Organic/inorganic hybrid materials prepared by the sol-gel approach have rapidly become a fascinating new field of research in biomaterials [45]. Its unique low temperature processing characteristic also provides unique opportunities to make pure and well-controlled composition organic/inorganic hybrid materials through the incorporation of low molecular weight and oligomeric/polymeric organic molecules with appropriate inorganic moieties at temperatures under which the organics can survive [46]. For the past decade, organic/inorganic nanocomposites prepared by the sol-gel process have attracted a great deal of attention,

especially in the fields of ceramics, polymer chemistry, organic and inorganic chemistry and physics [47, 48]. The preparation, characterization, and applications of organic/inorganic hybrid materials have became a fast expanding area of research in material science. The major driving forces behind the intense activities in this area are the new and different properties of the nanocomposites which the traditional macroscale composites and conventional materials do not have. Through the combinations of different inorganic and organic components in conjunction with appropriate processing methods, various types of primary and secondary bonding can be developed leading to materials with new properties for related applications.

1.3.2 Electrospinning

With the emergence of nanotechnology, researchers became more interested in studying the unique properties of nanoscale materials. Electrospinning, is a fiber processing technique that involves applying a high voltage to a polymeric solution, which results in nanometer to several micrometers diameter scale fibers (Figure 1-1) [49]. The interconnected porous network, high surface area, and tailorable surface morphology has made electrospinning a popular fiber processing technique ideal for a variety of applications, such as filtration, optical and chemical sensors, electrode materials and biological scaffolds [50]. This technique has been known for over 60 years in the textile industry for non-woven fiber fabric. In recent years, there has been an increasing interest in exploiting this technology to produce nanoscale fibers, especially for the fabrication of the nanofibrous scaffold from a variety of natural and synthetic polymers for bone tissue engineering [51-53].

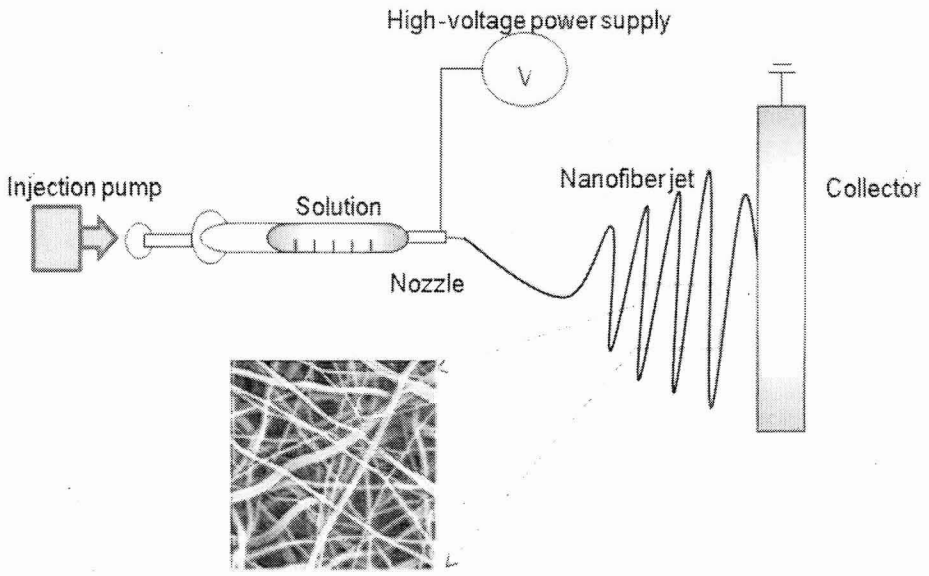

Figure1-1 The process of electrospinning.

References

[1] US Census Bureau. Health and nutrition. US Census Bureau statistical abstracts of the United States. Washington, DC: US Census Bureau; 2006.

[2] Logeart-Avramoglou D, Anagnostou F, Bizios R, Petite H. Engineering bone: challenges and obstacles. J Cell Mol Med 2005; 9:72-84.

[3] Vastel L, Meunier A, Siney H, Sedel L, Courpied J. Effect of different sterilization processing methods on the mechanical properties of human cancellous bone allografts. Biomaterials 2004; 25:2105-10.

[4] Palmer S, Gibbons C, Athanasou N. The pathology of bone allograft. J Bone Joint Surg 1999; 81B:333-5.

[5] Harner CD, Olson E, Irrgang JJ, Silverstein S, Fu FH, Silbey M. Allograft versus autograft anterior cruciate ligament reconstruction: 3- to 5-year outcome. Clin Orthop Relat Res. 1996;

324:134-44.

[6] Poehling GG, Curl WW, Lee CA, Ginn TA, Rushing JT, Naughton MJ, Holden MB, Martin DF, Smith BP. Analysis of outcomes of anterior cruciate ligament repair with 5-year followup: allograft versus autograft. Arthroscopy. 2005; 21:774-85.

[7] Hutmacher DW. Scaffolds in tissue engineering bone and cartilage. Biomaterials 2000; 21:2529-43.

[8] Kohn DH, Ducheyne P. A parametric study of the factors affecting the fatigue strength of porous coated Ti-6A1-4V implant alloy. J Biomed Mater Res 1990; 24:1483-501.

[9] Bermudez MD, Carrion FJ, Martinez-Nicolas G, Lopez R. Erosion–corrosion of stainless steels, titanium, tantalum and zirconium. Wear 2005; 258:693-700.

[10] Hench LL. Bioceramics: from concept to clinic. J Am Ceram Soc 1991; 74:1487-510.

[11] Hyakuna K, Yamamuro T, Kotoura Y, Kakutani Y, Kitsugi T, Takagi H, et al. The influence of calcium phosphate ceramics and glass-ceramics on cultured cells and their surrounding media. J Biomed Mater Res 1989; 23:1049-66.

[11] El-Ghannam A, Ducheyne P, Shapiro IM. Effect of serum proteins on osteoblast adhesion to surface-modified bioactive glass and hydroxyapatite. J Orthop Res 1999; 17:340-5.

[13] Ducheyne P, Qiu Q. Bioactive ceramics: the effect of surface reactivity on bone formation and bone cell function. Biomaterials 1999; 20:2287-303.

[14] Hench LL, Parhall HH. Direct chemical bond of bioactive glass ceramic materials to bone and muscle. J Biomed Mater Res 1973; 5:25-42.

[15] Hench LL, Splinter R, Greenlee T, Allen W. Bonding mechanisms at the interface of

ceramic prosthetic materials. J Biomed Mater Res 1971; 2:117-41.

[16] Hench LL, Polak JM. Third-generation biomedical materials. Science 2002; 295:1014-7.

[17] Mata A, Geng Y, Henrikson KJ, Aparicio C,.Stock SR,Satcher RL, Stupp S. Bone regeneration mediated by biomimetic mineralization of a nanofiber matrix. Biomaterials. 2010; 31:6004-12.

[18] Fujihara K, Kotaki M, Ramakrishna S. Guided bone regeneration membrane made of polycaprolactone/calcium carbonate composite nanofibers. Biomaterials 2005; 26:4139-47.

[19] Lee Y et al. Tissue-engineered growth of bone by marrow cell transplantation using porous calcium metaphosphates matrices. J Biomed Mater Res 2001; 54:216-33.

[20] Khan SN, Tomin E, Lane JM. Clinical applications of bone graft substitutes. Orthop Clin North Am 2000; 31:389-98.

[21] Perry CR. Bone repair techniques, bone graft, and bone graft substitutes. Clin Orthop 1999; 360:71-86.

[22] Day RM, Boccaccini AR, Shurey S, Roether JA, Forbes A, Hench LL,et al. Assessment of polyglycolic acid mesh and bioactive glass for soft-tissue engineering scaffolds. Biomaterials 2004; 25:5857-6.

[23] Rezwan K, Chen QZ, Blaker JJ, Boccaccini AR. Biodegradable and bioactive porous polymer/inorganic composite scaffolds for bone tissue engineering. Biomaterials 2006; 27:3413-31.

[24] Pereira MM, Clark AE, Hench LL. Calcium phosphate formation on sol-gel-derived bioactive glasses *in vitro*. J Biomed Mater Res 1994; 28:693-8.

[25] Xynos ID, Edgar AJ, Lee DKB, Hench LL, Polak JM. Gene-expression profiling of human osteoblasts following treatment with the ionic products of Bioglass? 45S5 dissolution. J Biomed Mater Res 2001; 55:151-7.

[26] Schepers E, De Clercq M, Ducheyne P, Kempeneers R. Bioactive glass particulate material as a filler for bone lesions. J Oral Rehabil 1991; 18:439-52.

[27] Roether JA, Gough JE, Boccaccini AR, Hench LL, Maquet V, Jerome R. Novel bioresorbable and bioactive composites based on bioactive glass and polylactide foams for bone tissue engineering. J Mater Sci Mater Med 2002; 13:1207-14.

[28] Hench LL. Bioceramics. J Am Ceram Soc 1998; 81:1705-28.

[29] Hench LL. Bioceramics-from concept to clinic. J Am Ceram Soc 1991; 74:1487-510.

[30] Pereira MM, Clark AE, Hench LL. Calcium-phosphate formation on sol–gelderived bioactive glasses *in-vitro*. J Biomed Mater Res 1994; 28:693-8.

[31] Vallet-Regí M, Arcos D, Pérez-Pariente J. Evolution of porosity during *in vitro* hydroxycarbonate apatite growth in sol–gel glasses. J Biomed Mater Res 2000; 51:23-8.

[32] Vallet-Regí M, Ragel CV, Salinas AJ. Glasses with medical applications. Eur J Inorg Chem 2003:1029-42.

[33] Peter M, Binulal NS, Nair SV, Selvamurugan N,Tamura H, Jayakumar R. Novel biodegradable chitosan–gelatin/nano-bioactive glass ceramic composite scaffolds for alveolar bone tissue engineering. Chem Eng J 2010; 158: 353-61.

[34] Mozafari M, Rabiee M, Azami M, Maleknia S. Biomimetic formation of apatite on the surface of porous gelatin/bioactive glass nanocomposite scaffolds. Appl Sur Sci 2010;

257:1740-9.

[35] Mozafari M, Moztarzadeh F, Rabiee M,Azami M,Maleknia S, Tahriri M, Moztarzadeh Z, Nezafari N. Development of macroporous nanocomposite scaffolds of gelatin/bioactive glass prepared through layer solvent casting combined with lamination technique for bone tissue engineering. Ceram Int 2010; 36(8):2431-9.

[36] Valliant E.M, Jones JR. Softening bioactive glass for bone regeneration: sol-gel hybrid materials. Soft matter 2011; 7:5083-95.

[37] Rezwan K, Chen QZ, Blaker JJ, Boccaccini AR. Biodegradable and bioactive porous polymer/inorganic composite scaffolds for bone tissue engineering. Biomaterials 2006; 27:3413-31.

[38] Mahony O, Tsigkou O, Ionescu C, Minelli C, Ling L. Silica-gelatin hybrids with tailorable degradation and mechanical properties for tissue regeneration. Adv Func Mater. 2010; 20:3835-45.

[39] Venugopal J, Low S, Choon AT,Kumar TSS, Ramakrishna S. Mineralization of osteoblasts with electrospun collagen/hydroxyapatite nanofibers. J Mater Sci: Mater Med. 2008; 19:2039-46.

[40] Brown RF, Day DE, Day TE, Jung S, Rahaman MN, Fu Q. Growth and differentiation of osteoblastic cells on 13-93 bioactive glass fibers and scaffolds. Acta Biomater 2008; 4:387–96.

[41] Zhong J, Greenspan DC. Processing and properties of sol–gel bioactive glasses. J Biomed Mater Res 2000; 53:694-701.

[42] Avnir D, Braun S. Biochemical aspects of sol-gel science and technology: a special issue of the journal o sol-gel science and technology. New York: Springer-Verlag; 1996.

[43] Coradin T, Boissiere M, Livage J. Sol–gel chemistry in medicinal science. Curr Med Chem 2006; 13:99.

[44] Hamadouche M, Meunier A, Greenspan DC, Blanchat C, Zhong JP, LaTorre GP, et al. Long term *in vivo* bioactivity and biodegradability of bulk sol–gel bioactive glasses. J Biomed Mater Res 2001; 54:560-6.

[45] Avnir D, Coradin T, Lev O, Livage J. Recent bio-applications of sol–gel materials. J Mater Chem 2006; 16:1013-30.

[46] Ren L,Tsuru K,Hayakawa S, Osaka A. *In vitro* Evaluation of Osteoblast Response to Sol-Gel Derived Gelatin-Siloxane Hybrids. J Sol-Gel Sci Techn. 2003; 26, 1137-40.

[47] Mahony O, Tsigkou O, Ionescu C, Minelli C, Ling L. Silica-gelatin hybrids with tailorable degradation and mechanical properties for tissue regeneration. Adv Func Mater. 2010; 20:3835-45.

[48] Smitha S, Shajesh P, Mukundan P, Nair TDR,Warrier KGK. Sythesid of biocompatible hydrophobic silica-gelatin nano-hybrid by sol-gel process. Colloids Surf B 2007; 55:38-43.

[49] Agarwal S, Wendorff JH, Greiner A. Use of electrospinning technique for biomedical applications. Polymer 2008; 49:5603-21.

[50] Jang JH, Castano O, Kim HW. Electrospun materials as potential platforms for bone tissue engineering. Adv Drug Delivery Rev 2009; 61:1065-83.

[51] Pham QP, Sharma U, Mikos AG. Electrospinning of polymeric nanofibers for tissue

engineering applications: a review. Tissue Eng 2006; 12:1197-1211.

[52] Choktaweesap N, Arayanarakul K, Aht-ong D, Meechaisue C, Supaphol P. Electrospun gelatin fibers: effect of solvent system on morphology and fiber diameters. Polym J. 2007; 39: 622-31.

[53] Venugopal J, Low S, Choon AT,Kumar TSS, Ramakrishna S. Mineralization of osteoblasts with electrospun collagen/hydroxyapatite nanofibers. J Mater Sci: Mater Med. 2008; 19:2039-46.

CHAPTER 2 Literature Review

2.1 Increasing demand for more effective bone grafts

Human lifespan has been continuously increasing over the last decades, mainly due to the constant advances in the medical research, the improvements in the health care system, and the improvement of general life conditions. According to a US Census Bureau the population of 65 years and older is expected to more than double in the course of the next 25 years [1]. This increasing in the aging population is concomitant with an increase in bone fractures and a growing crisis in organ transplantation, but also in elderly diseases like Parkinson and Alzheimer, which have driven a search for new and alternative therapies [2].

2.2 Problems with current bone grafts

Self-repair of bone tissue depends on the defect size and host source of osteoprogenitors. Whereas minor injuries heal spontaneously, critical size defects will not completely repair by this self-regeneration process [3]. Moreover, the defects caused by trauma, tumors and infections will compromise the host source of osteoprogenitors for bone repair is not practical. Therefore, bone replacement procedures using autografts, allograft tissue and synthetic materials have been proposed. However, limited source and immunological rejection restrict the administration of autograft and allograft tissue replacement [4, 5]. Therefore, there is a great need for the use of synthetic bone grafts. Nowadays, numerous synthetic bone graft materials have been used to repair fractures and other bone defects. However, these substitutes are far from ideal as each has its own specific problems and limitations [6].

2.2.1 Autografts

An autograft is a bone graft that is derived from the patient's own tissue. The bone tissue may be harvested from the iliac crest, femur, or tibia, and then placed in the defect site. Autografts have been considered as the "gold standard" for bone grafts [7]. They provide an osteoconductive, osteogenic scaffold for bone cells as well as endogenous biological healing factors, such as bone morphogenetic factors and angiogenic growth factors to promote new bone formation and blood vessel development, respectively [8]. However, an obvious disadvantage with autografts is the need for separate surgical procedure to produce donor tissue, which increases surgery time and the likelihood of infection, inflammation, donor-site pain, and other complications [9]. The incidence of complications has been reported to be as high as 50% [10]. Moreover, there is only a finite amount of tissue available for autografting needs.

2.2.2 Allografts

An allograft is tissue produced from screened cadavers and is processed as fresh, frozen, or freeze-dried tissue [11]. Allografts are similar to autografts, but the main difference is that the tissue is coming from a cadaver as opposed to the patient. Like autograft, allografts are osteoconductive, and depending on the processing methods used, they can even retain osteoinductive factors (i.e., bone –healing factors) such as bone morphogenetic protein (BMP) [12]. Although allografts are unlimited in supply, concerns with disease transmission and foreign body response limit their clinical use [13].

2.2.3 Xenografts

Xenograft is the transplantation of living cells, tissues or organs from one species to another [14]. Such cells, tissues or organs are called xenografts (xenotransplants). In contrast, the term allograft refers to a same-species transplant [15]. Attempts at xenograft transplantation were first performed in the early twentieth century. At present, the relative shortage of human organs and tissue available for transplantation has amplified interest in xenografts as alternatives to human tissue transplants [16]. Although the obvious advantage of xenograft is the almost infinite amount of nonhuman animal tissue that might be considered for transplantation, the major disadvantage is the risk of cross-species disease transmission [17].

2.2.4 Metals and metal alloys

To overcome the drawbacks associated with autografts, allografts and xenografts, many biomaterials have been synthesized and successfully used as bone grafts. Metals and metal alloys, have been used in clinical settings for centuries, primarily because of their mechanical properties [18, 19]. However, the average longevity of current metal-based orthopedic implants is only 10 to 15 years [20]. Implant loosening over time is the leading cause of clinical failure in the short term, as a result of insufficient osteoblast functions and excessive fibroblast activities. Moreover, mismatches in the mechanical properties of metallic implants and physiological bone result in "stress shielding" problems in the long term according to Wolff's law [21-23]. That is, the implanted material shields healing bone from mechanical loading, resulting in necrosis of the surrounding bone and subsequent implant loosening.

2.3 Basic science of bone

Bone is a highly vascular mineralized connective tissue, consisting of cells and an intercellular or extracellular matrix (ECM), in which the majority of its cells are embedded [24]. It is a natural composite material, composed of organic materials (30% dry weight in mature bone), which are mainly collagen fibers (Figure 2-1), inorganic slats rich in calcium and phosphate (60% in weight) and water (10% in weigh) [25]. The fibers present in the ECM are mainly constituted of collagen type Ⅰ (90%) and other non-collagenous protein like osteonectin, osteopontin, bone siaoprotein, osteocalcin, decorin and biglycan [26]. Microscopically, living bone is white and it has either a dense texture (compact or cortical bone), or it is composed by large cavities resembling a honeycomb, where the bone element is reduce to a network of bars and plates (trabeculae) (Figure 2-1). The compact bone is mainly in the cortices of mature bone, providing increased strength, while the rest of the bone is trabecullar (also known as a cancellous or spongy bone), housing the bone marrow (long bones) or filled with air (pneunatized) in many internal cavities of some bones in the skull [27].

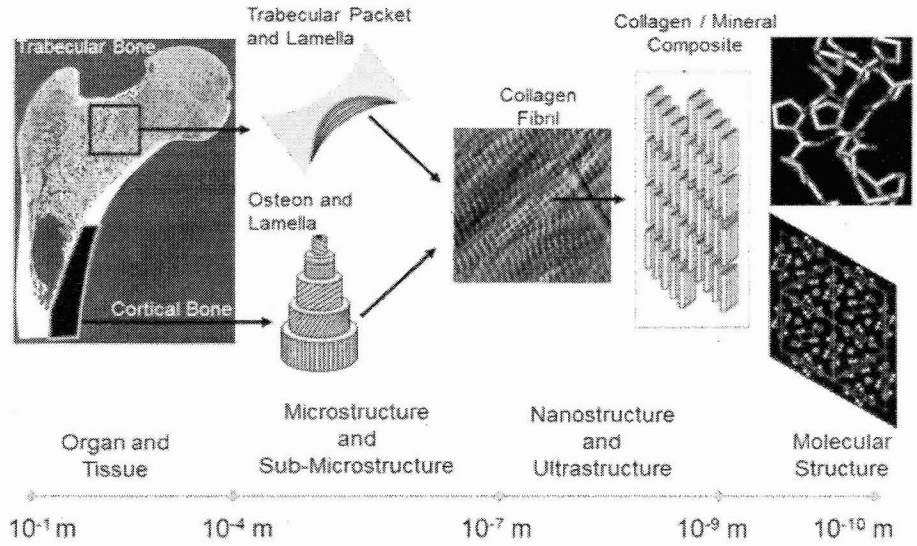

Figure 2-1 Micrometer and nanometer structure features of bone and cartilage.

(http://biomechanism.com/wp-content/uploads/2011/05/bone.png)

2.3.1 Bone remodeling and bone cells

Bone remodeling is an essential process for the maintenance of our skeleton, since it enables adaption of the bone mass and architecture to changes in external loads [28], and prevents accumulation of damage by promoting a frequent turnover to repair micro-damages created during normal daily lading [29]. In most bones, four different cells can be present: osteoclasts, osteoblasts, osteocytes and bone lining cells.

2.3.1.1 Osteoblasts

Osteoblasts are the cells that form new bone. They also come from the bone marrow and are related to structural cells. They have only one nucleus. Osteoblasts work in teams to build bone. They produce new bone called "osteoid" which is made of bone collagen and other protein [30]. Then they control calcium and mineral deposition. They are found on the surface of the new

bone.

2.3.1.2 Osteocytes

Osteocytes are cells inside the bone [31]. They also come from osteoblasts. Some of the osteoblasts turn into osteocytes while the new bone is being formed, and the osteocytes then get surrounded by new bone. They are not isolated, however, because they send out long branches that connect to the other osteocytes. These cells can sense pressures or cracks in the bone and help to direct where osteoclasts will dissolve the bone.

2.3.1.3 Osteoclasts

Osteoclasts are large cells that dissolve the bone [32]. They come from the bone marrow and are related to white blood cells. They are formed from two or more cells that fuse together, so the osteoclasts usually have more than one nucleus. They are found on the surface of the bone mineral next to the dissolving bone.

2.3.1.4 Bone lining cells

When the team of osteoblasts has finished filling in a cavity, the cells become flat and look like pancakes [33]. They line the surface of the bone. These old osteoblasts are also called lining cells. They regulate passage of calcium into and out of the bone, and they respond to hormones by making special proteins that activate the osteoclasts.

2.4 Bone tissue engineering

Tissue engineering has emerged as a promising approach for the repair and regeneration of tissues and organs lost or damaged as a result of trauma, injury, disease or aging [34]. A tissue

engineering approach for bone regeneration is illustrated in Figure 2-2 [35]. It has the potential to overcome the problem of a shortage of living tissues and organs available for transplantation. In the most common approach, a biomaterial scaffold with a well-defined architecture serves as a temporary structure for cells and guide their proliferation and differentiation into the desired tissue. Growth factors and other biomolecules can be incorporated into the scaffold, along with the cells, to guide the regulation of cellular functions during tissue regeneration [36].

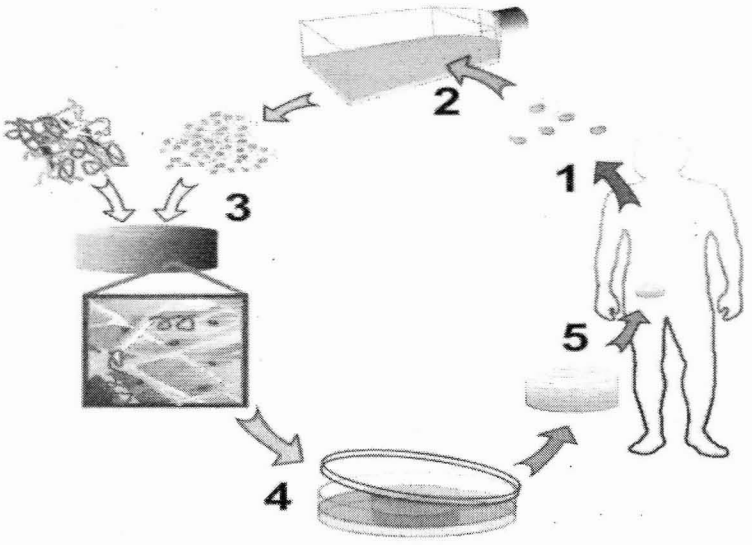

Figure 2-2 Basic principle of tissue engineering.

(http://www.centropede.com/UKSB2006/ePoster/images/background/TE_model_large.jpg)

2.4.1 Essential requirements for biomaterials

2.4.1.1 Biocompatibility

Biomaterials should be compatible to cells and be well integrated into the host tissue without eliciting a severe immune response, cytotoxicity, or formation of scar tissue [37]. Factors that

determine cytocompatibility can be affected not only by intrinsic chemistry of materials but also by techniques used for material synthesis and fabrication [38]. For example, residual chemicals involved in polymer processes (such as organic solvents, initiators, stabilizers, cross-linking agents, catalysts, or unreacted monomers) may leach out of implanted materials under physiological conditions. Therefore, not only the intact biomaterial, but also any leachable components and degradation products, must be biocompatible. Specifically, the release of acidic byproducts from some degradable materials may cause tissue necrosis or inflammation due to a quick drop in local pH [39].

2.4.1.2 Biodegradability

The ideal biomaterials should be biodegradable and bioresorbable with a controllable degradation and resorption rate to match cell/tissue growth *in vitro* and *in vivo* [40]. The degradation rate of the materials and the rate of new tissue formation must be appropriately coupled to each other in such a way that by the time the injury site is totally regenerated, the implant is totally degraded. The degradation rate of an implant can be altered by many factors, such as its structure and the molecular weight of the component materials [41]. The structures in prostheses (such as surface-to-volume ratio, porosity, pore size and shape) may also play important roles in degradation kinetics, as do dimensions and geometries. The choice of implantation site, the amount of mechanical loading, and the rate of metabolism of degradation products *in vivo* also influence the degradation time of the implanted prostheses.

2.4.1.3 Mechanical Properties

The ideal biomaterials should also have adequate mechanical properties to match the intended site of implantation. *In vitro*, the scaffolds should have sufficient mechanical strength to withstand hydrostatic pressures and to maintain spacing required for cell ingrowth and matrix production [42]. *In vivo*, because bone is always under physiological stresses (such as compression, tension, torsion, and bending), the mechanical properties of the implanted materials should closely match those of living bone so that early healing of the injured site can be possible. If the mechanical strength of an implant is much higher than bone, resulting stress-shielding effects will slow down bone healing. If the mechanical strength of an implant is much lower than bone, obviously, it will break down under load-bearing conditions

2.4.1.4 Surface Properties

An appropriate surface is very important to favor cell attachment, proliferation and differentiation. Surface properties, both chemical and topographical, can control and affect bioactivity and osteoconductivity [43]. Chemical properties are related to the ability of proteins to initially adsorb and, subsequently, for cells to adhere to the material surface. Topographical properties are of particular interest when osteoconductivity is concerned. Osteoconduction is the process by which osteogenic cells migrate to the surface of the scaffold through a fibrin clot, which is established immediately after the material is implanted [44]. This migration of osteogenic cells through the clot will cause retraction of the temporary fibrin matrix. Hence, it is of the utmost importance that the fibrin matrix is well secured to the implant, otherwise, when

osteogenic cells start to migrate, the fibrin will detach from the implant due to wound contraction. As opposed to a smooth surface, it has been previously shown that a rough surface will be able to imprison the fibrin matrix and hence facilitate the migration of osteogenic cells to the implant surface [45, 46].

2.4.1.5 Osteoinductivity

Osteoinduction is the process by which mesenchymal stem cells and pluripotent osteoprogenitor cells are recruited to a bone healing site [47]. These cells are then stimulated to the osteogenic differentiation pathway. However, when the portion of bone that requires regeneration is large, natural osteoinduction is not enough for accelerating bone healing. Therefore, the orthopedic implant itself should be osteoinductive to promote bone formation. Recombinant human bone morphogenetic proteins (rhBMPs), such as rhBMP-2 and rhBMP-7, were found to be osteoinductive and capable of inducing new bone formation [48]. Recent research has demonstrated that combining rhBMPs with bone scaffolds could significantly increase osteoinductivity of the scaffolds and hence promote new bone growth and accelerate healing [49].

2.4.1.6 Interconnected 3D Structures

The ideal orthopedic prostheses should have 3D bone-like interconnected porous structures with appropriate organization, porosity and scale to favor tissue integration and vascularization, as well as support flow transportation of nutrients and metabolic waste [50]. Pore size is a very important factor because bone scaffolds with large void volume and large surface area-to-volume

ratio maximize space to help cells, tissues, and blood vessels penetrate [51]. To attain a high surface area per unit volume, however, smaller pores are preferable as long as the pore size is greater than the diameter of osteoblasts (typically, 10 μm). If the pores employed are too small, pore occlusion by the cells may happen. This will prevent cellular penetration and neovascularization of the inner areas of bone scaffolds. It is reported that interconnected larger pores facilitate diffusion and cell migration within the scaffolds, improving nutrient supply and waste removal, and, thus, increasing the viability of cells at the center of the scaffolds [52]. Currently, researchers are still searching for the optimal pore size and shape for various bone tissue engineering applications. It is also crucial to control the suitable porosity of scaffolds by adjusting available fabrication techniques to match the porosity of true bone. Importantly, the porosity, pore structures, and pore size affect the mechanical and biological properties of scaffolds [53].

2.4.1.7 Feasible Fabrication Techniques and Sterilizability

Orthopedic prostheses should be fabricated reproducibly on a large scale using versatile processing techniques for a variety of shapes and sizes to match bone defects in patients [54]. As with all implanted materials, bone substitutes must be easily sterilizable to prevent infection. The method of sterilization, however, must not interfere with bioactivity of biomaterials or alter their chemical composition, which could influence their cytocompatibility or degradation properties.

2.4.2 Suitable biomaterials for bone tissue engineering

Scaffolds for bone tissue engineering are commonly constructed from biodegradable

polymeric materials, synthetic or natural. However, for the regeneration of load-bearing bones, the use of biodegradable polymer scaffolds is challenging because of their low mechanical strength [55]. Attempts have been made to reinforce the biodegradable polymers with a biocompatible inorganic phase, commonly bioactive glass and calcium phosphate based bioceramics [56, 57].

2.4.2.1 Selected Inorganic

2.4.2.1.1 Bioactive glass

Since the report of its bone-bonding properties nearly 40 years ago, the bioactive glass designed 45S5, sometimes referred to by its commercial name Bioglass®, has been the most widely researched glass for biomedical applications [58]. This glass is a silicate glass based on the 3-D glass-forming SiO_2 network in which Si is fourfold coordinated to O. The key compositional features that are responsible for the bioactivity of 45S5 glass are it low SiO_2 content when compared to more chemical durable silicate glass, high Na_2O and CaO (glass network modifiers) content, and high CaO/P_2O_5 ratio.

The mechanisms of bioactivity and bone bonding of 45S5 glass have been widely studied, and described in detail elsewhere [59]. Based on those studies, the bonding of 45S5 glass to bone has been attributed to the formation of a carbonate substituted hydroxyapatite-like (HCA) layer on the glass layer in contact with the body fluid [60]. Because this HCA layer is similar to the mineral constituent of bone, it bonds firmly with living bone and tissue. While some details of the chemical and structural changes are not clear, the HCA layer is generally believed to form as

a result of a sequence of reactions on the surface of the bioactive glass implant, as describe by Hench [61]:

Stage 1: Rapid ion exchange reactions between the glass network modifiers (Na^+ and Ca^{2+}) with H^+ ions from the solution, leads to hydrolysis of the silica groups and the creation of silanol(Si-OH) groups on the glass surface: e.g.

$$\mathbf{Si—O—Na^+ + H^+ \rightarrow Si—OH^+ + Na^+ \quad (aq)} \qquad \mathbf{(1)}$$

The pH of the solution increases due to the consumption of H^+ ions.

Stage 2: The increase in pH (or OH^- concentration) leads to attack of the SiO2 glass network, and the dissolution of the silica, in the form of silica acid, $Si(OH)_4$, into the solution, and the continued formation of Si-OH groups on the glass surface:

$$\mathbf{Si—O—Si + H_2O \rightarrow Si—OH + OH—Si} \qquad \mathbf{(2)}$$

While the solubility of silica is low, the products of 45S5 glass and glass-ceramic dissolution in aqueous solutions have shown an increase in Si concentration, indicating that dissolution of silica is an important mechanism. However, other mechanisms could also contribute to the increase in Si concentration.

Stage 3: Condensation and polymerization of an amorphous SiO2-rich layer (typical 1-2μm thick) on the surface of the glass depleted in Na^+ and Ca^{2+}.

Stage 4: Further dissolution of the glass, coupled with migration of Ca^{2+} and PO_4^{3-} ions from the glass through the SiO_2-rich layer and from the solution, leading to the formation of an amorphous calcium phosphate (ACP) layer on the surface of the SiO_2-rich layer.

Stage 5: The glass continues to dissolve, as the ACP layer incorporates OH^- and CO_3^{2-} from

the solution and crystallized as a layer.

With the initial formation of an HCA layer, the biological mechanisms of bonding to bone are believed to involve adsorption of growth factors, followed by attachment, proliferation and differentiation of osteoprogenitor cells [62]. Osteoblasts creat extracellular, which mineralizes to form a nanocrystalline mineral and collagen on the surface of the glass implant while the degradation and coversion of glass continues over time [63].

2.4.2.2 Selected Organic

2.4.2.2.1 Synthetic polymer PVA

The synthetic polymer, poly(vinyl alcohol) (PVA), is soluble in water, nontoxic, biocompatible, and biodegradable, and it has been shown to provide mechanical stability and flexibility to conventional scaffolds made from natural polymers [64, 65]. It has been used extensively in applications such as soft contact lenses, drug delivery matrices, cartilage implants, temporary skin covers or burn dressings, and artificial organs [66–68]. PVA is available in a variety of degree of hydrolysis, because it is derived from the hydrolysis (or alcoholysis) of poly (vinyl acetate). We have been specifically interested in fully hydrolyzed PVA which has higher crystallinity and more hydroxyl groups for chemical reactions. Although PVA has been regarded as a promising material in bone tissue engineering applications, its poor bioactivity and weak integration with the host bone limit its application as a scaffold material for bone repair [69]. In an attempt to improve the performance of PVA, recent studies have investigated the incorporation of hydroxyapatite (HAp) nanoparticles into PVA fibers to improve the bioactivity

and mechanical properties of the material [70, 71]. However, the ease of agglomeration of HAp nanoparticles, presents challenges for dispersion in the PVA solution, which can result in poor mechanical properties. Furthermore, the formation of uniform composite nanofibers with a high particle content (>20%) still remains a challenge [72].

2.4.1.2.2 Natural derived polymer Gelatin

Gelatin was selected as the organic phase in the present work because it is a denatured form of collagen, with a composition almost identical to that of collagen. Because gelatin is a denatured form of collagen, its use as a scaffold material can avoid the concerns of immunogenicity and pathogen transmission associated with collagen [73]. Electrospun fibrous mats of gelatin have received much attention recently for potential applications in bone regeneration [74, 75]. However, most of the reported methods included the use of pungent fluorine-containing reagents. In this work, an aqueous solution of acetic acid was used to dissolve the gelatin for use in the electrospinning process. In addition, a cross-linking agent was needed to stabilize the as-prepared structure and to improve the stability of the electrospun gelatin fibers in aqueous media. While several physical and chemical methods have been used to crosslink gelatin [76–78], many suffer from drawbacks such as low efficiency and toxicity.

References

[1] U.S. Interim Projections by Age, Sex, Race, and Hispanic Origin. Washington (DC): U.S. Census Bureau, Population Division, Populations Projection Branch. 2004. Also available at http://www.census.gov/ipc/www/usinterimproj/.

[2] Bone Health and Osteoporosis: A Report of the Surgeon General. Rockville, MD: U.S.

Department of Health and Human Services, Public Health Service, Office of the Surgeon General. 2004, 68-70.

[3] Wilson JW. Blood supply to developing, mature, and healing bone. In: Sumner-Smith G, Dubendorf, editors. Bone in Clinical Orthopedics. AO Publishing 2002; 23-118.

[4] Enneking WF, Eady JL, Burchardt H. Autogenous cortical bone grafts in the reconstruction of segmental skeletal defects. J Bone Joint Surg Am 1980; 7:1039-58.

[5] Stevenson S. The immune response to osteochondral allografts in dogs. J Bone Joint Surg Am 1987; 4:573-82.

[6] Bauer T W, Muschler G F. Bone graft materials. An overview of the basic science. ClinOrthopRelatRes2000; 371:10-27.

[7] Matsumura G, Hibino N, Ikada Y, Kurosawa H, Shin' oka T. Successful application of tissue engineered vascular autografts: clinical experience. Biomaterials 2003; 13:2303-8.

[8] Weiland AJ, Moore JR, Daniel RK. Vascularized bone autografts. Experience with 41 cases. Clin Orthop Relat Res 1983; 174:87-95.

[9] Sowa DT, Weiland AJ. Clinical applications of vascularized bone autografts. Orthop Clin North Am 1987; 2:257-73.

[10] Taylor GI. The current status of free vascularized bone grafts. Clin Plast Surg 1983; 1:185-209.

[11] Glowacki J. A review of osteoinductive testing methods and sterilization processes for demineralized bone. Cell Tissue Bank 2005; 1:3-12.

[12] Mankin HJ, Gebhardt MC, Tomford WW. The use of frozen cadaveric allografts in the

management of patients with bone tumors of the extremities. Orthop Clin North Am 1987; 2:275-89.

[13] Lord CF, Gebhardt MC, Tomford WW, Mankin HJ. Infection in bone allografts. Incidence, nature, and treatment. J Bone Joint Surg Am 1988; 3:369-76.

[14] http://en.wikipedia.org/wiki/Xenotransplantation

[15] Michler, R. Xenotransplantation: Risks, Clinical Potential, and Future Prospects. EID 1996; 2(1).

[16] Dooldeniya M, Warrens A. Xenotransplantation: where are we today? J R Soc Med 2003; 96: 111-17.

[17] Bols PE, Aerts JM, Langbeen A, Goovaerts IG, Leroy JL. Xenotransplantation in immunodeficient mice to study ovarian follicular development in domestic animals. Theriogenology 2010; 73 (6): 740-7.

[18] Friedman RJ, Black J, Galante JO, Jacobs JJ, Skinner HB. Current concepts in orthopaedic biomaterials and implant fixation. J Bone Joint Surg 1993; 75A:1086-109.

[19] Cook SD, Georgette FS, Skinner HB, Haddad Jr RJ. Fatigue properties of carbonand porous-coated Ti-6A1-4V alloy. J Biomed Mater Res 1984; 18:497-512.

[20] Kohn DH, Ducheyne P. A parametric study of the factors affecting the fatigue strength of porous coated Ti-6A1-4V implant alloy. J Biomed Mater Res 1990; 24:1483-501.

[21] Yue S, Pilliar RM, Weatherly GC. The fatigue strength of porous-coated Ti-6% Al-4% V implant alloy. J Biomed Mater Res 1984; 18:1043-58.

[22] Bobyn JD, Stackpool GJ, Hacking SA, Tanzer M, Krygier JJ. Characteristics of bone

ingrowth and interface mechanics of a new porous tantalum biomaterial. J Bone Joint Surg Br 1999; 81B:907-14.

[23] Bermudez MD, Carrion FJ, Martinez-Nicolas G, Lopez R. Erosion-corrosion of stainless steels, titanium, tantalum and zirconium. Wear 2005; 258: 693-700.

[24] Currey JD. Bones: structure and mechanics. Princeton, NJ: Princeton University Press; 2002.

[25] Black DM, Bouxsein ML, Marshall LM, Cummings SR, Lang TF, Cauley JA. Proximal femoral structure and the prediction of hip fracture in men: a large prospective study using QCT. J Bone Miner Res 2008; 23:1326-33.

[26] De Laet CEDH, van Hout BA, Burger H, Hofman A, Pols HAP. Bone density and risk of hip fracture in men and women: cross sectional analysis. BMJ 1997; 315:221-5.

[27] Noble B. Bone microdamage and cell apoptosis. Eur Cell Mater 2003; 6:46-55.

[28] Teitelbaum SL. Osteoclasts, integrins, and osteoporosis. J Bone Miner Metab 2000; 18:344-55.

[29] Schilling AF, Filke S, Brink S, Korbmacher H, Amling M, Reuger JM. Osteoclasts and biomaterials. Eur J Trauma 2006; 32:107-14.

[30] Ringe J, Leinhase I, Stich S, Loch A, Neumann K, Haisch A. Human mastoid periosteum-derived stem cells: promising candidates for skeletal tissue engineering. J Tissue Eng Regen M 2008; 2 (2-3): 136-46.

[31] Tate M L, Adamson J R, Tami A E, Bauer T W. Cells in Focus, The osteocyte. Int J Biochem Cell B 2004: 36:1-8.

[32] Vaananen H, Zhao H, Mulari M, Halleen. The cell biology of osteoclast function. J Cell Sci 2000; 113 (3):377-81.

[33] Norrmatsu H C, Vander Wrel C J , Talmage R V. Morphologrcal support of a role for cells lining bone surfaces in marntenance of plasma calcrum concentratron. Clan Orthop 1978; 138:254-62.

[34] Langer R, Vacanti JP. Tissue engineering. Science 1993; 260(5110):920-6.

[35]Griffith LG, Naughton G. Tissue engineering-current challenges and expanding opportunities. Science 2002; 295:1009.

[36] Ma PX. Scaffolds for tissue fabrication. Mater Today 2004;7:30-40.

[37] Hutmacher DW. Scaffold design and fabrication technologies for engineering tissues-state of the art and future perspectives. J Biomater Sci: Polym Ed 2001; 12:107-24.

[38] Griffith LG. Emerging design principles in biomaterials and scaffolds for tissue engineering. Ann NY Acad Sci 2002; 961:83-95.

[39] Roy TD, Simon JL, Ricci JL, Rekow ED, Thompson VP, Parsons JR. Performance of degradable composite bone repair products made via three-dimensional fabrication techniques. J Biomed Mater Res A 2003; 66(2):283-91.

[40] Shin M, Abukawa H, Troulis MJ, Vacanti JP. Development of a biodegradable scaffold with interconnected pores by heat fusion and its application to bone tissue engineering. J Biomed Mater Res A 2008; 84(3):702-9.

[41] Hermawan H, Dube D, Mantovani D. Developments in metallic biodegradable stents. Acta Mater 2009; 6: 1693-7.

[42] Kokubo T, Kim HM, Kawashita M. Novel bioactive materials with different mechanical properties. Biomaterials 2003; 24:2161-75.

[43] Chua PH, Neoh KG, Kang ET, Wang W. Surface functionalization of titanium with hyaluronic acid/chitosan polyelectrolyte multilayers and RGD for promoting osteoblast functions and inhibiting bacterial adhesion. Biomaterials 2008; 29(10):1412-21.

[44] Rezania A, Healy KE. The effect of peptide surface density on mineralization of a matrix deposited by osteogenic cells. J Biomed Mater Res 2000; 52(4):595-600.

[45] Paletta JR, Bockelmann S, Walz A, Theisen C, Wendorff JH, Greiner A, et al. RGD-functionalisation of PLLA nanofibers by surface coupling using plasma treatment: influence on stem cell differentiation. J Mater Sci Mater Med 2010; 21(4):1363-9.

[46] Garcia AJ, Reyes CD. Bio-adhesive surfaces to promote osteoblast differentiation and bone formation. J Dent Res 2005; 84(5):407-13.

[47] Cao X, Chen D. The BMP signaling and *in vivo* bone formation. Gene 2005; 357:1-8.

[48] Smith E, Yang J, McGann L, Sebald W, Uludag H. RGD-grafted thermoreversible polymers to facilitate attachment of BMP-2 responsive C2C12 cells. Biomaterials 2005; 26:7329-38.

[49] Hall J, Sorensen RG, Wozney JM, Wikesjo UM. Bone formation at rhBMP-2-coated titanium implants in the rat ectopic model. J Clin Periodontol 2007; 34:444-51.

[50] Karageorgiou V, Kaplan D. Porosity of 3D biomaterial scaffolds and osteogenesis. Biomaterials 2005; 26:5474-91.

[51] Hollister SJ. Porous scaffold design for tissue engineering. Nat Mater 2005; 4:518-24.

[52] Shin M, Abukawa H, Troulis MJ, Vacanti JP. Development of a biodegradable scaffold with

interconnected pores by heat fusion and its application to bone tissue engineering. J Biomed Mater Res A 2008; 84(3):702-9.

[53] Conzone SD, Day DE. Preparation and properties of porous microspheres made form borate glass. J Biomed Mater Res 2009; 88A:531-42.

[54] Hutmacher DW, Sittinger M, Risbud MV. Scaffold-based tissue engineering: rationale for computer-aided design and solid free-form fabrication systems.Trends Biotechnol 2004; 22(7):354-62.

[55] Griffith LG. Polymeric biomaterials. Acta Mater 2000; 48:263-77.

[56] Sepulveda P, Jones JR, Hench LL. Bioactive sol–gel foams for tissue repair. J Biomed Mater Res 2002; 59:340-8.

[57] Lee Y et al. Tissue-engineered growth of bone by marrow cell transplantation using porous calcium metaphosphates matrices. J Biomed Mater Res 2001; 54:216–33.

[58] Hench LL. Bioceramics-from concept to clinic. J Am Ceram Soc 1991; 74:1487-510.

[59] Hench LL, Polak JM. Third-generation biomaterials. Science 2002; 295:1014-7.

[60] Hench LL. Bioceramics. J Am Ceram Soc 1998; 81:1705-28.

[61] Hench LL, Wilson J. Surface active biomaterials. Science 1984; 226:630-6.

[62] Hench LL, Splinter RJ, Allen WC, Greenlee Jr TK. Bonding mechanisms at the interface of ceramic prosthetic materials. J Biomed Mater Res 1971; 5:117-41.

[63] Ducheyne P, Qiu Q. Bioactive ceramics: the effect of surface reactivity on bone formation and bone cell function. Biomaterials 1999; 20:2287-303.

[64] Schmedlen RH, Masters KS, West JL. Photocrosslinkable polyvinyl alcohol hydrogels that

can be modified with cell adhesion peptides for use in tissue engineering. Biomaterials 2002; 23:4325-32.

[65] Sailaja GS, Sreenivasan K, Yokogawa Y. Kumary TV, Varma HK. Bioinspired mineralization and cell adhesion on surface functionalized poly (vinyl alcohol) films. Acta Biomater 2009; 5:1647-55.

[66] Matsumura K, Hayami T, Hyon SH, Tsutsumi S. Control of proliferation and differentiation of osteoblasts on apatite-coated poly(vinyl alcohol) hydrogel as an artificial articular cartilage material. J Biomed Mater Res A 2010; 92:1229-32.

[67] Fundueanu G, Constantin M, Ascenzi P. Poly (vinyl alcohol) microspheres with pH- and thermosensitive properties as temperature-controlled drug delivery. Acta Biomater 2010; 6:3899-3907.

[68] Kang YO, Yoon IS, Lee SY, Kim DD, Lee SJ, Park WH, Hudson SM. Chitosan-coated poly(vinyl alcohol) nanofibers for wound dressings. J Biomed Mater Res B Appl Biomater 2010 92B:568-76.

[69] Sheich FA, Barakat NA, Kanjwal MA, Park SJ, Park DK, Kim HY. Synthesis of poly(vinyl alcohol) (PVA) nanofibers incorporating hydroxyapatite nanoparticles as future implant materials. Macromol Res 2010; 59-66.

[70] Degirmenbasi N, Kalyon DM, Birinci E. Biocomposites of nanohydroxyapatite with collagen and poly (vinyl alcohol). Colloids Surf B Biointerfaces 2006; 48:42-9.

[71] Sinha A, Das G, Sharma B.K, Roy R.P, Pramanick A.K and Nayar S. Poly (vinyl alcohol)-hydroxyapatite biomimetic scaffold for tissue regeneration. Mater Sci Eng C 2007;

27:70-4.

[72] Mansur HS, Costa HS. Nanostructured poly (vinyl alcohol)/bioactive glass and poly (vinyl alcohol)/chitosan/bioactive glass hybrid scaffolds for biomedical applications. Chem Eng J 2008; 137:72-83.

[73] Murphyt SBR. Structure and rheology of gelatin gels: recent progress. Polymer 1992; 33(12): 2622-7.

[74] Choktaweesap N, Arayanarakul K, Aht-ong D, Meechaisue C, Supaphol P. Electrospun gelatin fibers: effect of solvent system on morphology and fiber diameters. Polym J. 2007; 39: 622-31.

[75] Chen HC, Jao WC, Yang MC. Characterization of gelatin nano-fibers electrospun using ethanol/formic acid/water as a solvent. Polym. Adv. Technol. 2009; 20: 98-103.

[76] Zhang YZ, Venugopal J, Huang ZM, Lim CT, Ramakrishna S. Crosslinking of the electrospun gelatin nano-fibers. Polym. 2006 ; 47: 2911-7.

[77] Ko JH, Yin HY, An J, Chung DJ. Characterization of cross-linked gelatin nanofibers through electrospinning. Macromol Res. 2010; 18: 137-43.

[78] Panzavolta S, Gioffre M, Focarete ML, Gualandi C, Foroni L. Electrospun gelatin nanofibers : optimization of genipin cross-linking to preserve fiber morphology after exposure to water. Acta Biomater. 2011; 7:1702-9.

CHAPTER 3: Preparation and *in vitro* bioactivity of novel mesoporous borosilicate bioactive glass nanofibers

3.1 Abstract

Mesoporous borosilicate bioactive glass nanofibers consisting of a network of interconnected macropores and mesopores were developed using electrospinning technology combined with a polymer/surfactant co-template. The morphology and structure of the nanofibrous scaffolds were studied by scanning electron microscopy, energy-dispersive spectroscopy, Fourier transform infrared spectroscopy, and X-ray diffraction. The morphology and mesoporous structure of the borosilicate glass nanofibers can be adjusted by altering the concentrations of the glass precursor solution and surfactant. The *in vitro* bioactivity of the bioglass nanofibers was investigated by immersion in simulated body fluid. Results from these experiments suggested that the mesoporous borosilicate glass nanofibrous scaffold had great potential for bone regeneration because it promoted rapid growth of hydroxyapatite crystals.

3.2 Introduction

Bioactive silicate glasses were first developed by Hench and co-workers in 1969 and represent a group of surface reactive materials that are able to bond to bone through the formation of mineral-like hydroxyapatite (HAp) layers in physiological environments [1]. Bioactive glasses have traditionally been used to fill and restore bone defects [2]. More recently, they are emerging as materials for bone tissue engineering applications [3]. The bioactive glasses used most widely in biomedical applications consist of a silicate network incorporating sodium, calcium, and phosphorus in different proportions. It is now widely accepted that a key parameter for evaluating biomedical materials is their ability to form a new crystalline HAp layer on the surface of biomaterials under physiological conditions [4, 5]. Therefore, promoting the ability of biomaterials to form mineral-HAp layers is considered to be of critical importance in this field. Recent studies discovered that, by introducing reactive borate (BO_3^{3-}) into the silicate glass network, borosilicate glasses showed rapid precipitation of the mineral-like HAp phase in simulated body fluid (SBF) and exhibited controllable degradation behavior [6,7,8,9].

Many techniques have been employed to synthesize bioglasses, producing various structures including macroporous scaffolds [10], mesoporous particles [11], hierarchical porous scaffolds [12,13], and nanofibrous nonwoven structures [14,15]. Among these structures, the silicate bioglass with a nanofibrous structure reported by Xia et al [14]. and Kim et al. [15], which was fabricated by an electrospinning technique, has attracted great attention, because of its large specific surface area and 3D structure consisting of an interconnected macroporous network. The large specific surface area of bioglasses with a nanofibrous structure allows not only rapid

release of ions but also the ability to absorb a large amount of protein, which enhances its bioactivity. Such bioglasses possess high bioactivity and show potential for bone regeneration applications. More recently, Hong et al [16, 17] reported silicate glass with a more sophisticated hierarchical nanofibrous structure, which shows potential for application in the absorption of large proteins and drug delivery. To date, borosilicate bioactive glasses composed of nanofibers with a hierarchical structure have not been reported.

In this study, hierarchical nanofibers of borosilicate glass ($47SiO_2$-$23B_2O_3$-$25CaO$-$5P_2O_5$ (mol %)) were successfully fabricated by combining electrospinning technology and a co-template composed of poly(vinyl butyral) (PVB) / nonionic tri-block copolymer (Pluronic F127). The effects of the concentrations of the borosilicate glass precursor solution and surfactant F127 on the morphology and structure of the resulting borosilicate glass nanofibers were investigated. Furthermore, the *in vitro* bioactivity of the nanofibers was evaluated by immersion in SBF.

3.3 Experimental procedure

3.3.1 Materials

Tetraethyl orthosilicate (TEOS), tributyl borate (TBB), calcium nitrate tetrahydrate ($Ca(NO_3)_2 \cdot 4H_2O$, 99 %), triethylphosphate (TEP), tri-block nonionic surfactant Pluronic F127 (poly(ethylene oxide)100-poly(propylene oxide)65-poly(ethylene oxide)100, Mn=12600), PVB, (Mw=144000), acetic acid (CH_3COOH) of analytical grade, and all the chemicals for preparation of the simulated body fluid (SBF) were purchased from Wako Chemicals (Japan) and used as

received.

3.3.2 Preparation of borosilicate glass precursor solution

The composition of borosilicate glass used was $47SiO_2$-$23B_2O_3$-$25CaO$-$5P_2O_5$ (mol%), which was chosen based on bulk borosilicate bioglasses developed previously [7,8]. The glass precursor solution was prepared by sequentially adding TEOS, TBB, TEP and $Ca(NO_3)_2 \cdot 4H_2O$ at 6 h intervals into a solution of water/ethanol (1:1 molar ratio) that contained acetic acid (6.5 mol/L) as a catalyst. The overall concentration of the glass precursor solution can be adjusted by changing the water/ethanol content. A predetermined amount of surfactant F127 (1, 1.5 or 2 wt %) was then slowly added to the glass precursor solution. After stirring at room temperature for 48 h, the solution was aged in an oven at 40°C for 24 h followed by a further 12 h at 60°C.

3.3.3 Electrospinning

The electrospinning setup (Kato Tech, Japan) used in this study consisted of a syringe with a flat-end metal needle (1.20×38 mm), a syringe pump for controlling the feeding rate, a grounded cylindrical stainless steel mandrel, and a high voltage DC power supply. For the electrospinning procedure, the aged glass precursor solution was first mixed with an equal volume of 10 wt% PVB. After stirring for 12 h, the solution was loaded into a syringe coupled with nozzles and electrospun under a high DC voltage of 7 kV with a distance from the needle tip to the collector of 8 cm and a feeding speed of 3.75 mL/h. The electrospun fibers were collected directly on aluminum foil. To obtain nanofibrous borosilicate mats, the composite fibers were heated at 700°C for 3 h in air.

3.4 Characterization

The morphologies of the electrospun composite nanofibers and borosilicate bioglass nanofibers were observed by field-emission scanning electron microscopy (FE-SEM, S-5000, Hitachi, Japan). Energy-dispersive spectroscopy (EDS) analysis was performed to determine the ratio of Ca to P, in the borosilicate glass nanofibers before and after immersion in SBF. Chemical analysis of the nanofibers was conducted with a Fourier transform infrared spectrometer (FT-IR, IRPrestige-21, Shimadzu, Japan). Wide-angle X-ray diffraction (WAXD) measurements of the borosilicate bioglass nanofibers were carried out with an X-ray generator (Rotorflex RU200B, Rigaku, Japan) operating at 40 kV and 150mA. Ni-filtered Cu Kα (λ=1.5402 Å) radiation was used with a scanning speed of 2θ=4°/min.

3.4.1 Assessment of *in vitro* bioactivity

The *in vitro* bioactivity of the nanofibrous borosilicate bioglasses was assessed by incubating samples in SBF (Tab.3-1), which contains similar ion concentrations to human body plasma, as described by Kokubo et al.[18] In this study, the bioglass sample (50 mg) was immersed in SBF (50 mL) at 37 °C for up to 5 days without refreshing. The bioglass samples were removed from the SBF, rinsed three times with distilled water and dried overnight at 40 °C after immersion for 1, 3 or 5 days. The structure and composition of these samples were measured using FE-SEM, EDS, FT-IR, and X-ray diffraction (XRD).

Table 3-1 Ion concentrations of SBF and human blood plasma

Ion	Concentration (mM)	
	SBF	Blood plasma
Na^+	142.0	142.0
K^+	5.0	5.0
Mg^{2+}	1.5	1.5
Ca^{2+}	2.5	2.5
Cl^-	148.8	103.0
HCO_3^{2-}	4.2	27.0
HPO_4^{2-}	1.0	1.0

3.5 Results and discussion

3.5. 1 Characterization of borosilicate glass nanofibers

XRD analysis revealed that the borosilicate glass nanofibers were amorphous after calcination at 700 °C (Fig. 3-8 (a)). FT-IR spectra of the nanofibers showed that the heat-treated borosilicate glass nanofibers did not contain any residual PVB or impurities. As shown in Fig.3-1, the typical bands associated with Si-O-Si bonds appeared at 810 and 1049 cm^{-1} [18]. The band at 1417 cm^{-1} corresponds to B-O symmetric stretching vibrations from the [BO_3^{3-}] units [19]. The appearance of a band from [BO_3^{3-}] illustrates that [BO_3^{3-}] partially replaces [SiO_4^{4-}] sites in the glass structure. Broad bands at 3483 and 1636 cm^{-1} are attributed to the stretching and bending vibrational modes of O-H in water molecules and Si-OH stretching of surface silanols [20] ,

respectively.

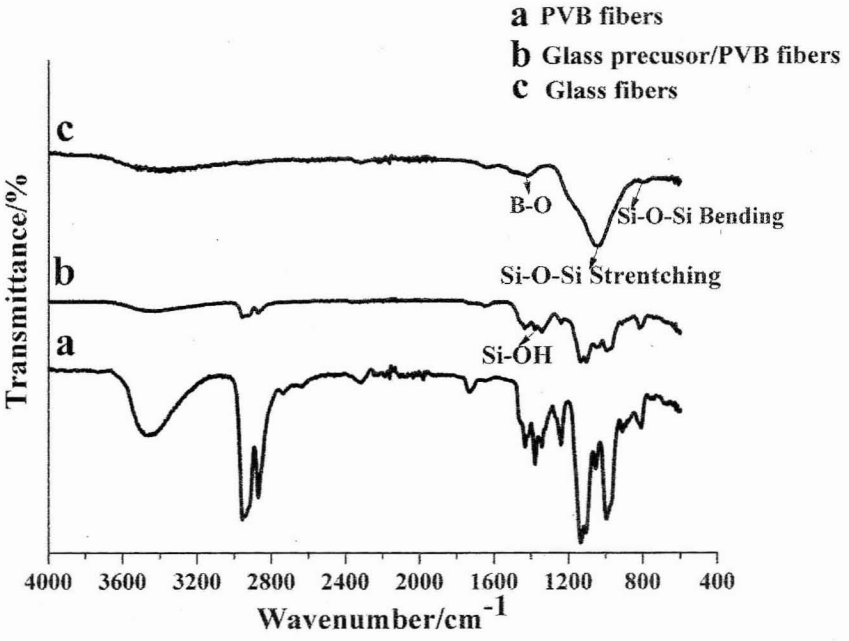

Figure 3-1. FTIR spectra of electrospun PVB, borosilicate/PVB composite and borosilicate glass nanofibers.

3.5.2 Effect of the concentration of the glass precursor solution

The sol-gel process generally includes three steps: hydrolysis, condensation, and gelation [21]. In this work, the rate of TEOS hydrolysis and condensation has to be controlled to avoid gelation before electrospinning. The effect of the concentration of the glass precursor solution on the morphology of the as-spun fibers was investigated over the range of 0.2 to 2 M. Fig.3-2 showed the morphology of glass precursor/PVB composite nanofibers and glass nanofibers obtained after calcination at 700 °C. Uniform composite nanofibers were obtained when the concentration of PVB was 5 wt% in the precursor solution. Compared with the composite fibers, the diameter of

the borosilicate glass fibers was reduced greatly upon the removal of PVB and other impurities by calcination at 700 °C. The morphology of the glass fibers was influenced by the concentration of the glass precursor solution. When the concentration of the glass solution was 0.2 M, the fibers were curled and show a random distribution of diameters. When the concentration of the glass precursor solution was increased, the fibers lengthened, became uniform, and the average diameter increased from about 150 nm to 450 nm. Therefore, the morphology of glass nanofibers can be easily controlled to meet the requirements of specific applications by adjusting the concentration of the glass precursor solution.

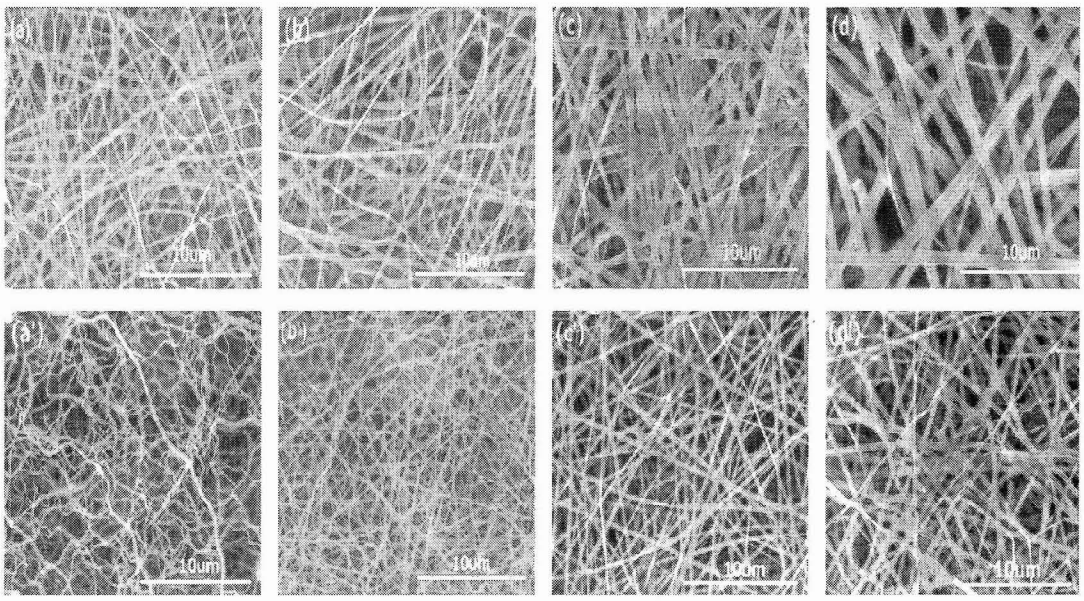

Figure 3-2. Effect of the concentration of the glass precursor solution on the morphology of electrospun composite fibers (a-d) and calcined borosilicate glass (a'-d') ((a) 0.2, (b) 0.6, (c) 1, and (d) 2 M).

3.5.3 Effects of surfactant F127 on the mesoporous glass

It was found that the concentration of surfactant F127 in the precursor solution significantly

affected the mesoporous structure formed. As shown in Fig. 3-3, addition of different amounts of F127 resulted in mesopores of different sizes and nanofibrous borosilicate glass with varying surface morphology. As the concentration of F127 was increased, the size of the mesopores increased and the diameter of the fibers decreased from 360 nm to 270 nm. Compared with the smooth glass fibers obtained without F127, the presence of F127 (Fig.3-3 (b, c, d)) caused the formation of obvious mesoporous structures. It was determined that the optimum concentration of F127 was 2 wt%, because it resulted in structures with larger mesopores and fibers of smaller diameter. For this reason, 2 wt% F127 was used in subsequent experiments.

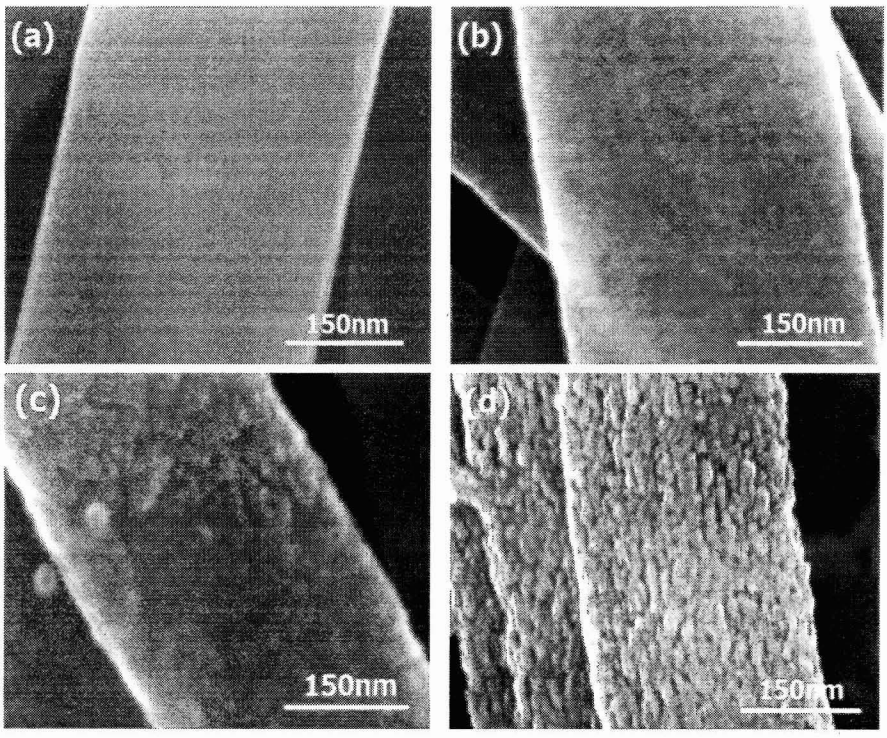

Figure 3-3. Effect of the concentration of F127 on the morphology of borosilicate glass nanofibers ((a) 0, (b) 1%, (c) 1.5%; and (d) 2%).

The formation of borosilicate glass nanofibers containing different mesoporous can be

illustrated as shown in Fig.3-4. Because of induction from the applied electric field, PVB and F127 molecules aligned along the axis of the fibers. When the as-spun fibrous mats were removed from the Al foil, the F127 self-organized into micelles to minimize the entropy. During the course of heating, both PVB and F127 assembled into coils of phase-separated microdomains. The diameter of these domains increased in direct proportion to the concentration of F127. Mesoporous borosilicate glass nanofibers were produced after removal of the templates by calcination. However, if a larger microdomain was formed, a fibrous morphology was not produced. When the concentration of F127 in the precursor solution was increased to 2.5wt%, the product obtained after calcination exhibited a monolithic rather than a fibrous morphology.

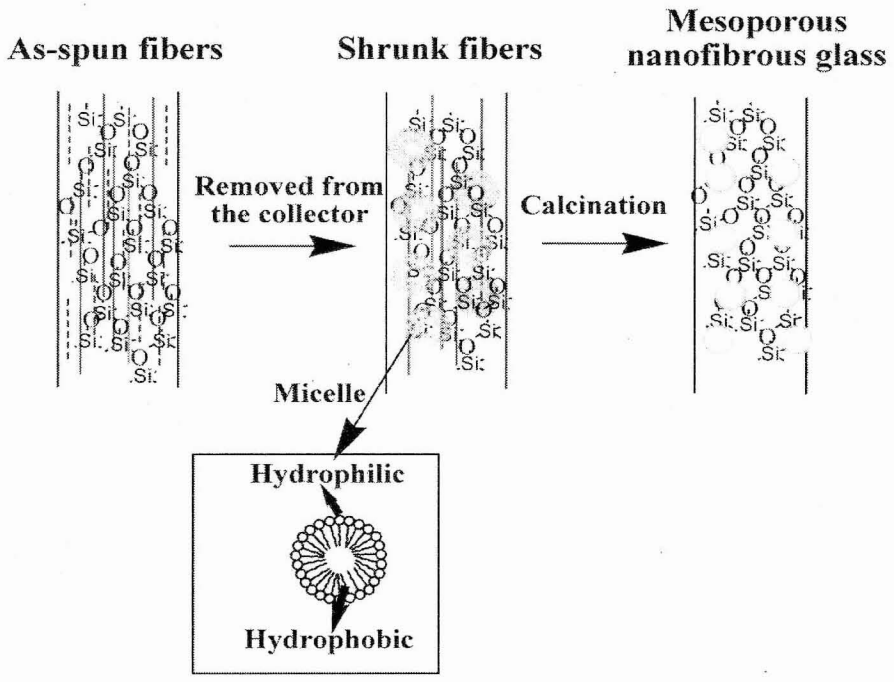

Figure 3-4. Schematic illustration of the formation process of mesoporous bioglass fibers.

3.5.4 *In vitro* bioactivity of nanofibrous bioglasses

A significant characteristic of bioactive glasses is their ability to bond with living bone both *in vitro* and *in vivo* through the formation of a HAp layer on their surface [20]. To understand the bioactivity of the mesoporous borosilicate glass nanofibers, it was of primary importance to investigate the ability of the fibers to form HAp. The *in vitro* bioactivity of the borosilicate glass nanofibers was assessed by monitoring the formation of HAp on the surface after immersing samples in SBF for different periods. As shown in Fig. 3-5, many nanoparticles of HAp formed on the surface of the samples after incubation for 1 day in SBF. The density of the nanoparticles increased with the immersion time. When the immersion time reached 3 days (Fig.3-5 (b''')), the morphology of the fibers became more significant, with numerous needle-like crystals formed over almost the entire surface of the fibers. High magnification images of the fibers incubated for 3 days showed that the size of the crystals formed on the nanofiber surfaces was a few tens of nanometers. After incubation for 5 days, the needle-like crystals had grown into crystalline plates of higher density. Moreover, some of the plates aggregated to form flower-like clusters, which is a typical morphology of HAp crystals. More importantly, it was found that the fibrous structure of the bioglass was still maintained after immersion for 5 days, which is an essential feature for their application as a scaffold in bone tissue engineering.

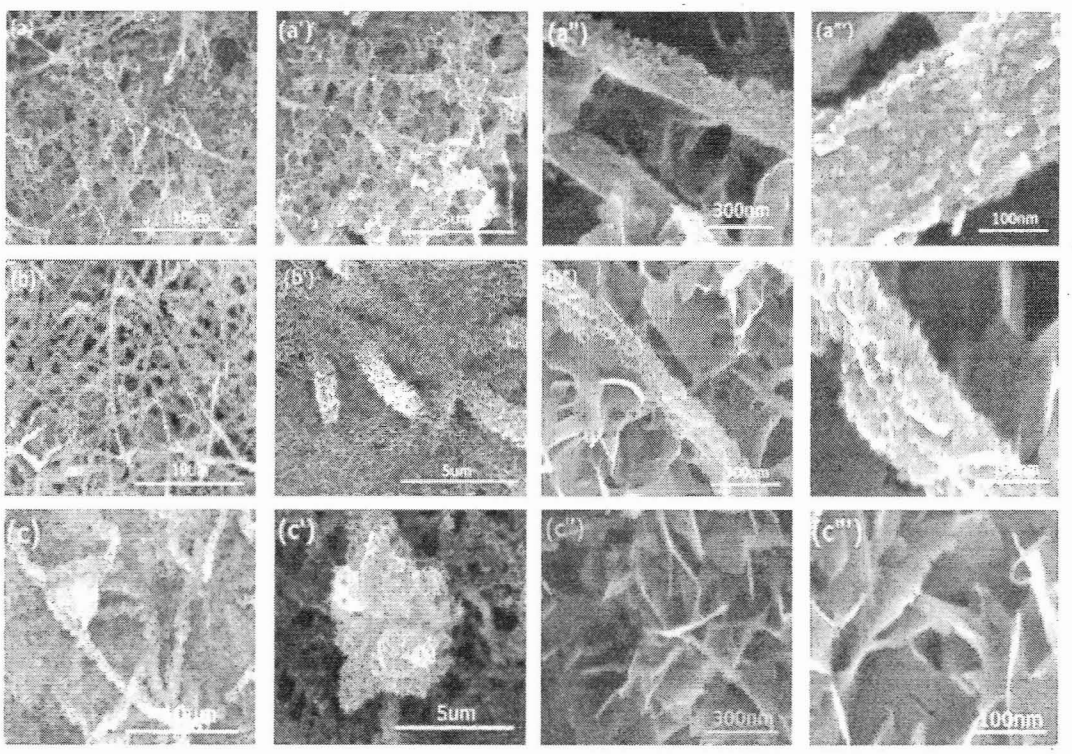

Figure 3-5. SEM images of mesoporous borosilicate glass fibers incubated in SBF for: (a-a''') 1 day, (b-b''') 3 days, and (c-c''') 5 days.

The results obtained from FE-SEM were confirmed by EDS analysis as shown in Fig.3-6. After immersion in SBF, the concentrations of Ca and P increased significantly, and were accompanied by a decrease in the concentration of Si, which signified the extended development of HAp. That HAp crystals formed on the surface of the mesoporous borosilicate glass nanofibers after incubation in SBF was further confirmed by performing FTIR spectroscopy after different incubation times, as shown in Fig.3-7. Before immersion in SBF, peaks at 490, 798, and 1080 cm^{-1} can be attributed to Si-O-Si bands [22]. After immersion in SBF for 1 day, obvious bands from P-O appeared at 574, 607, and 1033 cm^{-1} indicating the growth of a HAp layer on the surface of the borosilicate glass nanofibers. As the incubation time increased, the bands related to

the borosilicate glass (490, 798, 1080 cm^{-1}) became attenuated, while those attributed to HAp (574, 607, and 1033 cm^{-1}) increased in intensity. In addition, a band consistent with carbonate appeared at 877 cm^{-1}, suggesting the formation of carbonate-HAp, which is of similar composition to bone mineral.

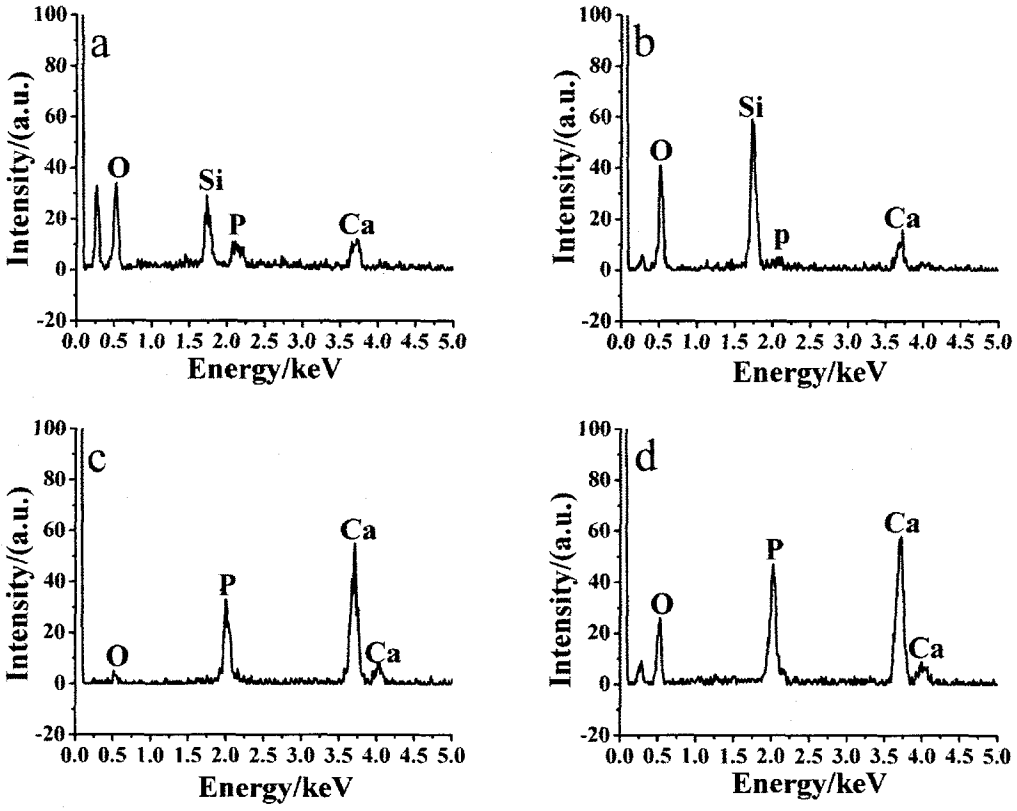

Figure 3-6. EDS spectra of bioglass samples immersed in SBF for (a) 0, (b) 1, (c) 3 and (d) 5 days.

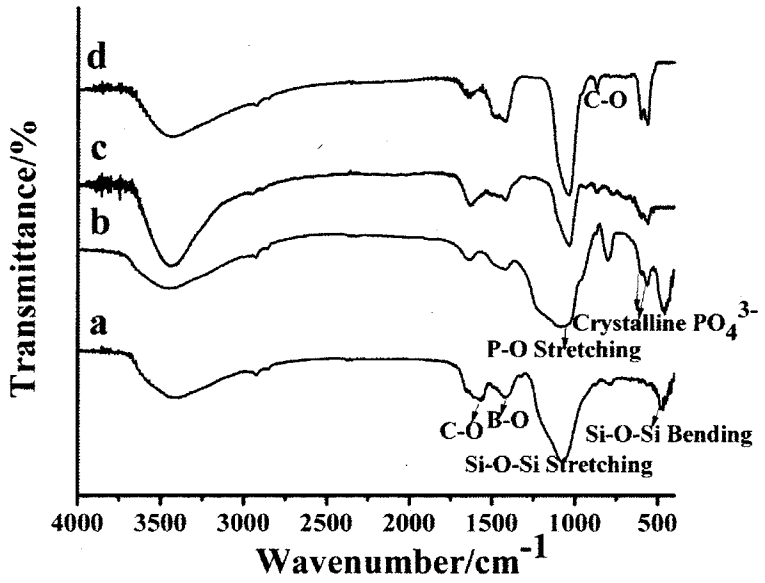

Figure 3-7. FTIR spectra of borosilicate glass nanofibers after immersion in SBF for different times (a: before immersion, b: 1 day, c: 3 days, and d: 5 days).

XRD analysis results for the bioglass before and after soaking in SBF were shown in Fig.3-8. The pattern of the untreated borosilicate glass showed that it was in an amorphous state, which is indicative of the internal disorder and glassy nature of this material. There were obvious changes in the structure of the glass after immersion for 1 day in SBF. New peaks emerged at 31.7° and 25.8° that corresponded to the (211) and (002) reflections of HAp according to the standard JCPDS card (72-1243). After immersion for 3 days, the intensities of these two peaks increased and some other peaks consistent with HAp at 40°, 46°, 49°, and 53° also appeared. After immersion for 5 days, all of the Hap peaks became more intense, suggesting that the borosilicate glass had transformed into well-crystallized HAp.

It is of special note that, when compared with bulk borosilicate and even conventional silicate

glass nanofibers that usually need several days to weeks for nucleation and growth of pure HAp crystals [22,23], the mesoporous nanofibrous borosilicate glass exhibited faster nucleation and growth of HAp crystals. This was mainly attributed to the large surface area of the nanofibers, resulting in faster dissolution and supersaturation of the medium promoting the nucleation of HAp crystals. Meanwhile, the mesoporous surface morphology enhanced the bioactivity because of the large surface area of the mesopores, which could substantially increase the reaction kinetics at the bioglass surface. Besides the morphology and structure of the nanofibers, the introduction of [BO_3^{3-}] decreases the chemical durability of the glass network structure, which should promote the leaching of calcium ions from the glass surface and encourage precipitation of HAp crystals.

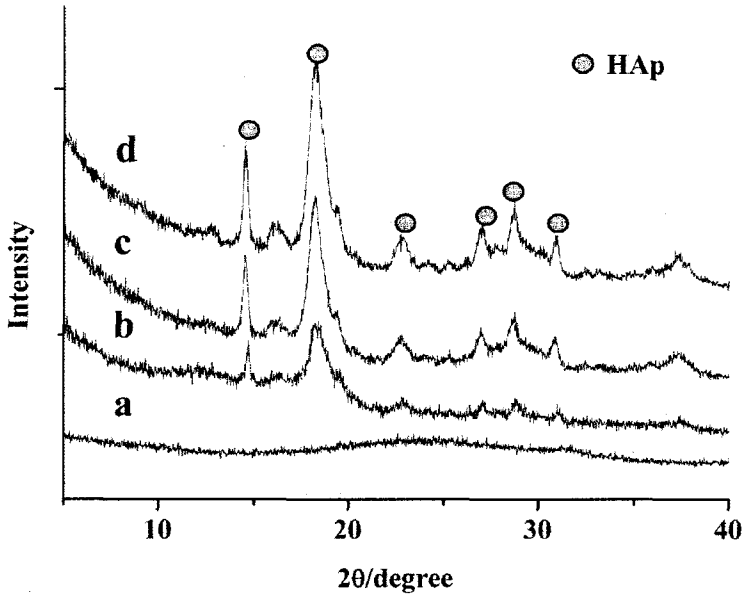

Figure 3-8. XRD patterns of borosilicate glass nanofibers after immersion in SBF for different times (a: before immersion, b: 1 day, c: 3 days and d: 5 days)

3.6 Summary

In this study, a novel borosilicate bioglass consisting of hierarchical nanofiber mats was fabricated by electrospinning and using polymer/Pluronic F127 as co-templates. Compared with other borosilicate bioglasses, the mesoporous borosilicate bioglass nanofibers exhibited a larger specific surface area and pore volume, which enhanced the deposition rate of a HAp layer in SBF. Because of the unique nanoscale mesoporous structure and structure/bioactivity correlation, the borosilicate bioglass nanofibers are expected to find application in *in vivo* bone-formation and hold great promise as scaffolds with drug delivery potential.

References

[1] L. L. Hench and H. A. Paschall, "Direct chemical bond of bioactive glass-ceramic materials to bone and muscle," J. Biomed. Mater. Res., 7[3], 25-42 (1973).

[2] L. L. Hench, "Bioceramics: From Concept to Clinic," J. Am. Ceram. Soc., 74[7], 1487-1510 (1991).

[3] I. D. Xynos, M. V. Hukkanen, J. J. Batten, L. D. Buttery, L. L. Hench and J. M. Polak, "Bioglass 45S5 Stimulates Osteoblast Turnover and Enhances Bone Formation *In Vitro*: Implications and Applications for Bone Tissue Engineering," Calcif. Tissue Int., 67[4], 321-329 (2000).

[4] T. Kokubo, "Bioactive glass ceramics: properties and applications,"Biomaterials, 12[2], 155-163 (1991).

[5] T. Kokubo, H. Kushitani, S. Sakka, T. Kitsugi and T. Yamamuro "Solutions able to reproduce *in vivo* surface-structure changes in bioactive glass-ceramic A-W," J. Biomed. Mater. Res., 24[6], 721-734 (1990).

[6] X. Liu, W. Huang, H. Fu, A.Yao, D.Wang, H. Pan, W. Lu, X. Jiang and X. Zhang, "Bioactive borosilicate glass scaffolds: *in vitro* degradation and bioactivity behaviors," J. Mater. Sci. Mater. Med., 20[6], 1237-1243 (2009).

[7] S. B. Jung and D. E. Day, "Conversion kinetics of silicate, borosilicate, and borate bioactive glasses to hydroxyapatite, " Phys. Chem. Glasses-B, 50[2], 85-88 (2009).

[8] K. Singh, I. Bala and V. Kumar, "Structural, optical and bioactive properties of calcium borosilicate glasses," Ceramics International, 35 (8), 3401-3406 (2009).

[9] W. Huang, D. E. Day, K. Kittiratanapiboon and M. N. Rahaman, "Kinetics and mechanisms of the conversion of silicate (45S5),borate, and borosilicate glasses to hydroxyapatite in dilute phosphate solutions," J. Mater. Sci. Mater. Med., 17[7], 583-596 (2006).

[10] C. V. Brovarone, E. Verné and P. Appendino, "Macroporous bioactive glass-ceramic scaffolds for tissue engineering," J. Mater. Sci. Mater. Med., 17[11], 1069-1078 (2006).

[11] X. Yan, X. Huang, C. Yu, H. Deng, Y. Wang, Z. Zhang, S. Qiao, G. Lu and D. Zhao, "The *in-vitro* bioactivity of mesoporous bioactive glasses," Biomaterials, 27[18], 3396-3403 (2006).

[12] X. Li, X. Wang, H. Chen, P. Jiang, X. Dong, and J. Shi, "Hierarchically Porous Bioactive Glass Scaffolds Synthesized with a PUF and P123 Cotemplated Approach," Chem. Mater., 19 [17], 4322-4326 (2007).

[13] J. R. Jones, P. D. Lee and L. L. Hench, "Hierarchical porous materials for tissue engineering," Philos. Transact. A Math. Phys. Eng. Sci., 364[1838], 263-281(2006)

[14] W. Xia, D. Zhang and J. Chang, "Fabrication and *in vitro* biomineralization of bioactive glass (BG) nanofibres, " Nanotechnology,18, 135601,7pp (2007).

[15] H.W. Kim, H. E. Kim, J. C. Knowles, "Production and Potential of Bioactive Glass Nanofibers as a Next-Generation Biomaterial," Adv. Funct. Mater., 16[12], 1529-1535(2006).

[16] Y. Hong, X. Chen, X. Jing, H. Fan, B. Guo, Z. Gu and X. Zhang, "Preparation, Bioactivity, and Drug Release of Hierarchical Nanoporous Bioactive Glass Ultrathin Fibers," Adv. Mater., 22[6], 754-758(2010).

[17] Y. Hong, X. Chen, X. Jing, H. Fan, Z. Gu and X. Zhang, "Fabrication and Drug Delivery of Ultrathin Mesoporous Bioactive Glass Hollow Fibers," Adv. Funct. Mater., 20[9], 1503–1510(2010).

[18] T. Kokubo and H.Takadama, "How useful is SBF in predicting *in vivo* bone bioactivity?," Biomaterials, 27[15], 2907-2915 (2006).

[19] A. Yao, D. Wang, W. Huang, Q. Fu, M. N. Rahaman and D. E. Day, "*In Vitro* Bioactive Characteristics of Borate-Based Glasses with Controllable Degradation Behavior," J. Am. Ceram. Soc., 90[1], 303-306 (2007).

[20] H. Morgan, R. M. Wilson, J. C. Elliott, S. E. P. Dowder, and P. Anderson, "Preparation and Characterization of Monoclinic Hydroxyapatite and its Precipitated Carbonate Apatite Intermediate-a Combined IR and XRD Rietveld Analysis, " Biomaterials, 21[6], 617-627 (2000).

[21] L. L. Hench and J. K. West, "The Sol-Gel Process," Chem. Rev., 90[1], 33-72(1990).

[22] J. Ning, A. Yao, D.Wang, W. Huang, H. Fu, X. Liu, X. Jiang and X. Zhang, "Synthesis and

in vitro bioactivity of a borate-based bioglass," Mater. Lett., 61[30], 5223-5226 (2007)

[23] X. Zhang, W. Jia, Y. Gu, W. Xiao, X. Liu, D. Wang, C. Zhang, W. Huang, M. N. Rahaman, D. E. Day and N. Zhou, "Teicoplanin-loaded borate bioactive glass implants for treating chronic bone infection in a rabbit tibia osteomyelitis model," Biomaterial, 31[22], 5865-5874 (2010)

CHAPTER 4: Preparation and *in vitro* characterization of electrospun PVA scaffolds coated with bioactive glass for bone regeneration

4.1 Abstract

An important objective in bone tissue engineering is to fabricate biomimetic three-dimensional scaffolds that stimulate mineralization for rapid regeneration of bone. In this chapter, scaffolds of electrospun poly(vinyl alcohol) (PVA) fibers (diameter = 286 ± 14 nm) were coated with a sol–gel derived bioactive glass (BG), and evaluated *in vitro* for potential applications in bone repair. Structural and chemical analyses showed that the BG coating was homogeneously deposited on the PVA fibers. *In vitro* cell culture studies showed that the BG-coated PVA scaffold had a greater capacity to support proliferation of osteogenic MC3T3-E1 cells, alkaline phosphatase activity, and mineralization than the uncoated PVA scaffold. The BG coating improved the tensile strength of the PVA scaffold from 18 ± 2 MPa to 21 ± 2 MPa, but reduced the elongation to failure from 94 ± 4% to 64 ± 5%. However, immersion of the BG-coated PVA scaffolds in a simulated body fluid (SBF) for 5 days resulted in an increase in the tensile strength (24 ± 2 MPa) and elongation to failure (159 ± 4%). Together, the results show that these BG-coated PVA scaffolds could be considered as candidate materials for bone tissue engineering applications.

4.2 Introduction

Scaffold-based tissue engineering is an attractive approach for the repair and regeneration of bone defects resulting from trauma, resection for tumors, and congenital deformities [1, 2]. An ideal bone scaffold should be biocompatible, biodegradable and bioactive, easy to use in clinical practice, and cost effective. In addition, the scaffold should serve as a structural support and, in some applications, as a drug delivery device. While the creation of such ideal scaffolds remains a major challenge [3, 4], the nanoscale dimensions and physical structure of the bone extracellular matrix (ECM) could provide a framework for the design of synthetic scaffolds. Based on these features of the ECM, electrospun fibers have been studied as a class of promising scaffold materials for bone tissue engineering [5–7].

Since reported by Hench et al. [8], the silicate glass designated 45S5 (sometimes referred to by its commercial name Bioglass®) has been the most widely researched bioactive glass (BG) for biomedical applications [9,10]. The biocompatibility and bioactivity of BGs in the form particles, dense solids, and porous scaffolds, as well as the ability of BGs to form a firm bond with bone and tissues *in vivo*, have been widely studied and reported [9, 11]. Developments in nanotechnology have resulted in the fabrication of BGs into various nanostructures, such as nanoparticles, nanofibers, and mesoporous nanofibers in an attempt to maximize their biological activity [12–14]. With an architecture that mimics the ECM, a high surface area, and a high bioactive potential, nanofibrous BGs may have promising potential as a biomaterial for bone regeneration. However, biomedical applications of nanofibrous BGs may be limited by their brittle characteristics and difficulty in handling.

The use of electrospinning to form fibrous composites of polymers and BG can provide an attractive approach for creating scaffolds with desirable properties for bone generation [15, 16]. However, BG nanoparticles are commonly prone to agglomeration, and they cannot be easily mixed homogeneously with polymer solutions [17]. Consequently, electrospinning of BG–polymer mixtures often results in the formation of fibers with a morphology mimicking that of "beads on a string" [18, 19]. In view of these difficulties, a coating of BG deposited, for example, by a solution sol–gel process on electrospun polymeric fibers could provide an alternative approach for combining the bioactive properties of BG with the plasticity of polymeric fibers. In particular, the sol–gel derived BG coating can impart bioactivity to the surface of the fibers, while the desirable morphological and plastic properties of the electrospun polymeric fibers are retained. These BG-coated fibrous scaffolds could potentially be applied to bone regeneration because of their desirable surface bioactivity, coupled with an architecture that mimics the ECM.

The synthetic polymer, poly(vinyl alcohol), PVA, is soluble in hot water, nontoxic, biocompatible; in addition, it has been shown to provide mechanical stability and flexibility to conventional scaffolds made from natural polymers [20, 21]. PVA has been used extensively in applications such as soft contact lenses, drug delivery devices, cartilage implants, temporary skin covers or burn dressings, and artificial organs [22–24]. Although PVA has been regarded as a promising material in bone tissue engineering, its poor bioactivity and weak integration with host bone limit its application as a scaffold material for bone repair [25]. Recent studies have investigated the incorporation of hydroxyapatite (HA) nanoparticles to improve the bioactivity

and mechanical properties of PVA [26, 27]. However, dispersing HA nanoparticles homogeneously in PVA solution is challenging because of the ease of agglomeration of the fine particles. As a result, the composite fibers often have poor mechanical properties. Furthermore, the formation of uniform composite nanofibers with a high particle content (>20%) remains a challenge [16].

One aim of the present study was to develop a facile method for creating a fibrous composite scaffold that would combine the bioactivity of BG with the desirable structure and properties of a nanofibrous biodegradable polymer. Our approach was to deposit a sol–gel derived BG coating on cross-linked electrospun PVA fibers. PVA was selected as a model polymer because it can be electrospun from aqueous solutions, in addition to its acceptable biomechanical properties, biocompatibility, and chemical stability [28, 29]. A second aim of the present study was to evaluate the effect of the BG coating on the mechanical response of the electrospun PVA fibers and their response to osteogenic cells *in vitro*. We hypothesized that the electrospun PVA scaffolds coated with BG would show improved response to mechanical loading and to cells *in vitro*, when compared to the uncoated PVA scaffolds.

4.3 Materials and methods

4.3.1 Electrospinning of fibrous PVA scaffolds

PVA (99.9% hydrolyzed; molecular weight M_w = 140,800) was kindly provided by Kuraray Co. Ltd. (Tokyo, Japan); the cross-linking agent K-FJD (N,N'-trimethylenebis[2-(vinyl sulfony) acetamide]) was purchased from Fujifilm Co. Ltd. (Tokyo, Japan). The PVA solution for

electrospinning was prepared by dissolving PVA (6 w/v%) in 3 wt% dilute acetic acid solution at 85°C, and stirring continuously for >4 h. After cooling the solution to room temperature, 20 wt% K-FJD crosslinking agent (based on the mass of PVA) was added, and the mixture was ultrasonicated for 10 min, then stirred for 30 min before electrospinning.

The main components of the electrospinning apparatus (Kato Tech; Kyoto, Japan) used in this study were a syringe with a flat-end metal needle (1.20 mm internal diameter × 38 mm), a syringe pump for controlling the feeding rate of the solution, a grounded cylindrical stainless steel mandrel, and a high voltage DC power supply. The PVA solution was electrospun under an applied DC voltage of 10 kV, using a distance of 14 cm between the needle and the collector plate, and a feeding rate of 1.5 ml/h. The as-spun PVA mats were treated for 30 min at 110°C to crosslink the PVA chains.

4.3.2 Preparation of bioactive glass (BG)-coated PVA scaffolds

The bioactive glass (BG) composition used in this work, $70SiO_2$–$25CaO$–$5P_2O_5$ (mol %), was based on a composition reported previously [30, 31]. A solution sol–gel process was used to deposit the BG coating on the PVA scaffolds. Tetraethyl orthosilicate (TEOS), calcium nitrate tetrahydrate ($Ca(NO_3)_2 \cdot 4H_2O$, 99%), triethylphosphate (TEP) and acetic acid (CH_3COOH) were used to prepare the BG precursor solution for the coating process. These chemicals were analytical grade reagents purchased from Wako Pure Chem. Ind., Ltd. (Japan) and were used without further purification.

The BG precursor solution was prepared by sequentially adding 5 ml TEOS, 0.545 ml TEP,

and 1.89 g $Ca(NO_3)_2 \cdot 4H_2O$ at 1 h intervals into 32 ml of water/ethanol mixture (1:1 molar ratio) containing acetic acid (13.65 g) as a catalyst. After stirring for 24 h at room temperature, the solution was aged for 12 h at 40°C, and then for a further 12 h at 60°C. BG-coated PVA scaffolds were prepared by immersing the cross-linked fibrous PVA mats in the aged precursor solution for 5 min at room temperature. The BG-coated scaffolds were dried at room temperature for ~30 min, rinsed with distilled water until the pH was neutral, freeze-dried, and stored for subsequent evaluation.

4.3.3 Characterization of scaffold structure and composition

The morphology of the PVA and BG-coated PVA scaffolds was investigated using field-emission scanning electron microscopy SEM (Hitachi S-5000; Japan) at an accelerating voltage of 20 kV and a working distance of 15 mm. Compositional analysis of the scaffolds was performed using energy-dispersive X-ray (EDS) spectroscopy in the SEM, and Fourier transform infrared (FT-IR) spectroscopy (IRPrestige-21; Shimadzu, Japan). FT-IR was performed in the wavenumber range 500–4000 cm^{-1} on disks prepared from a mixture of 5 mg of the sample and 150 mg of high-purity KBr powder. Each FTIR spectrum was obtained from 40 scans at a resolution of 2 cm^{-1}. The crystalline structure of the samples was analyzed using wide-angle X-ray diffraction, XRD (Rotorflex RU200B; Rigaku, Japan); XRD was performed using Ni-filtered CuKα radiation (λ=1.5402 Å) in a step-scan mode at a rate of 2°/min in the 2θ range 10–60°.

4.3.4 Evaluation of *in vitro* bioactivity

The bioactivity of the BG-coated PVA scaffolds was evaluated *in vitro* from samples immersed for varying times in a simulated body fluid (SBF) described elsewhere [33]. Scaffolds with the shape of discs (12 mm in diameter × ~10 μm) were placed individually in the wells of a static 24-well plate containing 2 ml of SBF per well, and the system was kept at 37°C in 5% CO_2 atmosphere for up to 5 days without replacing the SBF. The samples were removed from the SBF at intervals of 1 day, rinsed three times with distilled water, and freeze-dried. The morphology, structure, composition, and Ca/P atomic ratio of the samples were evaluated using SEM, XRD, FT-IR and EDS, using the procedures described previously.

4.3.5 Mechanical testing

Mechanical testing of the PVA and BG-coated PVA scaffolds was performed in tension at a constant deformation rate of 2 mm/min using a testing machine (RTC-1250A, A&D Co., Ltd., Japan). The specimens were 60 mm long, 5 mm wide, and ~10 μm thick, with a gauge length of 40 mm. Prior to testing, the thickness and width of the specimens were measured at three locations along the sample length using a micrometer, and the average values were taken. Ten samples per group were tested.

4.3.6 *In vitro* cell culture

The established line of mouse pre-osteoblastic MC3T3-E1 cells, obtained from the RIKEN Cell Bank (Tsukuba, Japan), was used in this study. This cell line was selected because it is widely used in assays to evaluate the response of scaffolds to osteogenic cells [30]. The cells were cultured in alpha-modified minimum essential medium (α-MEM; GIBCO), supplemented

with 10% heat-inactivated fetal bovine serum (FBS, GIBCO), 100 U/ml penicillin and 100 U/ml streptomycin. The cultures were incubated at 37°C in a humidified atmosphere containing 5% CO_2, with the medium changed every 2 days.

Prior to seeding with cells, discs (15 mm in diameter × ~10 μm thick) were cut from PVA and BG-coated PVA scaffolds and placed in 24-well plates. The samples were sterilized by soaking for 1 h in 70% ethanol, and washed three times with sterile PBS for 30 min each to remove residual ethanol. The scaffolds were then placed individually in cell culture medium overnight using standard culture conditions. After the culture medium was removed as completely as possible, each scaffold was seeded with cells by adding an MC3T3-E1 cell suspension dropwise onto the scaffolds (1×10^4 cells in 100 μl of medium per well). The cell suspension was fully absorbed, allowing the cells to be distributed within the porous scaffolds. The cell-seeded scaffolds were incubated for 3 h to allow the cells to adhere to the scaffolds, after which additional culture medium was added (1 ml/well). The control group consisted of the same number of cells seeded on tissue culture plastic (TCP) substrates (high-grade polystyrene Nunc™ Dishes; Thermo Fisher Scientific, Denmark).

4.3.7 Cytotoxicity assay

The viability of cells grown on the scaffolds was determined using a lactate dehydrogenase (LDH) Cytotoxicity Kit (Wako, Japan). The LDH assay is used for the quantitative determination of cell death by measuring the LDH activity liberated from cells with cell membrane injuries. For this assay, MC3T3-E1 cells were seeded (5×10^4 cells/well) on sterilized PVA and BG-coated

PVA scaffolds, and also on tissue culture plastic(TCP) as a control, as described previously. After an incubation time of 24 h, the LDH in the supernatant and in the adherent cells was measured separately, using the procedure described by the manufacturer. For estimation of cell death, the cell membrane damage was expressed as the percent of cell lysis.

4.3.8 Cell proliferation assay

MC3T3-E1 cells were seeded on the PVA and BG-coated PVA scaffolds and on the TCP control substrates (1×10^4 cells/well), as described previously. After incubation for 1, 3, 5, 7 and 14 days, 10 μL of TetraColor ONE reagent containing tetrazolium monosodium salt (Seikagaku Corporation, Tokyo, Japan) was added to each well, and the cells were incubated for an additional 2 h. The absorbance at 450 nm was measured using a Biotrack II plate reader (GE Healthcare; USA).

4.3.9 Alkaline phosphatase activity

Alkaline phosphatase (ALP) activity, an early indicator of osteoblastic differentiation, was measured using an ALP substrate kit (Wako, Japan). Scaffolds and TCP controls were seeded with MC3T3-E1 cells (1×10^4 cells/well) as described previously, and incubated in α-MEM supplemented with 0.1% β-glycerol phosphate to induce osteoblast differentiation. The ALP activity was measured after incubation times of 7, 10, and 14 days. After each incubation, 500 μL of β-nitrophenyl phosphate solution containing 1 mM $MgCl_2$ (Sigma–Aldrich; USA) and the mixture was incubated for a further 10 min at 37 °C. The enzymatic reaction was stopped by adding 500 μL of 0.2 M NaOH, and the absorbance was measured at 405 nm.

4.3.10 Calcium content assay and alizarin red S staining

In the late stages of differentiation, osteoblasts produce a mineralized matrix that consists of extracellular protein and calcium phosphate minerals [34]. The calcium content of the scaffolds and the TCP control substrates was determined using a Calcium C Test Kit (Wako Pure Chemical Industries, Ltd., Osaka, Japan), using a procedure described elsewhere [35]. After incubation for 7, 10 and 14 days, the cell-seeded scaffolds and TCP control substrates were washed twice with PBS, and soaked overnight in 1N hydrochloric acid. Extracts of the solutions were used for calcium assay according to the manufacturer's instructions. Briefly, extracts (10 μg) were pipetted into each well of a 96-well plate, and 200 μl of a reagent mixture was added to the well. The calcium content in each well was measured at 570 nm in a Biotrack II plate reader.

Mineralization in the cell layers was assessed by alizarin red S staining. After incubating for 7, 10 and 14 days, the cell-seeded scaffolds were washed three times with phosphate-buffered saline (PBS), fixed with 10% formaldehyde for 1 h and then rinsed 5 times for 5 min each with deionized water. A solution of alizarin red S stain (1%) was added to each well and the system was incubated for 5 min at room temperature. Excess dye was removed by washing with deionized water. After washing ten times with deionized water, the scaffolds were examined in an optical microscope.

4.3.11 Cell morphology

After incubation for 1, 3, and 5 days, scaffolds with attached cells were removed, washed three times with PBS and placed in 2.5% glutaraldehyde in PBS. After an overnight soak at 4°C, the

scaffolds were washed 3 times with PBS and dehydrated through a graded series of ethanol (50–99%). After the final washing with 99% ethanol, the scaffolds were treated three times with t-butyl alcohol for 10 min each. Finally, the samples were sputter-coated with gold and examined in an SEM (Hitachi S-5000), using the procedure described previously.

4.4 Statistical analysis

All biological experiments were (3 samples in each group) run in duplicate or triplicate. The data are presented as the mean ± standard deviation (SD). Statistical analysis was performed using one-way analysis of variance (ANOVA) with the level of significance set at $p < 0.05$.

4.5 Results

4.5.1 Structure and composition of scaffolds

SEM showed that the electrospun PVA scaffolds prepared in this work had a homogeneous microstructure of randomly distributed fibers (Fig. 4-1a) with a nearly uniform diameter (Fig. 4-1a; inset), and that the fibers were free from beads. While the microstructure of the BG-coated PVA scaffolds was also homogeneous, the deposition of the coating resulted in a change in the microstructure and the fiber morphology (Fig.4-1c); the BG-coated PVA scaffold appeared to be less porous than the PVA scaffold, and the fiber morphology was less uniform (Fig.4-1c; inset). Analysis of >100 fibers using the Image J software showed that the PVA fibers had a diameter of 286 ± 14 nm while the BG-coated fibers had a diameter of 318 ± 36 nm. EDS analysis showed the presence of sulfur (S) on the surface of the PVA nanofibers, which resulted presumably from the crosslinking reagent K-FJD (Fig. 1b). After deposition of the BG coating, silicon (Si) was

also detected on the surface of the nanofibers (Fig. 4-1d), indicating the presence of an Si-based coating on the surface of the PVA fibers.

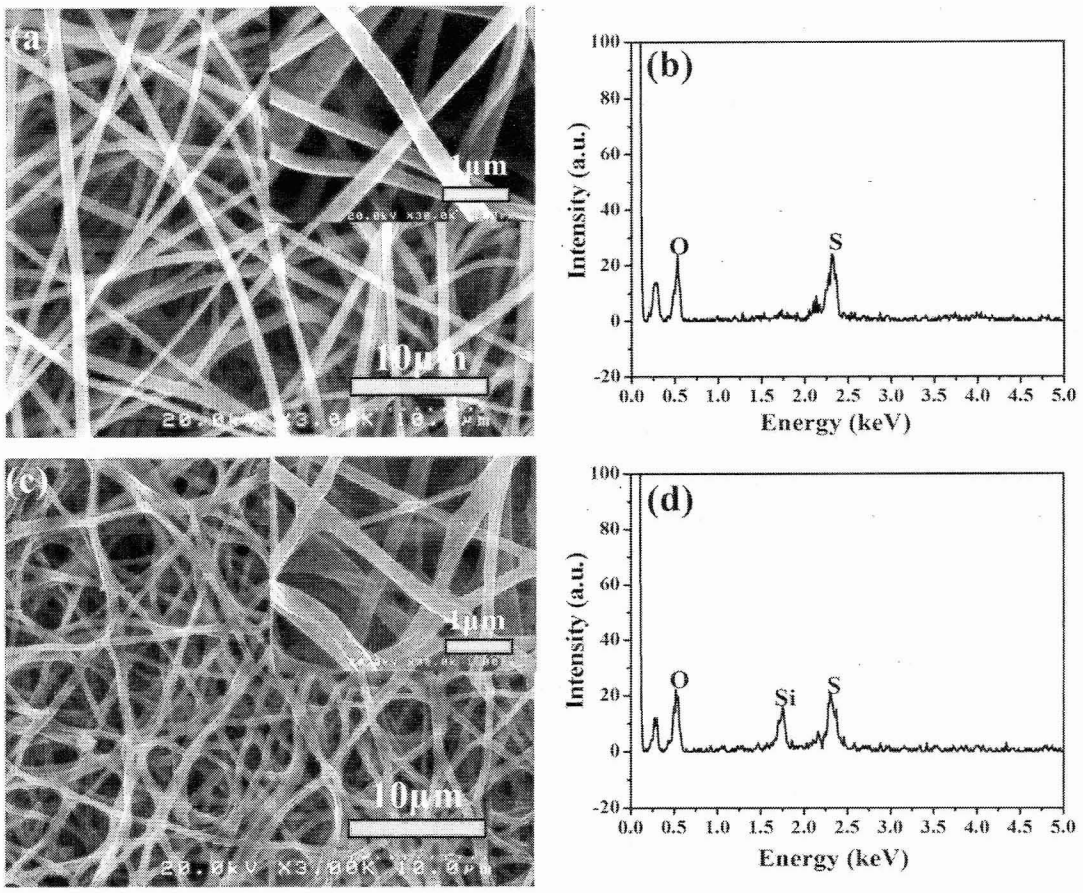

Figure 4-1. SEM images and EDS spectra of electrospun PVA fibrous scaffold (a, b), and bioactive glass (BG)-coated PVA fibrous scaffold (c, d). (a, c; inset: higher magnification SEM image of PVA fibers and BG-coated PVA fibers)

FTIR spectroscopy of the crosslinked PVA fibers (Fig.4-2a) showed a resonance at 1665 cm^{-1}, attributed to the C=O stretching vibration of the crosslinking agent (K-FJD), and a broad resonance at 3400 cm^{-1}, characteristic of the –OH stretching vibration in PVA [26]. For the BG-coated PVA fibers, resonances appeared at 1085 cm^{-1} and 817 cm^{-1}, characteristic of Si–O–Si

stretching and bending vibrations [28], which support the EDS observations for the presence of Si on the surface of BG-coated PVA scaffolds. The FTIR spectrum for the BG-coated PVA also showed a resonance at 1655 cm^{-1}, which was attributed to the stretching vibration of –OH groups in the PVA which were hydrogen-bonded to silanol groups (Si–OH) in the sol–gel derived silicate coating. Silanol groups commonly result from incomplete polycondensation of TEOS in sol-gel silicates. This FTIR observation indicated that intermolecular hydrogen bonds were formed at the interface between the BG coating and PVA fibers.

XRD patterns of the electrospun PVA and BG-coated PVA scaffolds (Fig.4-2b) showed a peak at 19.8° 2θ which corresponds to reflections from the (101) plane in semi-crystalline PVA [21]. This peak was broader and less intense (smaller peak height) in the pattern for the BG-coated PVA scaffold, presumably because of the presence of the amorphous BG coating. Together, the SEM, EDS, FTIR, and XRD results confirmed the presence of an amorphous silicate coating on the PVA fibers coated with the sol–gel derived BG.

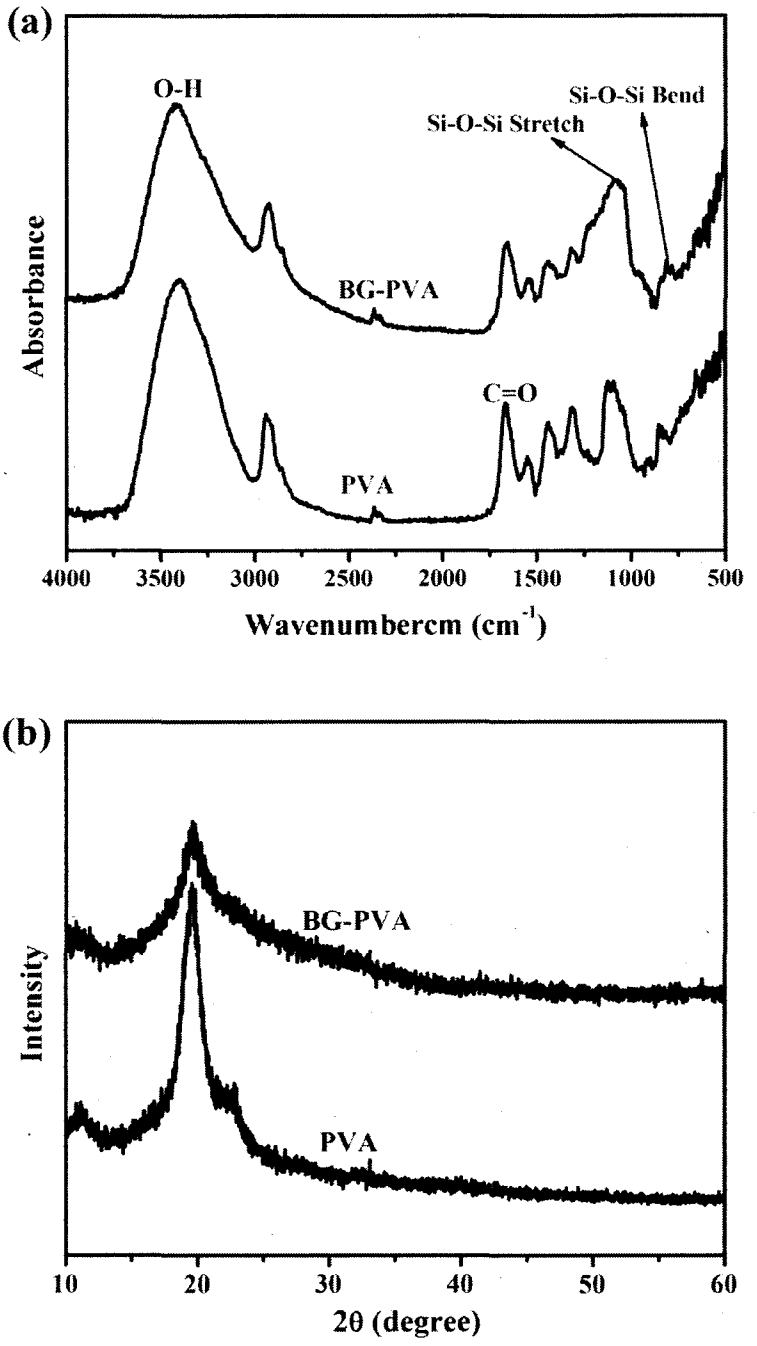

Figure 4-2. (a) FTIR spectra and (b) XRD patterns of electrospun PVA and BG-coated PVA scaffolds.

4.5.2 *In vitro* bioactivity

Immersion of the BG-coated PVA scaffolds for 1–5 days in SBF resulted in considerable morphological changes on the surface of the BG-PVA fibers (Fig. 4-3a, c, e). In comparison, little change occurred on the uncoated PVA fibers even after 5 days in SBF (Fig. 4-3g). After immersion for 1 day, fine particles of a reaction product, with a spherical geometry, appeared on the surface of the BG-coated PVA fibers; the particles appeared to be well-attached to the fiber surface (Fig. 4-3a). The spherical particles increased in size and number with immersion time, but individual spherical particles could still be observed after an immersion time of 3 days (Fig. 4-3c). After 4 days, the surface of the scaffold was completely covered by a layer of reaction product (image was not shown); this layer became denser after 5 days (Fig.4-3e).

High resolution SEM images showed that the reaction product consisted initially (day 1) of a mesoporous structure of fine, needle-like particles with a morphology typical of nanostructured HA (Fig.4-3a; inset). This structure became denser with an increase in the immersion time to 3 and 5 days (Fig.4-3c, e; inset), but a mesoporous structure of fine particles was still evident. The SEM images indicated that BG-coated PVA fibrous scaffolds can support rapid formation of a reaction product, presumably an HA-like material, when immersed in SBF.

EDS analysis of the reaction product formed on the surface of the BG-coated PVA scaffolds showed that the major elements consisted of C, S, Ca, P, and O (Figs.4-3b, d and f). Sulfur presumably resulted from the cross-linking agent, while C presumably resulted from the PVA fibers (carbon-based polymer) and the sol-gel derived coating (unhydrolyzed organic groups).

Since the PVA fibers did not contain Ca and P, these elements could be taken to come from the BG coating and/or the reaction product (presumably an HA-like material). The concentration of Ca and P (taken to be proportional to the peak intentisy) increased with immersion time in the SBF (Figs.4-3b, d and f), while the S peak became smaller and disappeared after 4 days (EDS spectrum was not shown). At day 5, the Ca/P atomic ratio was found to be 1.63, which is similar to the ratio for stoichiometric HA (1.67).

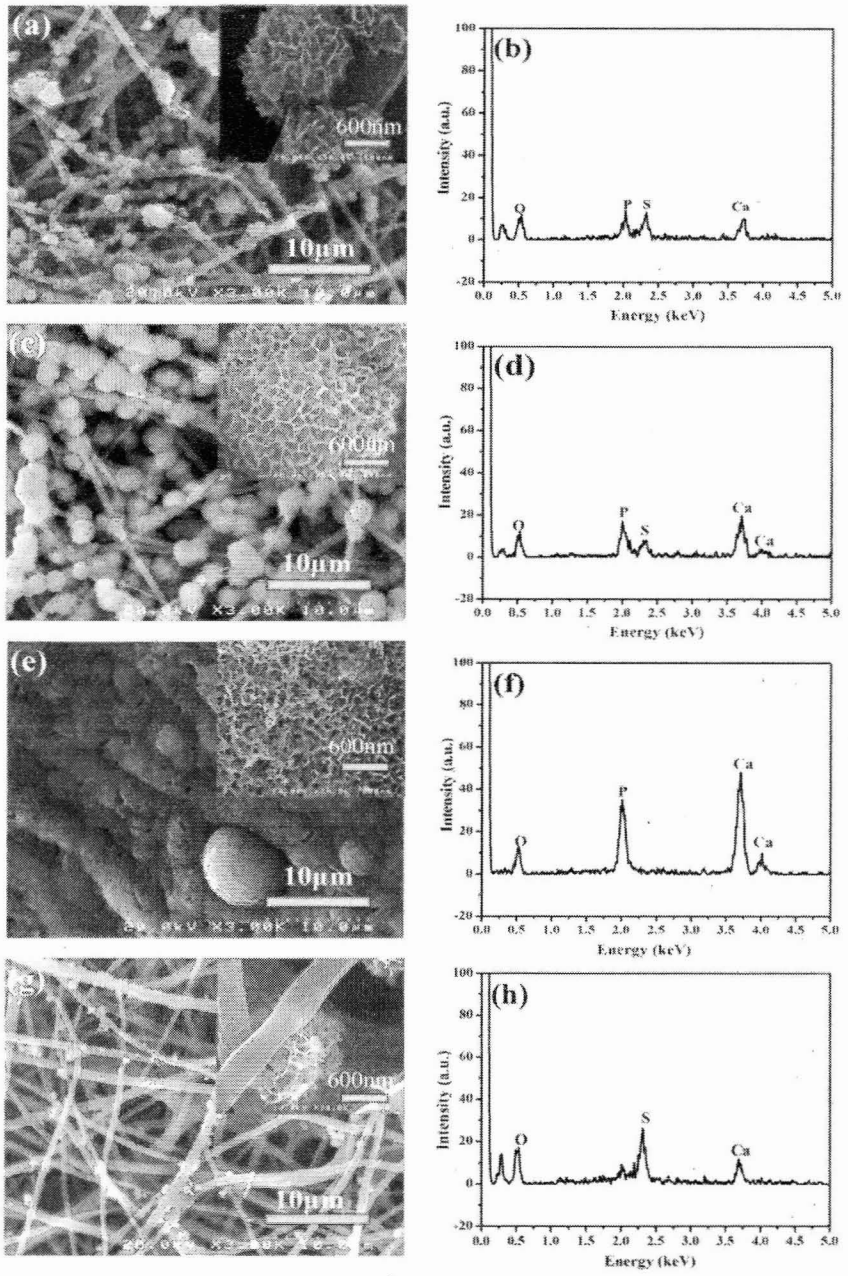

Figure 4-3. SEM images and EDS spectra of BG-coated PVA scaffolds immersed in a simulated body fluid (SBF) for (a, b) 1 day; (c, d) 3 days; (e, f) 5 days. For comparison, an SEM image and EDS spectrum of the uncoated PVA scaffold immersed in SBF for 5 days are shown (g, h). (a, c, e; inset: higher magnification SEM images of the reaction product on the surface of the fibrous scaffolds; scale bar = 600 nm)

Fig.4-4 shows the FTIR spectra of BG-coated PVA scaffolds immersed in the SBF for 1, 3 and

5 days. The presence of P–O resonances at 574, 607 and 1033 cm^{-1}, is attributed to the formation of a crystalline HA-like material [36]. The intensity of the resonances increased with increasing immersion time, indicating continued formation of the reaction product with time.

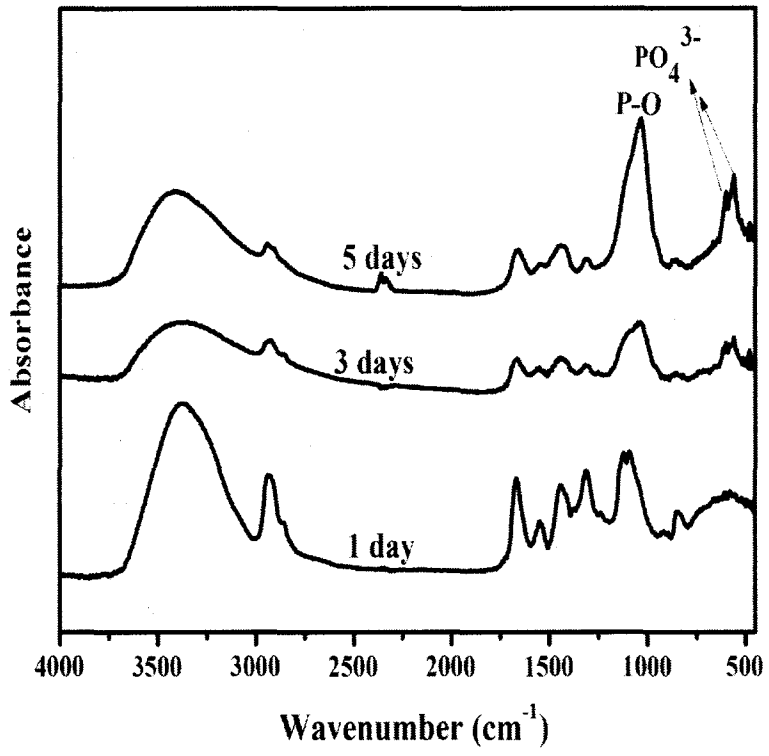

Figure 4-4. FTIR spectra of BG-coated PVA fibrous scaffolds immersed in SBF for 1, 3, and 5 days.

Taken together, the SEM images, EDS analysis, and FTIR spectra strongly indicated the rapid conversion of the BG coating to an HA-like product upon immersion of the BG-coated PVA fibers in SBF.

4.5.3 Mechanical response

The mechanical response in tension for fibrous mats of PVA, BG-coated PVA, and BG-coated PVA immersed for 5 days in SBF are shown in Fig.4-5. The stress vs. deformation response for all three groups showed the same general trend: an initial region in which the stress increased more rapidly with deformation, followed by region with a more gradual increase, and eventually failure. When compared to the PVA sample, the BG-coated PVA sample showed a higher Young's modulus (taken as the slope of the initial steep region), no significant change in the tensile strength (strength at failure), and a smaller elongation to failure (Table 4-1). Immersion of the BG-coated PVA scaffolds for 5 days in SBF resulted in an increase in the tensile strength and elongation to failure when compared to the PVA sample.

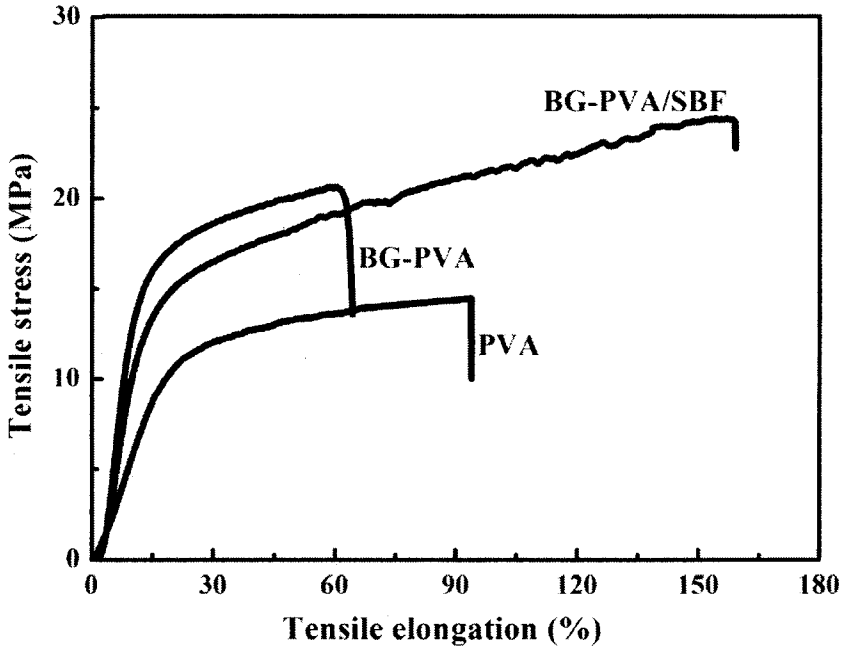

Figure 4-5. Mechanical response in tension of (a) electrospun PVA scaffold; (b) BG-coated

PVA scaffold (BG-PVA), and (c) BG-coated PVA scaffold immersed in SBF for 5 days. (BG-PVA/SBF).

Table 4-1. Tensile mechanical properties of electrospun PVA, BG-coated PVA (BG-PVA), and BG-coated PVA immersed in a simulated body fluid (SBF) for 5 days (BG-PVA/SBF).

Scaffold	Young's modulus (MPa)	Tensile strength (MPa)	Enlongation to failure (%)
PVA	126 ± 5	18 ± 2	94 ± 4
BG-PVA	275 ± 8	21 ± 2	64 ± 5
BG-PVA/SBF	205 ± 10	24 ± 2	159 ± 4

4.5.4 Response of scaffolds to cells

The amount of LDH released from the cell-seeded scaffolds into the culture medium was used to quantitatively evaluate cell death and, therefore, cell viability. Figure 4-6a shows the amount of LDH released from the cell-seeded PVA and BG-coated PVA scaffolds as well as from the TCP control substrate after an incubation time of 24 h. There was no significant difference in cytotoxicity among the PVA scaffold, the BG-coated PVA scaffold, and the TCP control, indicating the biocompatibility of the BG-coated PVA material.

Results for the proliferation of MC3T3-E1 cells on PVA and BG-coated PVA scaffolds and the TCP control substrate after incubation times of 1–14 days are shown in Fig. 4-6b. Both groups of scaffolds and the TCP substrate supported cell proliferation at day 1, but the BG-coated PVA scaffold had a greater capacity to support cell proliferation than the PVA

scaffold at days 3–14. The number of cells on the BG-coated PVA scaffolds was lower than on the TCP control at days 3–7; however, at days 10 and 14, the number of cells on the BG-coated PVA and TCP was approximately the same, which is a further indication of the biocompatibility of the BG-coated PVA scaffolds.

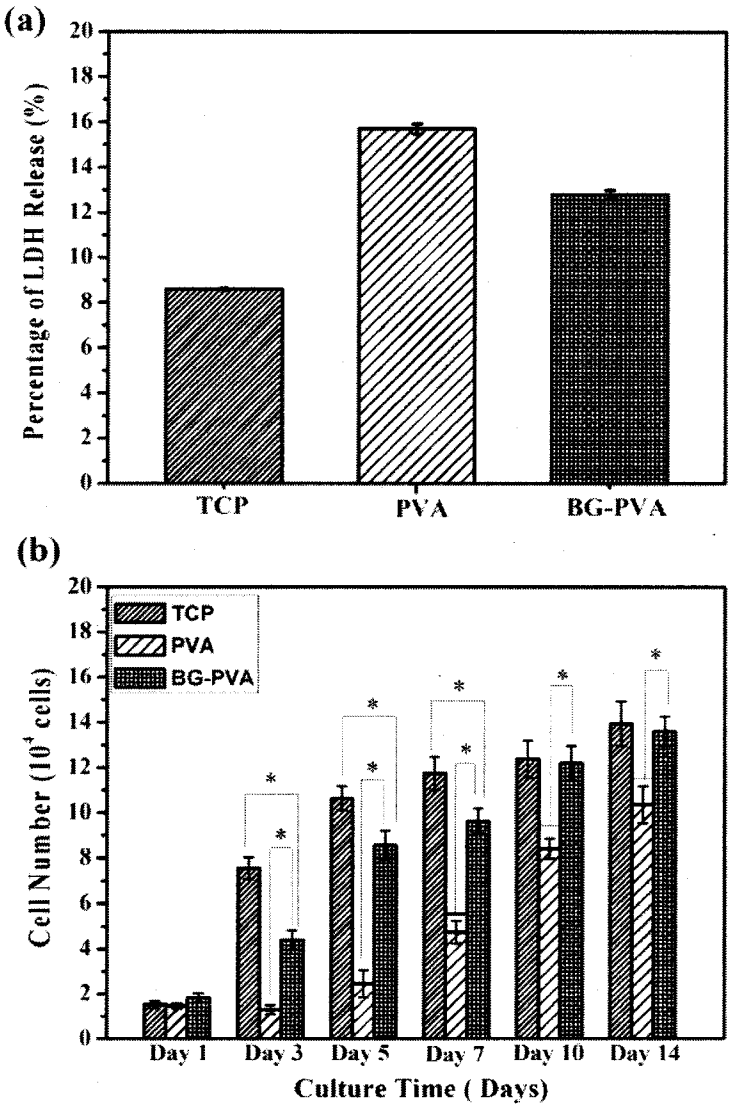

Figure 4-6. Response of MC3TC-E1 cells to fibrous scaffolds of PVA and BG-coated PVA, and to tissue culture plastic (TCP) control substrates: (a) lactate dehydrogenase (LDH) assay after

incubation for 24 h; (b) cell proliferation as a function of incubation time. *Significant difference between pairs of substrates shown ($p < 0.05$). (Mean ± SD; n = 5)

Figure 4-7a shows results for the spectrophotometric measurement of alkaline phosphatase (ALP) activity of MC3T3-E1 cells cultured on PVA and BG-coated PVA scaffolds and on TCP controls for 7, 10, and 14 days. The ALP activity of the BG-coated PVA scaffolds was higher than that of the TCP at all three incubation times, and it was higher than that of the PVA at days 10 and 14. Results for the calcium content of the PVA and BG-coated PVA scaffolds and TCP control substrates seeded with MC3T3-E1 cells are shown in Fig. 4-7b for incubation times of 7, 10, and 14 days. The calcium content of the PVA and BG-coated PVA scaffolds was higher than that of TCP at all three incubation times; in addition, the calcium content BG-coated PVA was higher than that of the PVA scaffold at days 10 and 14. Images of alizarin red S staining of the cell-seeded PVA and BG-coated PVA scaffolds after an incubation time of 14 days (Fig. 4-7b; inset) showed the presence of calcium on both scaffolds (red staining). The more intense staining of the BG-coated PVA scaffolds indicated higher calcium content in those scaffolds.

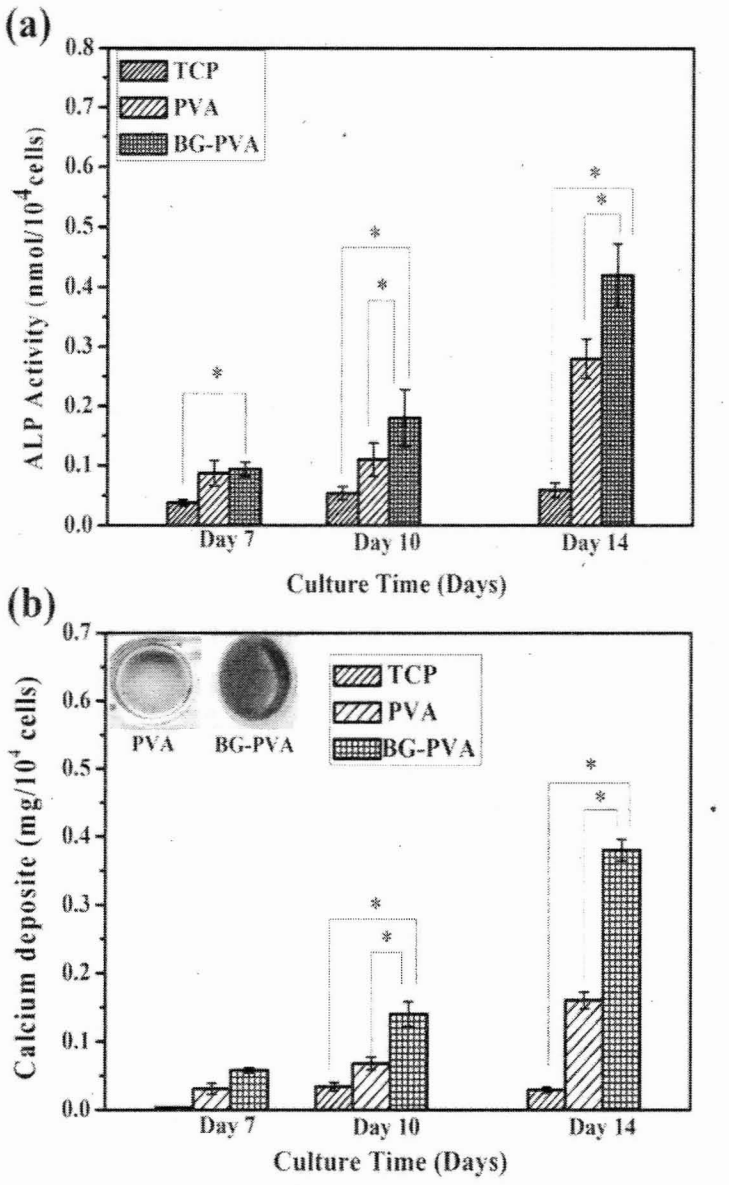

Figure 4-7. (a) Alkaline phosphatase (ALP) activity of MC3T3-E1 cells cultured on PVA and BG-coated PVA scaffolds, and on TCP control substrates for 7, 10, and 14 days; (b) Amount of calcium on the cell-seeded scaffolds and TCP control after incubation times of 7, 10, and 14 days. *Significant difference between pairs of substrates shown ($p<0.05$). (Mean ± SD; n=5) (b; inset: images of alizarin red S staining of cell-seeded PVA and BG-PVA scaffolds incubated for 14 days)

SEM images in Fig. 4-8 show the morphology and density of MC3T3-E1 cells incubated for 1,

3 and 7 days on the PVA and BG-coated PVA scaffolds. The cells showed an increase in density with incubation time for both scaffolds, but the increase was greater for the BG-PVA scaffold. Differences in morphology were also apparent between the cells cultured on the two groups of scaffolds. The cells visible on the PVA scaffold after day 1 had a more rounded shape (Fig. 4-8a); in comparison, the cells on the BG-coated PVA scaffold showed numerous projections and pseudopodia (Fig. 4-8d), indicating better biocompatibility of the BG-coated PVA scaffold. After 3 days of culture, the cell morphology on the BG-coated PVA scaffold was distinctly different from that on the PVA scaffold. The cells on the BG-coated PVA scaffold showed physical contact and aggregation with neighboring cells via multiple extensions (Figs. 4-7b, 7e). Mineralization can be seen on the surface of the BG-PVA scaffold (white phase) (Fig. 4-8e), and the cells appeared to be in intimate contact with the mineralized layer. After 7 days of culture (Fig. 4-8c, 8f), the major part of the BG-coated PVA scaffold was covered with a layer of cells and mineralized material.

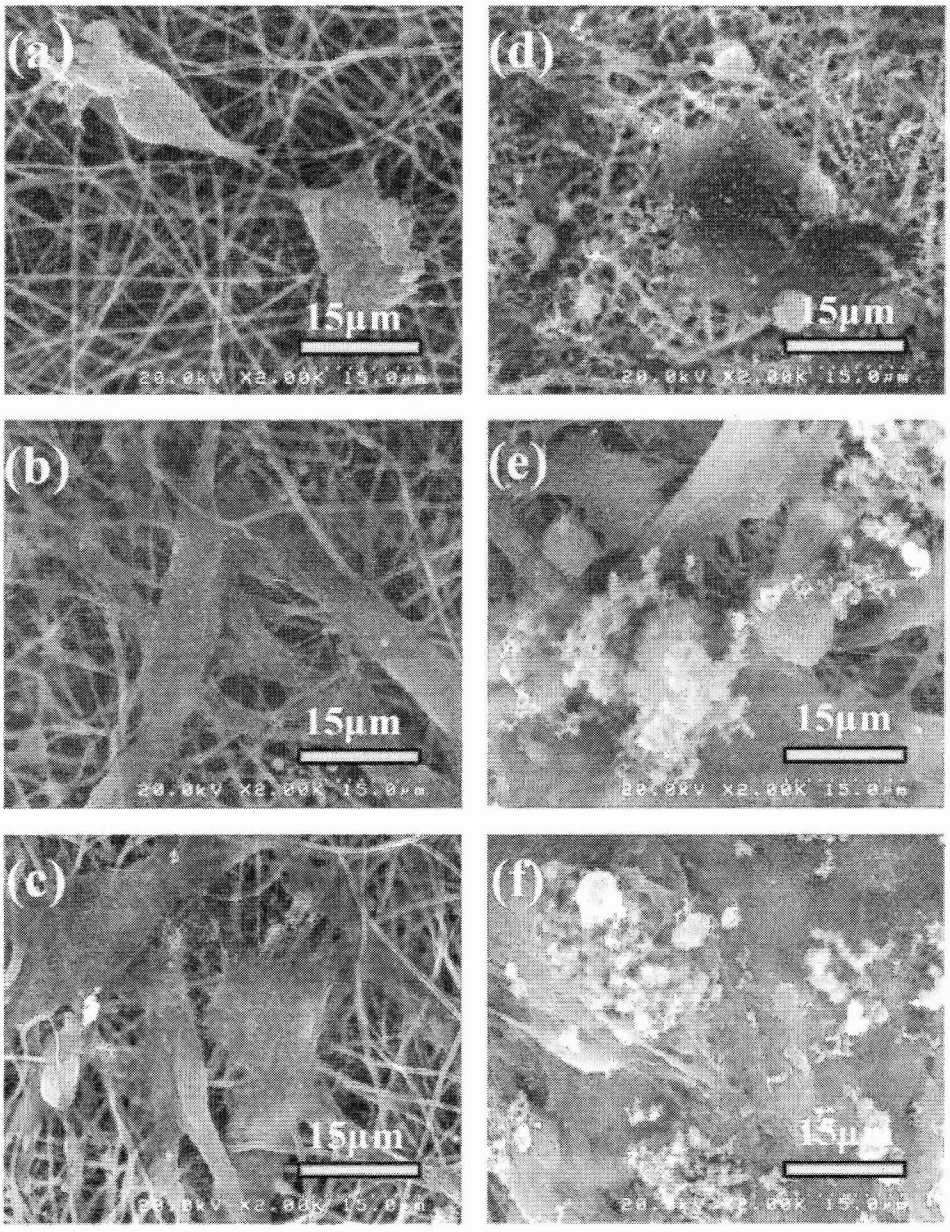

Figure 4-8. SEM images of MC3TC-E1 cell morphology on PVA (a–c), and BG-coated PVA fibrous scaffolds (d–f), after incubation for 1 day (a), (d); 3 days (b), (e); and 7 days (c), (f).

4.6 Discussion

Properties such as architecture (microstructure) and response to cells and tissues are critically important to the performance of scaffolds in tissue regeneration. Many materials have the desired

structural characteristics but often lack the requisite biocompatibility or bioactivity. Electrospun PVA scaffolds have a fibrous structure that mimics the extracellular matrix (ECM), but poor bioactivity and weak integration with host bone limit their application as a scaffold material for bone repair [25]. In this work, deposition of a sol–gel derived BG coating on electrospun PVA fibers was used to improve the bioactivity and response of PVA scaffolds to cells. The results showed that the BG coating did not markedly alter the desirable ECM-like architecture of the electrospun PVA scaffolds, while it improved the bioactivity and mechanical response of the scaffolds, as well as the capacity of the scaffolds to support cell proliferation, ALP activity, and mineralization *in vitro*. These BG-coated PVA scaffolds could potentially provide attractive materials for bone regeneration.

Examination of the morphology and structure showed that the electrospun PVA fibers were uniformly coated with the BG without markedly affecting the fibrous and porous structure of the scaffold. Small differences in the fiber morphology (Fig. 4-1a, 4-1c) could be caused by swelling of the PVA nanofibers as a result of exposure to the acidic silicate solution during the sol–gel coating process. FTIR spectroscopy showed evidence for the formation of hydrogen bonds between hydroxyl groups of the PVA and the BG coating (Fig. 4-2a) which is beneficial for developing strong interfacial adhesion between the BG coating and the PVA fibers.

An advantage of the BG-coated PVA scaffold, when compared to the uncoated PVA, is the potential for improved bioactivity. When immersed in SBF, an HA-like material formed rapidly on the surface of the BG-coated PVA scaffold (Fig. 4-3), resulting in the full coverage of the surface with HA within 5 days. In comparison, the PVA scaffold (no BG coating) showed little

ability to induce the formation of HA, as observed in previous studies which showed that PVA had limited ability to support the formation of HA *in vitro* [21, 25, 29]. When the BG-coated PVA is immersed in SBF, calcium ions released from the BG react with phosphate ions in the SBF to precipitate an HA-like material on the surface of the BG [9, 37]. Silanol groups on the surface of the BG coating are believed to serve as nucleation sites for the precipitation and growth of HA. The mesoporous structure and, presumably, high surface area of the BG coating, typical of materials formed by sol–gel processing, may be responsible for the rapid mineralization of the BG-coated PVA scaffold.

The BG coating improved the elastic modulus of the electrospun PVA scaffolds, had little effect on the tensile strength, and reduced the elongation to failure (Table 4-1); however, the elongation to failure of the BG-coated PVA was still large (64 ± 5%). Presumably, the homogeneous inorganic BG coating enabled the PVA nanofibers to better resist extension in response to an applied load, which resulted in an increase in elastic modulus. An interesting observation is that after immersion in SBF for 5 days, the BG-coated PVA scaffold showed an improvement in tensile strength and elongation to failure when compared to the as-fabricated PVA scaffolds (Table 4-1). A possible explanation might be the development of a strong interfacial adhesion between the PVA and the fine needle-like HA particles formed during the conversion of the BG coating. In addition the strengthening effect, the ability to the maintain a high ductility (elongation to failure) should be beneficial for the potential use of these BG-coated PVA as a membrane or scaffold for bone regeneration.

Scaffolds for bone tissue engineering applications must support the differentiated function of

bone progenitor cells. In addition, the production of a mineralized matrix by bone progenitor cells is an important requirement in the development of scaffolds for bone repair. When compared to the PVA scaffolds, the BG-coated PVA scaffolds showed a greater capacity to support the proliferation of osteogenic MC3T3-E1 cells and ALP activity *in vitro* (Figs. 4-6b, 4-7a). Overall, mineralization in the cell-seeded BG-coated PVA scaffolds was higher than in the cell-seeded PVA scaffolds (Fig. 4-7b). However, because of the mineralization of the BG coating (conversion to an HA-like material) in the culture medium, the effect of the BG-coated PVA scaffold to support mineralization in the cells themselves is unclear.

The present study showed that the sol–gel deposition of a BG coating provided an effective method to improve the bioactivity and biocompatibility of electrospun PVA fibrous scaffolds. The favorable *in vitro* cell culture response, ECM-like architecture, and mechanical properties indicate that these BG-coated PVA scaffolds could be potentially useful in bone regeneration. Ongoing research is aimed at evaluating the ability of these BG-coated PVA scaffolds to heal bone defects in an animal model.

4.7 Summary

A sol–gel method provided a facile process for coating electrospun PVA fibers (diameter = 286 ± 14 nm) with a layer of bioactive glass (BG) (composition $70SiO_2$–$25CaO$–$5P_2O_5$; mol%). The BG coating resulted in mineralization of the fiber surface (conversion to a hydroxyapatite-like material) within 3 days in a simulated body fluid (SBF). When compared to PVA scaffolds (no BG coating), the BG-coated PVA scaffolds showed a higher elastic modulus, no difference in tensile strength, and a reduction in elongation to failure. Immersion of the BG-coated PVA

scaffolds in SBF for 5 days resulted in an increase in the elastic modulus and elongation to failure when compared to the as-fabricated PVA scaffolds. *In vitro*, the BG-coated PVA scaffolds showed a better capacity to support the proliferation of osteogenic MC3T3-E1 cells, alkaline phosphatase activity, and mineralization when compared to the uncoated PVA scaffolds. These BG-coated PVA fibrous scaffolds could be potentially useful as scaffolds in bone regeneration.

References

[1] Stevens MM. Biomaterials for bone tissue engineering. Mater Today 2008; 11:18–25.

[2] Porter JR, Ruckh TT, Popat KC. Bone tissue engineering: a review in bone biomimetics and drug delivery strategies. Biotechnol Prog 2009; 25:1539–60.

[3] Burg KJ, Porter S, Kellam JF. Biomaterial developments for bone tissue engineering. Biomaterials 2000; 21:2347–59.

[4] Hutmacher DW. Scaffolds in tissue engineering bone and cartilage. Biomaterials 2000; 21:2529–43.

[5] Agarwal S, Wendorff JH, Greiner A. Use of electrospinning technique for biomedical applications. Polymer 2008; 49:5603–21.

[6] Pham QP, Sharma U, Mikos AG. Electrospinning of polymeric nanofibers for tissue engineering applications: a review. Tissue Eng 2006; 12:1197–1211.

[7] Jang JH, Castano O, Kim HW. Electrospun materials as potential platforms for bone tissue engineering. Adv Drug Delivery Rev 2009; 61:1065–83.

[8] Hench LL, Splinter RJ, Allen WC, Greenlee TK Jr. Bonding mechanisms at the interface of ceramic prosthetic materials. J Biomed Mater Res 1971; 5:117–41.

[9] Hench LL. Bioceramics. J Am Ceram Soc 1998; 81:1705–28.

[10] Hench LL. The story of bioglass. J Mater Sci Mater Med 2006; 7:967–78.

[11] Rahaman MN, Day DE, Bal BS, Fu Q, Jung SB, Bonewald LF, Tomsia AP. Bioactive glass in tissue engineering. Acta Biomater 2011;7:2355–73.

[12] Hong Z, Liu A, Chen L, Chen X, Jing X. Preparation of bioactive glass ceramic nanoparticles by combination of sol–gel and coprecipitation method. J Non-Cryst Solids 2009; 355; 368–372.

[13] Gao CX, Gao Q, Bao XX, Li YD, Teramoto A, Abe KJ. Preparation and *in vitro* bioactivity of novel mesoporous borosilicate bioactive glass nanofibers. J Am Ceram Soc 2011; 9: 2841–5.

[14] Hong YL, Chen XS, Jing XB, Fan HS, Guo B, Gu ZW, Zhang XD. Preparation, bioactivity, and drug release of hierarchical nanoporous bioactive glass ultrathin fibers. Adv Mater 2010; 22:754–8.

[15] Jang JH, Castano O, Kim HW. Electrospun materials as potential platforms for bone tissue engineering. Adv Drug Deliver Rev 2009; 61:1065–83.

[16] Wei J, Wu XH, Liu CS, Jia JF, Heo SJ, Kim SE, Hyun YT, Shin JW. Fabrication of bioactive scaffold of poly(ε-caprolactone) and nanofiber wollastonite composite. J Am Ceram Soc, 2009; 92:1017–23.

[17] Rezwan K, Chen QZ, Blaker JJ, Boccaccini AR. Biodegradable and bioactive porous polymer/inorganic composite scaffolds for bone tissue engineering. Biomaterials 2006; 27:3413–31.

[18] Fujihara K, Kotaki M, Ramakrishna S. Guided bone regeneration membrane made of polycaprolactone/calcium carbonate composite nanofibers. Biomaterials 2005; 26:4139–47.

[19] Sheikh FA, Barakat NAM, Kanjwal MA, Park SJ, Park DK, Kim HY. Synthesis of poly(vinyl alcohol) (PVA) nanofibers incorporating hydroxyapatite nanoparticles as future implant materials. Macromol Res 2010; 18:59–66.

[20] Schmedlen RH, Masters KS, West JL. Photocrosslinkable polyvinyl alcohol hydrogels that can be modified with cell adhesion peptides for use in tissue engineering. Biomaterials 2002; 23:4325–32.

[21] Sailaja GS, Sreenivasan K, Yokogawa Y. Kumary TV, Varma HK. Bioinspired mineralization and cell adhesion on surface functionalized poly (vinyl alcohol) films. Acta Biomater 2009; 5:1647–55.

[22] Matsumura K, Hayami T, Hyon SH, Tsutsumi S. Control of proliferation and differentiation of osteoblasts on apatite-coated poly(vinyl alcohol) hydrogel as an artificial articular cartilage material. J Biomed Mater Res A 2010; 92:1229–32.

[23] Fundueanu G, Constantin M, Ascenzi P. Poly (vinyl alcohol) microspheres with pH- and thermosensitive properties as temperature-controlled drug delivery. Acta Biomater 2010; 6:3899–3907.

[24] Kang YO, Yoon IS, Lee SY, Kim DD, Lee SJ, Park WH, Hudson SM. Chitosan-coated poly(vinyl alcohol) nanofibers for wound dressings. J Biomed Mater Res B Appl Biomater 2010 92B:568–76.

[25] Sheich FA, Barakat NA, Kanjwal MA, Park SJ, Park DK, Kim HY. Synthesis of poly(vinyl alcohol) (PVA) nanofibers incorporating hydroxyapatite nanoparticles as future implant materials. Macromol Res 2010; 59–66.

[26] Degirmenbasi N, Kalyon DM, Birinci E. Biocomposites of nanohydroxyapatite with collagen and poly (vinyl alcohol). Colloids Surf B Biointerfaces 2006; 48:42–9.

[27] Sinha A, Das G, Sharma B.K, Roy R.P, Pramanick A.K and Nayar S. Poly (vinyl alcohol)-hydroxyapatite biomimetic scaffold for tissue regeneration. Mater Sci Eng C 2007; 27:70–4.

[28] Mansur HS, Costa HS. Nanostructured poly (vinyl alcohol)/bioactive glass and poly (vinyl alcohol)/chitosan/bioactive glass hybrid scaffolds for biomedical applications. Chem Eng J 2008; 137:72–83.

[29] Dias LLS, Mansur HS, Donnici CL, Pereira MM. Synthesis and characterization of chitosan-polyvinyl alcohol-bioactive glass hybrid membranes. Biomatter 2011;1:114-9.

[30] Brown RF, Day DE, Day TE, Jung S, Rahaman MN, Fu Q. Growth and differentiation of osteoblastic cells on 13-93 bioactive glass fibers and scaffolds. Acta Biomater 2008; 4:387–96.

[31] Li R, Clark AE, Hench LL. An investigation of bioactive glass powders by sol-gel processing. J Appl Biomater 1991;2:231–9.

[32] Karpov M, Laczka M, Leboy PS, Osyczka AM. Sol-gel bioactive glasses support both osteoblast and osteoclast formation from human bone marrow cells. J Biomed Mater Res A 2008; 84A: 718-26.

[33] Kokubo T, Takadama H. How useful is SBF in predicting *in vivo* bone bioactivity? Biomaterials 2006;27:2907–15.

[34] Ma PX. Biomimetic materials for tissue engineering. Adv Drug Deliver Rev 2008; 60:184–98.

[35] Kim J, Magno MHR, Alvarez P, Hollinger JO. Osteogenic differentiation of pre-osteoblasts on biomimetic tyrosine-drived polycarbonate scaffolds. Biomacromolecules 2011;12:3520–7.

[36] Marelli B, Ghezzi CE, Barralet JE, Boccaccini AR, Nazhat SN. Three-dimensional mineralization of dense nanofibrillar collagen-Bioglass hybrid scaffolds. Biomacromolecules 2010;11:1470–9.

[37] Huang W, Day DE, Kittiratanapiboon K, Rahaman MN. Kinetics and mechanisms of the conversion of silicate (45S5),borate, and borosilicate glasses to hydroxyapatite in dilute phosphate solutions. J Mater Sci: Mater Med 2006; 17:583–96.

CHAPTER 5 *In vitro* evaluation of electrospun gelatin–bioactive glass hybrid scaffolds for bone regeneration

5.1 Abstract

Organic–inorganic hybrid materials composed of phases that interact on a nanoscale and a microstructure that mimics the extracellular matrix can potentially provide attractive scaffolds for bone regeneration. In the present work, hybrid scaffolds of gelatin and bioactive glass (BG) with a fibrous microstructure were prepared by a combined sol–gel and electrospinning technique and evaluated *in vitro*. Structural and chemical analyses showed that the fibers consisted of gelatin and BG was covalently linked by GPTMS to form a homogeneous phase. Immersion of the gelatin–BG hybrid scaffolds in a simulated body fluid (SBF) at 37 °C resulted in the formation of a hydroxyapatite (HA)-like material on the surface of the fibers within 12 h, showing the bioactivity of the scaffolds. After 5 days in SBF, the surface of the hybrid scaffolds was completely covered with an HA-like layer. The gelatin–BG hybrid scaffolds had a tensile strength of 4.3 ± 1.2 MPa and an elongation to failure of 168 ± 14%, compared to values of 0.5 ± 0.2 MPa and 63 ± 2% for gelatin scaffolds with a similar microstructure. The hybrid scaffolds supported the proliferation of osteoblastic MC3T3-E1 cells, alkaline phosphatase activity, and mineralization during *in vitro* culture, showing their biocompatibility. The results indicate that these gelatin–BG hybrid scaffolds prepared by a combination of sol-gel processing and electrospinning have potential for application in bone regeneration.

5.2 Introduction

Scaffold-based tissue engineering can provide an alternative approach to the use of autogeneic and allogeneic sources to meet the increasing need for implants to repair and regenerate bone. In general, the scaffold should be biocompatible and bioactive, have mechanical properties comparable to the bone to be replaced, and have a porous architecture to support bone ingrowth and integration [1]. A porous architecture that mimics the extracellular matrix (ECM) is desirable; in addition, the scaffolds should have the ability to serve as a temporary support structure to allow cells to synthesize new tissue and to degrade upon neogenesis of tissue [2–4]. The bone ECM consists of an organic–inorganic nanocomposite, in which type I collagen fibrils and nanocrystalline hydroxyapatite (HA)-like particles are intimately combined [5]. Biomaterials in the form of nanoparticles, nanofibers, and nanocomposites have been receiving increasing attention for bone repair applications in an attempt to mimic the physical structure of the inorganic HA-like phase of bone [6-8]. In addition, biomaterials have been developed to mimic the collagen fibrils using processing techniques such as electrospinning, phase separation, and self-assembly [9]. The use of electrospinning has been receiving considerable interest as a scaffold fabrication technique because of its ability to create scaffolds with a fibrous architecture that mimics the ECM [10, 11]. In addition, electrospinning can be used to process a wide range of materials, does not rely on expensive equipment, and has low operating costs.

In the present work, hybrid scaffolds composed of gelatin and a silicate bioactive glass (BG) were prepared by a combined sol–gel and electrospinning technique. This technique has clear differences from those described in previous studies. First, the present method relies on the use

of a homogeneous solution composed of the polymer (gelatin) and the BG precursor solution, instead of using of discrete phases of the polymer phase and the inorganic phase (typically in the form of particles) [12]. Second, the electrospinning technique is used in this work to create scaffolds with a fine-scale fibrous architecture that mimics the ECM, compared to the coarser architecture produced by the methods used in previous studies [13].

Gelatin was selected as the organic phase in the present work because it is a denatured form of collagen, with a composition almost identical to that of collagen. Because gelatin is a denatured form of collagen, its use as a scaffold material can avoid the concerns of immunogenicity and pathogen transmission associated with collagen [14]. Electrospun fibrous mats of gelatin have received much attention recently for potential applications in bone regeneration [15, 16]. However, most of the reported methods included the use of pungent fluorine-containing reagents. In addition, a cross-linking agent was needed to stabilize the as-prepared structure and to improve the stability of the electrospun gelatin fibers in aqueous media. While several physical and chemical methods have been used to crosslink gelatin [17–19], many suffer from drawbacks such as low efficiency and toxicity.

Previous studies have shown the ability to functionalize gelatin using 3-glycidoxyproyl–trimethoxysilane (GPTMS), and the use of GPTMS as a coupling agent to covalently link gelatin to silica to form a biocompatible hybrid material [20–22]. However, the hybrid materials in those studies did not have a nanofibrous ECM-like architecture or the silica inorganic phase had limited ability to enhance the bioactivity of the hybrid material. Recently, to improve the bioactivity, the Ca^{2+}-containing gelatin-siloxane fibrous mats were fabricated by

sol-gel and electrospinning procedure [23]. However, the effects of immersion time in SBF on the morphology of fibrous mats were not shown. Meanwhile, all Si content in the gelatin-siloxane hybrid was provided by GPTMS. It is difficult to control the Si content and the degree of covalent coupling [20, 24]. In our study, the changes in the morphology and structure of fibrous mats in *in vitro* bioactivity test were investigated in detail and ternary silicate BG was chose as inorganic phase.

A BG was selected as the inorganic phase in this work because of its attractive bioactive characteristics, such as its conversion to HA, ability to bond to bone and soft tissues, and the ability to support osteogenesis [25–27]. Fibrous composites composed of biodegradable polymers and inorganic particles have been studied recently for applications in bone regeneration [28]. However, most of the composites were prepared by electrospinning mixtures composed of discreet inorganic particles dispersed in a polymer solution [28, 29]. Consequently, the fabricated composites suffered from limited interaction between the organic and inorganic phases which resulted in weak mechanical performance.

The objective of this study was to prepare gelatin–BG hybrid scaffolds by a combined sol–gel and electrospinning technique, and to evaluate the bioactivity, biocompatibility, and mineralization of the scaffolds *in vitro*. A homogeneous solution composed of gelatin, the BG precursor, and GPTMS as a coupling agent, was used in the electrospinning process to enhance the mixing of the gelatin and BG phases and to covalently link the gelatin and BG at the nanoscale level. We hypothesized that the incorporation of the BG into the gelatin to form a hybrid material would improve the bioactivity and mechanical response of the gelatin, as well as

its ability to support the proliferation of osteogenic cells and mineralization *in vitro*. The mechanical response of the hybrid scaffolds was determined in tension, while structural and chemical techniques were used to evaluate the bioactivity of the scaffolds in SBF. The biocompatibility of the scaffolds was evaluated from their ability to support the proliferation of osteogenic MC3T3-E1 cells, alkaline phosphatase activity, and mineralization.

5.3 Materials and methods

5.3.1 Preparation and electrospinning of solutions

The BG composition used in this work, $70SiO_2$–$25CaO$–$5P_2O_5$ (mol %), was the same as that used in a previous study [30]. A precursor solution of the BG composition was prepared by sequentially adding 5 ml tetraethyl orthosilicate (TEOS), 0.545 ml triethylphosphate (TEP), and 1.89 g calcium nitrate tetrahydrate, $Ca(NO_3)_2 \cdot 4H_2O$ (purity = 99%) at 1 h intervals into 32 ml of distilled water containing 16 wt% acetic acid as a catalyst. (All chemicals were purchased from Wako Pure Chem. Ind. Ltd., Japan, and they were used as received unless otherwise stated). The solution was stirred for 24 h at room temperature, aged for 12 h at 40 °C, then for 12 h at 60 °C, and stored at room temperature for use as described below.

Gelatin (Porcine skin, Type A; Sigma–Aldrich Chemical Co; Japan) was dissolved in a solvent composed of 60 vol% acetic acid (≥99.7%; Sigma–Aldrich Chemical Co; Japan) and 40 vol% distilled water, to give a gelatin concentration of 35 wt% (pH=2.7). The solution was stirred at 50 °C for 3 h, after which the BG precursor solution was added. The effective ratio of BG to gelatin in the solution was 30 wt%. After stirring for another 2 h, the required amount of GPTMS

(50 wt% based on the weight of gelatin) was added to the gelatin–BG precursor solution, and the system (pH=3.1) was stirred for 4 h at room temperature before electrospinning.

The main components of the electrospinning apparatus (Kato Tech; Japan) used in this study were a syringe with a flat-end metal needle (1.20 mm internal diameter × 38 mm), a syringe pump for controlling the feeding rate of the solution, a grounded cylindrical stainless steel mandrel, and a high voltage DC power supply. The solution was electrospun under an applied DC voltage of 12 kV, using a distance of 14 cm between the needle and the collector, and a feeding rate of 1.5 ml/h. The as-prepared gelatin–BG constructs in the shape of thin sheets were heated for 6 h at 110°C with a heating rate of about 1°C/min prior to evaluation. For comparison, electrospun fibers were also prepared from gelatin solutions with or without the coupling agent GPTMS.

5.3.2 Structural and chemical characterization of gelatin–BG fibrous scaffolds

The morphology of the electrospun gelatin–BG scaffolds was examined using field-emission scanning electron microscopy, SEM (Hitachi; S-5000) at an accelerating voltage of 20 kV and a working distance of 14 mm. Conventional transmission electron microscopy, TEM (JEOL JEM-2010,120kV) was used to examine the microstructure of the gelatin–BG fibers. Compositional analysis of the scaffolds was performed using energy-dispersive X-ray (EDS) spectroscopy in the SEM (Hitachi; S-5000) and Fourier transform infrared (FTIR) spectroscopy (IRPrestige-21, Shimadzu, Japan). FTIR was performed in the wavenumber range 500–4000 cm^{-1}; each FTIR spectrum was obtained from 40 scans at a resolution of 2 cm^{-1}. Measurements

were performed in transmission mode using pellets which pressed from mixture of 3 mg sample and 197 mg spectroscopic-grade KBr. Wide-angle X-ray diffraction, XRD (Rotorflex RU200B, Rigaku, Japan) was used to determine any crystalline phases present in the gelatin–BG scaffolds; the XRD analysis was performed using Ni-filtered CuK_α radiation (λ=1.5402 Å) in a step-scan mode (2° per minute) in the 2θ range 10–60°.

5.3.3 Mechanical testing

Mechanical testing of electrospun gelatin and gelatin–BG scaffolds was performed in a tensile testing machine (RTC-1250A, A&D Co., Ltd., Japan) at a constant deformation rate of 2 mm/min. The specimens were 60 mm long, 5 mm wide, and ~10 μm thick, with a gauge length of 40 mm. Prior to testing, the thickness and width of the specimens were measured at three locations along the sample length using a micrometer, and the average values were taken. Ten samples per group were tested.

5.3.4 *In vitro* evaluation of bioactivity in a simulated body fluid (SBF)

The *in vitro* bioactivity of the electrospun gelatin–BG scaffolds was evaluated from their reaction in SBF. The SBF with a pH of 7.4 was prepared by dissolving reagent-grade NaCl, KCl, $NaHCO_3$, $MgCl_2 \cdot 6H_2O$, $CaCl_2$, and KH_2PO_4 in distilled water at 37 °C and buffering with TRIS (trishydroxymethyl aminomethane) and 1N HCl solution according to a method described elsewhere [31]. Constructs with the shape of thin discs (22 mm in diameter × ~10 μm thick) were placed individually in a static 12-well plate containing 3 ml of SBF per well, and the system was kept at 37 °C in 5% CO_2 atmosphere for up to 5 days, with the SBF replaced every 48 hours. The

samples were removed from the SBF after 12 h, 1 day, 3 days and 5 days, rinsed 3 times with distilled water and freeze-dried. The morphology, structure, composition, and Ca/P atomic ratio of the samples were investigated using SEM, EDS, and XRD using the procedures described previously.

5.3.5 Cell culture

The established line of mouse pre-osteoblastic MC3T3-E1 cells, obtained from the RIKEN Cell Bank (Tsukuba, Japan), were cultured until passage 7 and used in this study. The cells were cultured in alpha-modified minimum essential medium (α-MEM; GIBCO), supplemented with 10% heat-inactivated fetal bovine serum (FBS, GIBCO), 100 U/ml penicillin and 100 U/ml streptomycin. The cultures were incubated at 37 °C in a humidified atmosphere containing 5% CO_2, with the medium changed every 48 hours.

Discs (15 mm in diameter × ~10 μm thick) were cut from the gelatin–BG and gelatin scaffolds and placed in a 24-well tissue culture polystyrene (TCP) plate (high-grade polystyrene Nunc™ Dishes, Thermo Fisher Scientific, Denmark). The samples were sterilized in 70% ethanol for 1 h, and then washed 3 times with sterile phosphate-buffered saline (PBS) for 30 min each to remove residual ethanol. The scaffolds were then immersed in α-MEM overnight under conventional culture conditions. After the culture medium was removed as completely as possible, each scaffold was seeded with cells by adding a MC3T3-E1 cell suspension drop-wise onto the scaffolds (1×10^4 cells in 100 μL of medium per well). The cell suspension was fully absorbed, thereby allowing the cells to be distributed within the scaffolds. The cell-seeded scaffolds were

incubated for 3 h to allow the cells to adhere to the scaffolds, and additional culture medium was added (1 ml/well). The control group consisted of the same number of cells seeded on TCP substrates.

5.3.5.1 Morphological observation of cultured cells

After incubation for 1, 3, 7 and 14 days, each scaffold was removed, rinsed 3 times with PBS, and the cells were fixed with 2.5% glutaraldehyde solution (500 μl/well). After an overnight soak at 4 °C, the scaffolds were washed 3 times with PBS and dehydrated through a graded series of ethanol (50–99%) for 2 min at each concentration. After the final washing with 99% ethanol, the scaffolds were treated 3 times for 10 min each with t-butyl alcohol. Finally, the samples were sputter-coated with gold and observed in an SEM (Hitachi; S-5000) using the conditions described previously.

5.3.5.2 Alkaline phosphatase (ALP) activity

ALP activity of the cell-seeded scaffolds was measured using an alkaline phosphate substrate kit (Wako, Japan). Scaffolds and TCP controls were seeded with MC3T3-E1 cells as described previously, and incubated in α-MEM supplemented with 0.1% β-glycerol phosphate to induce osteoblast differentiation. The ALP activity was measured after incubation times of 3, 5, 7, 14, and 21 days. After each incubation, 500 μl of β-nitrophenyl phosphate solution containing 1 mM $MgCl_2$ (Sigma-Aldrich Chemical Co., Japan) was added and the mixture were incubated for a further 10 min at 37 °C. The enzymatic reaction was stopped by adding 500 μl of 0.2 N NaOH,

and the absorbance was measured at 405 nm using a microplate reader (Biotrack II; GE Healthcare, Japan).

5.3.5.3 Alizarin red S staining for mineralization

Alizarin red S (ARS) is a dye that selectively binds to calcium salts and it widely used for calcium mineral histochemistry [32]. In this study, staining with ARS (Sigma-Aldrich Chemical Co., Japan) was used to determine the presence of calcium in the as-prepared gelatin–BG hybrids. An ARS staining solution, prepared by mixing 2 g of ARS with 100 ml of water and using dilute ammonium hydroxide to adjust the pH value to 4.0, was added to the as-prepared gelatin–BG scaffolds. A control group, composed of gelatin–BG scaffolds previously washed 3 times in PBS for 20 min each, was also subjected to the same ARS staining process. After incubation for 10 min at room temperature, the excess dye was removed by washing with deionized water. The gelatin–BG scaffolds were subsequently washed 10 times with deionized water, and examined using an optical microscope (FluoView FV1000, Olympus, Japan); images were taken using a confocal laser scanner (HP Photosmart 3210a All-in-One).

Staining with ARS was also used to detect the matrix mineralization *in vitro*. After incubation for 14 days, the cell-seeded scaffolds were washed 3 times with PBS, fixed with 10% formaldehyde for 1 h, and then rinsed 5 times for 5 min each with deionized water. After adding the ARS stain, each well was incubated for 10 min at room temperature, and examined using the same procedure described above.

5.3.6 Statistical analysis

All biological experiments (3 samples in each group) were run in triplicate. The data are presented as the mean ± standard deviation (SD). Statistical analysis was performed using one-way analysis of variance (ANOVA) with the level of significance set at $p < 0.05$.

5.4 Results

5.4.1 Structural and chemical characteristics of electrospun gelatin–BG scaffolds

SEM showed that the as-prepared gelatin–BG scaffolds covalently linked by GPTMS were composed of randomly distributed fibers with a uniform diameter, which were free from bead-like defects (Fig.5-1a). After immersion for 12 h in PBS, the fiber diameter appeared to increase slightly (Fig. 5-1b), presumably as a result of swelling, but the scaffold maintained the porous fibrous architecture. TEM of the gelatin–BG fibers (Fig.5-1c) showed a smooth surface and a homogeneous single phase material. Higher resolution TEM (Fig. 5-1d) did not show a particulate phase or a crystalline phase, a finding that was confirmed by selected area diffraction (SAD) (Fig. 5-1d, inset). Therefore, within the limits of resolution of the TEM, the fibers consisted of an amorphous single-phase material. The average fiber diameter of the electrospun gelatin–BG scaffolds, determined from more than 100 randomly selected fibers using the Image J software was 192 ± 8 nm.

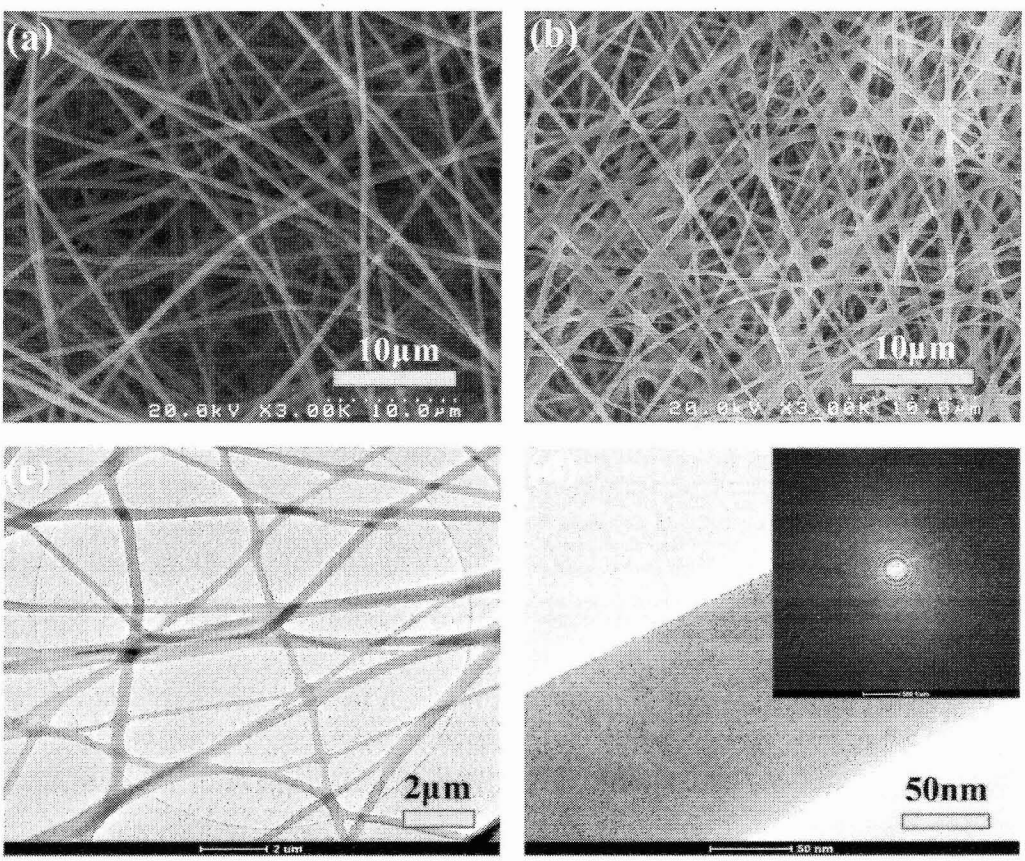

Figure 5-1. SEM images of electrospun gelatin–BG hybrid scaffolds: (a) as-fabricated, and (b) after immersion in PBS for 12 h; TEM images of as-fabricated gelatin–BG fibers: (c) lower magnification; (d) higher magnification. No particulate phase was observed in the TEM images, while the absence of diffraction rings in the selected area diffraction (SAD) image (d; inset) indicated the absence of a crystalline phase.

Figure 5-2a shows FTIR spectra of the as-prepared gelatin–BG hybrids and gelation fibers that contained the coupling agent GPTMS. For comparison, the FTIR spectra of the pure gelatin fibers without GPTMS and the BG gel are also shown for reference. The main characteristic resonances of pure gelatin and BG gel also appeared in spectra of gelatin−BG hybrids: at 1560 cm^{-1} attributed to the N–H bending vibration in the amide II, at 1670 cm^{-1} attributed to the C=O stretching vibration in the amide I, at 2952 cm^{-1} attributed to the C–H bending vibration for the

amide B, and at 3310 cm^{-1} attributed to N–H vibration for amide A [22]. In addition, the characteristic resonances of BG include those at 792 cm^{-1} attributed to the Si–O–Si symmetric stretching, at 1000–1110 cm^{-1} attributed to the Si–O–Si asymmetric stretching, and at 958 cm^{-1} attributed to the Si–OH asymmetric stretching [33].

Compared with the spectra of the BG gel, the resonance at 958 cm^{-1} became weak in the gelatin–BG hybrid due to the reduction in the number of Si–OH groups, indicating the enhanced formation of the silica network [33]. Moreover, the resonance at 1030 and 1103 cm^{-1} in the gelatin–BG hybrid attribute to the Si–O–Si asymmetric stretching (Fig. 5-2a) confirmed the formation of the silica network. The same phenomenon observed in the gelatin–GPTMS system indicated that the silane end of GPTMS has taken part in the formation of this silica network [34-36]. Additional resonance in the spectrum of the gelatin–BG fibers corresponded to Si-C stretching was found at 1235 cm^{-1}[35]. Combined with weak resonances appeared at 2942 and 2862 cm^{-1}, attributed to CH_2 stretching vibrations, presumably resulted from methyl groups of GPTMS, indicating the presence of GPTMS in the gelatin-BG hybrid [23, 35].

As described previously, alizarin red S (ARS) staining was used to characterize the presence of calcium element in the gelatin–BG hybrids. Figure 5-2b shows images of ARS-stained gelatin–BG hybrids as-prepared and after washing with PBS, and gelatin scaffolds (without BG). The large difference in red color between the as-prepared gelatin–BG hybrids and the gelatin (without BG) indicated the presence of calcium in the as-prepared hybrid material [22, 32]. After washing the as-prepared gelatin–BG hybrid with PBS (3 times for 20 minutes each), the red stain had a lower intensity but it was still clearly present (Fig. 5-2b), indicating the presence of

calcium in the gelatin–BG hybrid scaffold even after the prolonged washing process.

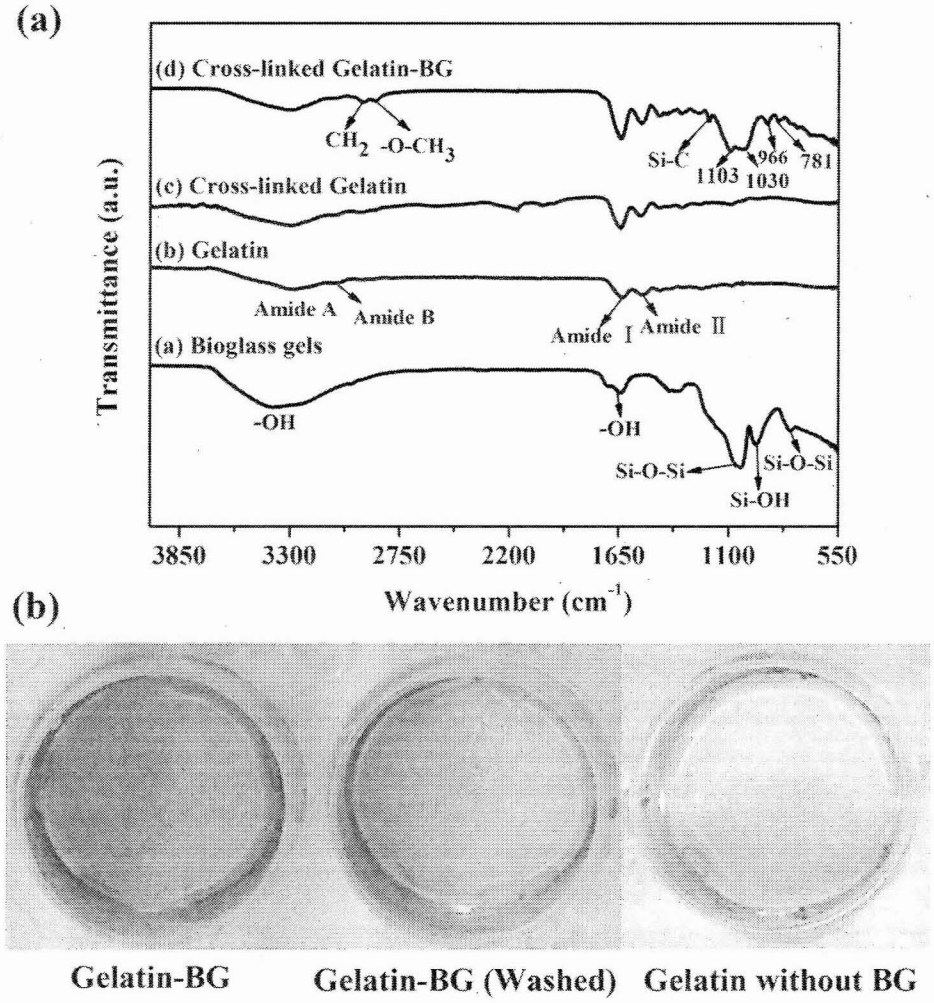

Figure 5-2. FTIR spectra of BG gels, gelatin fibers, cross-linked gelatin fibers and cross-linked gelatin-BG hybrid scaffolds prepared by electrospinning (a) and images of Alizarin Res S staining of fabricated gelatin-BG hybrids, washed gelatin-BG hybrids and the gelatin scaffolds.

5.4.2 Mechanical properties

Figure 5-3 shows the mechanical response in tension of the gelatin and gelatin–BG hybrid scaffolds prepared by the electrospinning process. For both materials, the stress initially increased more rapidly and almost linearly with the elongation, but the stress at any elongation

was far higher for the hybrid scaffolds. Subsequently, for the gelatin scaffold, the stress showed little increase with elongation until failure; in the case of the gelatin–BG hybrid, the stress continued to increase with elongation until failure. The tensile strength of the gelatin scaffolds was 0.5 ± 0.2 MPa and the elongation to failure was 63 ± 2 %. In comparison, the gelatin–BG scaffolds had a tensile strength of 4.3 ± 1.2 MPa and an elongation to failure of 168 ± 14 %.

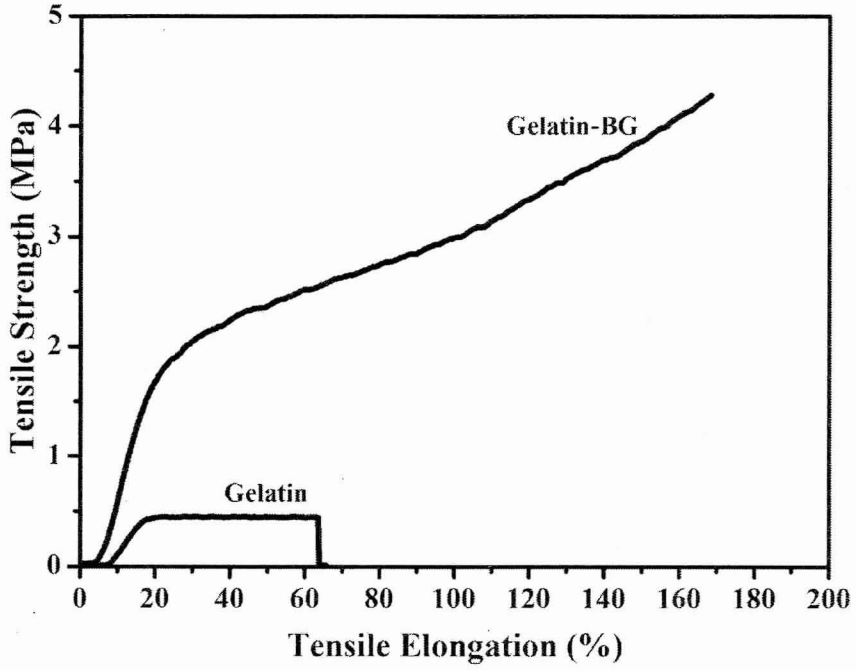

Figure 5-3. Mechanical response in tension for electrospun scaffolds of (a) gelatin, and (b) gelatin–BG hybrid.

5.4.3 *In vitro* bioactivity

The surface of the electrospun gelatin–BG hybrid scaffolds showed considerable morphological changes after immersion in SBF (Fig.5-4). Many fine, needle-like particles were

formed homogeneously on the surface of the fibers within 12 h (Fig. 5-4a), and they appeared to be well attached to the surface (Fig. 5-4a; inset). The size and number of these needle-like particles increased with immersion time. After 1 day, the surface of the fibers was almost completely covered with fine particles, but the porous and fibrous architecture of the scaffold was still evident (Fig. 5-4b). The particles increased in size and showed a more rounded morphology after 3 days. After immersion for 5 days, the surface of the scaffold was almost completely covered with a layer of reaction product, and the porous fibrous architecture of the scaffold was no longer visible (Fig. 5-4d); the surface of the reaction product consisted of fine, needle-like particles (Fig. 5-4d; inset).

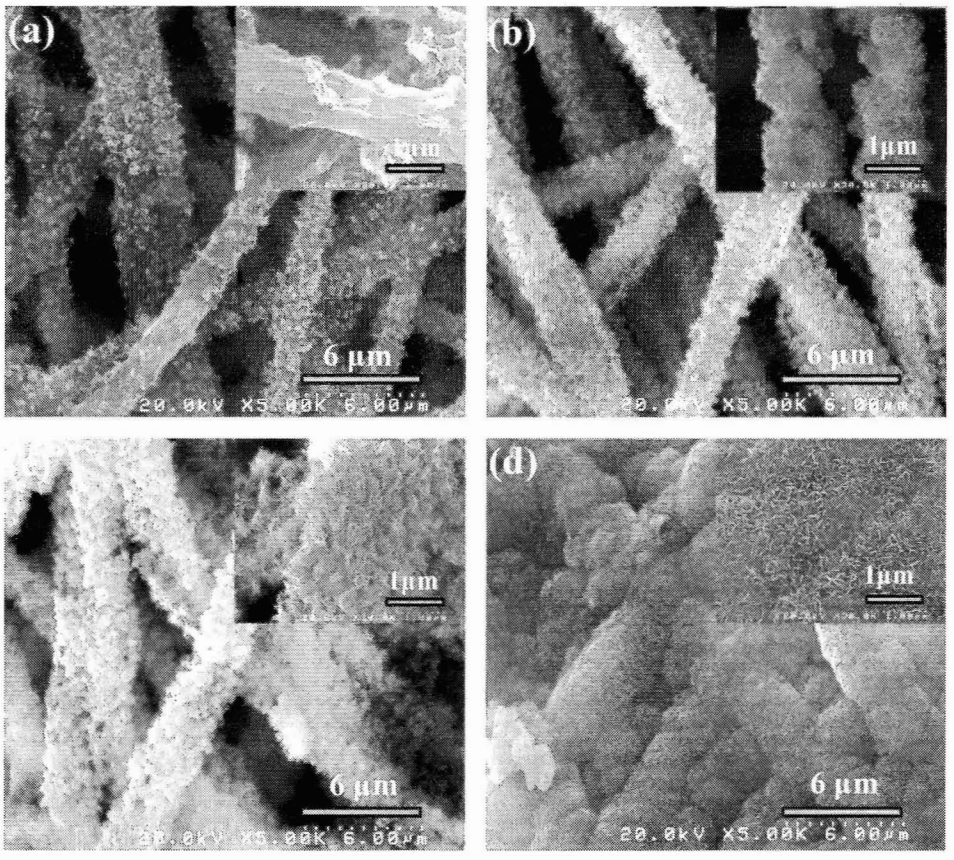

Figure 5-4. SEM images of electrospun gelatin–BG hybrid scaffolds after immersion in SBF for

(a) 12 h; (b) 1 day; (c) 3 days; (d) 5 days. The inset shows a higher magnification image of the reaction product for each immersion time.

EDS analysis showed that when compared to the as-prepared gelatin–BG scaffolds (Fig. 5-5a), immersion in SBF for 12 h resulted in an increase in the intensity (height) of both the Ca and the P peaks, and a decrease in the Si peak intensity (Fig. 5-5b). The intensities of the Ca and P peaks continued to increase with longer immersion time (Fig. 5-5c – 5e); in addition, a small Si peak was still present.

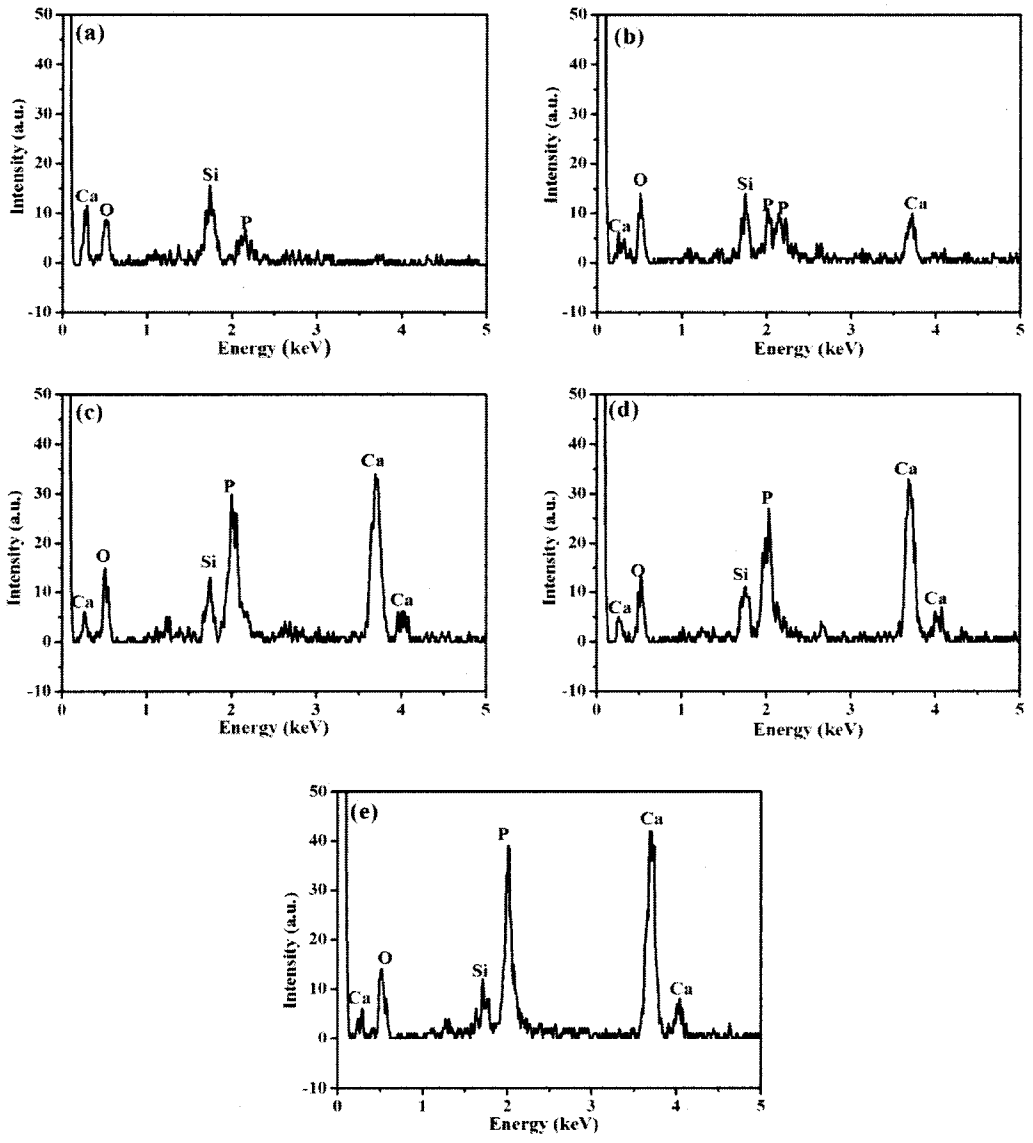

Figure 5-5. EDS spectra of electrospun gelatin–BG hybrid scaffolds as-prepared (a), and after immersion in SBF for 12 h (b); 1 day (c); 3 days (d); 5 days (e).

XRD analysis of the as-prepared gelatin–BG hybrid scaffold did not show any measureable diffraction peaks (Fig. 5-6), indicating an amorphous material. This finding is in agreement with the TEM observation described previously (Fig, 5-1d). However, after immersion of the scaffold

for 12 h in SBF, small peaks were detected at 26° and 32°, which corresponded to the dominant (002) and (211) reflection planes in a reference HA (JCPDS 72-1243). The intensity of these two peaks increased with immersion time (up to 5 days used in this study). Taken together, the EDS and XRD analyses indicated the formation of an HA-like reaction product on the surface of the gelatin–BG scaffold within 12 h of immersion in SBF which increased with immersion time.

SEM images show the morphology and density of MC3T3-E1 cells cultured for 3, 7 and 14 days on the gelatin–BG hybrids (Fig. 5-7a) and on the gelatin scaffolds (control) (Fig. 5-7b). For both scaffolds, the cells showed an increase in density with increasing incubation time. However, differences in morphology were also apparent between the cells cultured on the gelatin-BG scaffold and the gelatin scaffold. After incubation for 3 day, the cells appeared to be well attached to the surface of the both scaffolds, and they presented a typical characteristic of polygonal morphology. After 7 days, some particles could be found on the surface of the gelatin-BG scaffolds, whereas the surface of the cells cultured in the gelatin scaffolds were smooth. After 14 days of culture, the surface of gelatin-BG scaffold was covered with multi-cellular layers, associated with some small spherical structures and nodules on the surface of the cellular layer.

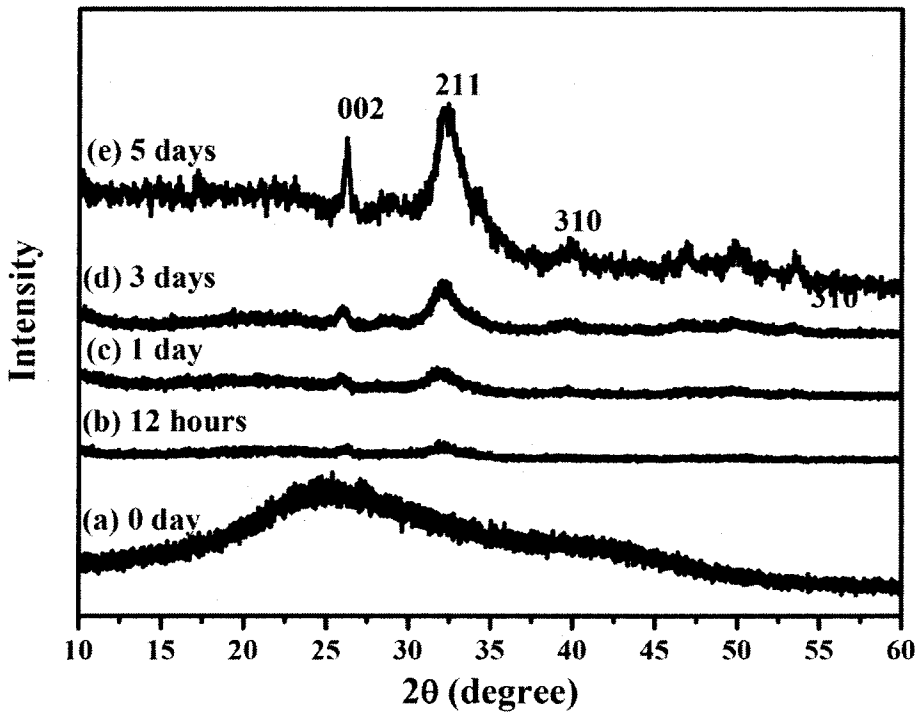

Figure 5-6. XRD patterns of electrospun gelatin–BG hybrid scaffolds as-prepared and after immersion in SBF for the times shown.

SEM at higher magnification (Fig. 5-7c) showed the morphology of the deposited nodules on the cellular surface of the gelatin-BG scaffolds after 14 days, while EDS analysis (Fig. 5-7d) showed that the nodules were composed of a calcium phosphate material with Ca/P atomic ratio of 1.39. In addition, ARS staining was used to evaluate the ability of the cell-seeded gelatin–BG scaffolds to support mineralization after an incubation time of 14 days (Fig. 5-7a, b; inset). Both scaffolds showed a bright red staining, indicating the presence of calcium. However, the greater intensity of the red stain indicated a greater ability of the gelatin-BG hybrids to support mineralization and formation of nodules.

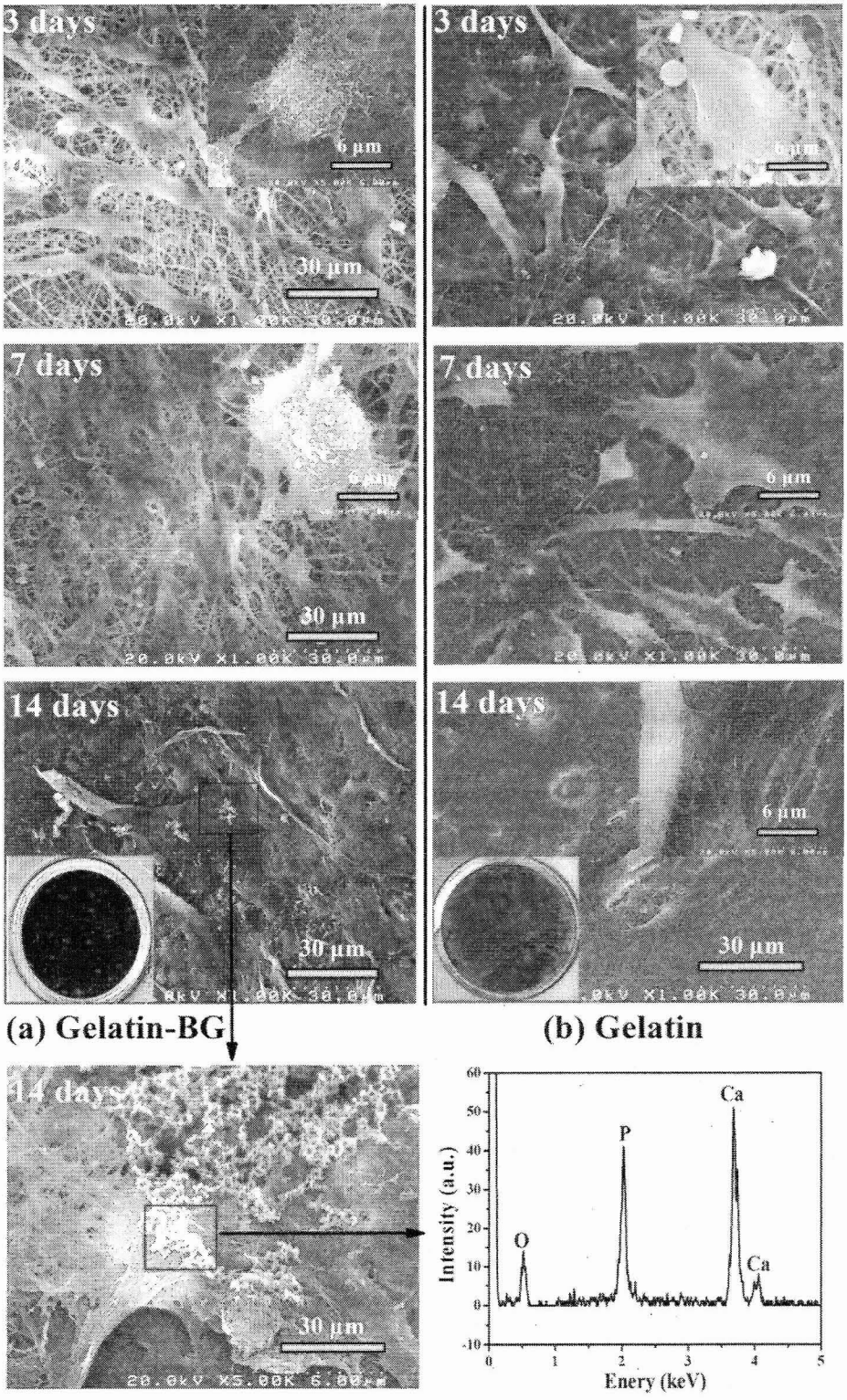

Figure 5-7. (a) SEM images of MC3TC-E1 cell morphology of gelatin-BG and gelatin scaffolds,

alizarin red S stained images of MC3T3-E1 cells incubated on electrospun gelatin–BG and gelatin scaffolds for14days (inset images) and the EDX for the formation of nodules.

5.4.4 Alkaline phosphatase (ALP) activity

Results of spectrophotometric measurement of ALP activity of MC3T3-E1 cells cultured on the gelatin–BG scaffolds, gelatin scaffolds and TCP controls for 3, 5, 7, 14, and 21 days are presented in Fig. 5-8. As shown, the ALP activity increased with time, indicating that the MC3T3-E1 cells were able to carry out an osteogenic function on the gelatin-BG and gelatin scaffolds. However, the ALP of the cells cultured on the gelatin-BG scaffolds was higher than that for cells cultured on the gelatin scaffolds and TCP at days 7, 14 and 21 days. This higher ALP activity showed that the gelatin–BG scaffolds had a greater capacity to support mineralization after incubation times of 7 days or longer when compared to the gelatin scaffolds and TCP control substrates.

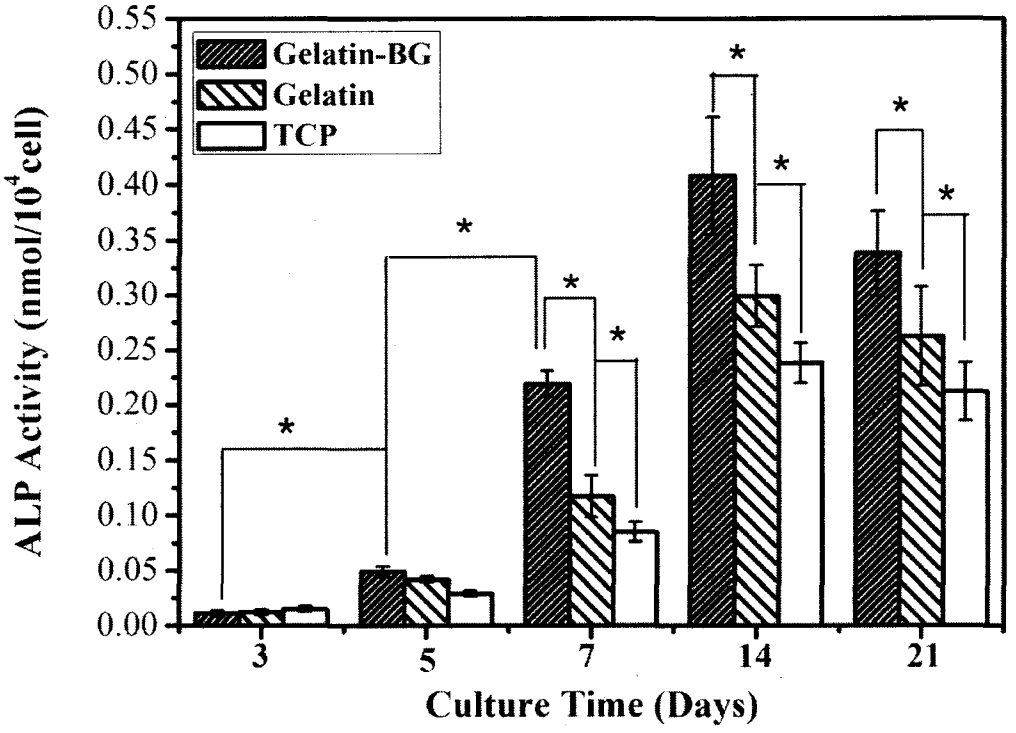

Figure 5-8. ALP activity of electrospun gelatin–BG, gelatin scaffolds and TCP control substrates seeded with MC3T3-E1 cells and incubated for 3, 5, 7, 14 and 21 days. Mean ± SD; *significant difference between pairs ($p<0.05$).

5.5 Discussion

The results show that gelatin–BG hybrid scaffolds prepared in this work by a combined sol–gel and electrospinning technique have desirable characteristics for potential application in bone repair. The scaffolds have a fibrous architecture that mimics the ECM, are bioactive, and support the proliferation of osteoblastic MC3T3-E1 cells, alkaline phosphatase activity, and mineralization *in vitro*.

SEM and TEM showed that the gelatin–BG scaffolds had a porous architecture consisting of

fibers with a nearly uniform diameter of ~200 nm (Fig. 5-1). Furthermore, the fibers in the as-prepared scaffolds were amorphous, as determined by XRD and selected area diffraction in the TEM, and they consisted of a homogeneous phase within the limits of resolution of the TEM (Figs. 5-1, 5-6). These results indicate that the fibers consist of a hybrid network in which gelatin polymers and presumably siloxane (Si–O–Si) chains present in the sol–gel derived BG precursor solution are covalently linked by GPTMS to form a homogenous phase.

It is well known that acid-catalyzed hydrolysis and condensation reactions in solution sol–gel processing of inorganic silicates lead to the formation of a siloxane (Si–O–Si) network. FTIR analysis confirmed the presence of amide bands of gelatin, (Si–O–Si) groups of BG in the as-prepared gelatin–BG scaffolds (Fig. 5-2). Meanwhile, the FTIR analysis also showed the presence of GPTMS in the spectrum of the gelatin–BG hybrid scaffolds. Presumably, the silane end of GPTMS has taken part in the formation of the silica network.

The incorporation of calcium and phosphate ions into the as-prepared gelatin–BG hybrid was shown using ARS staining and EDX analysis [22, 37]. The rapid mineralization in SBF also indicated the presence of calcium in the as-prepared gelatin–BG hybrid (Figs. 5-4, 5-5). However, the incorporation of calcium in the hybrid scaffolds is unclear. While some previous studies have indicated the incorporation of calcium in gelatin–siloxane hybrids [38], other studies have indicated that the incorporation of calcium in gelatin–silica hybrids was difficult [39]. Further work is being performed to more clearly determine the presence of calcium in the hybrid scaffolds prepared in this work.

A schematic diagram summarizing the main steps in the formation of the gelatin–BG hybrid

fibers is shown schematically in Fig. 5-9. Initially, hydrolysis and partial condensation of the BG precursor solution under acidic conditions presumably resulted in the formation of a siloxane network in which the Ca and P are incorporated into the network in the same proportions as the starting solution (Fig. 5-9a). After addition of the sol–gel derived BG solution to the gelatin solution and homogenization of the mixture by stirring, addition of GPTMS to the mixture resulted presumably in ring-opening reactions in the epoxy groups [40]. The protonated epoxy group is believed to attack nucleophilic groups such as $-NH_2$, and –COOH on the amino acid residues of the gelatin chains, resulting in the bonding of GPTMS molecules to the gelatin chains (Fig. 5-9b) [41]. Simultaneously, the methoxy silane groups ($Si\text{-}OCH_3$) of GPTMS are hydrolyzed to give silanol (Si-OH) groups. This mixture was used in the electrospinning step to prepare the fibrous scaffolds. Heating the electrospun constructs to 110°C resulted presumably in silica network by condensation between the hydroxyl groups of the GPTMS and the siloxane chains, to give a covalently bonded network of gelatin and siloxane chains (Fig. 5-9c).

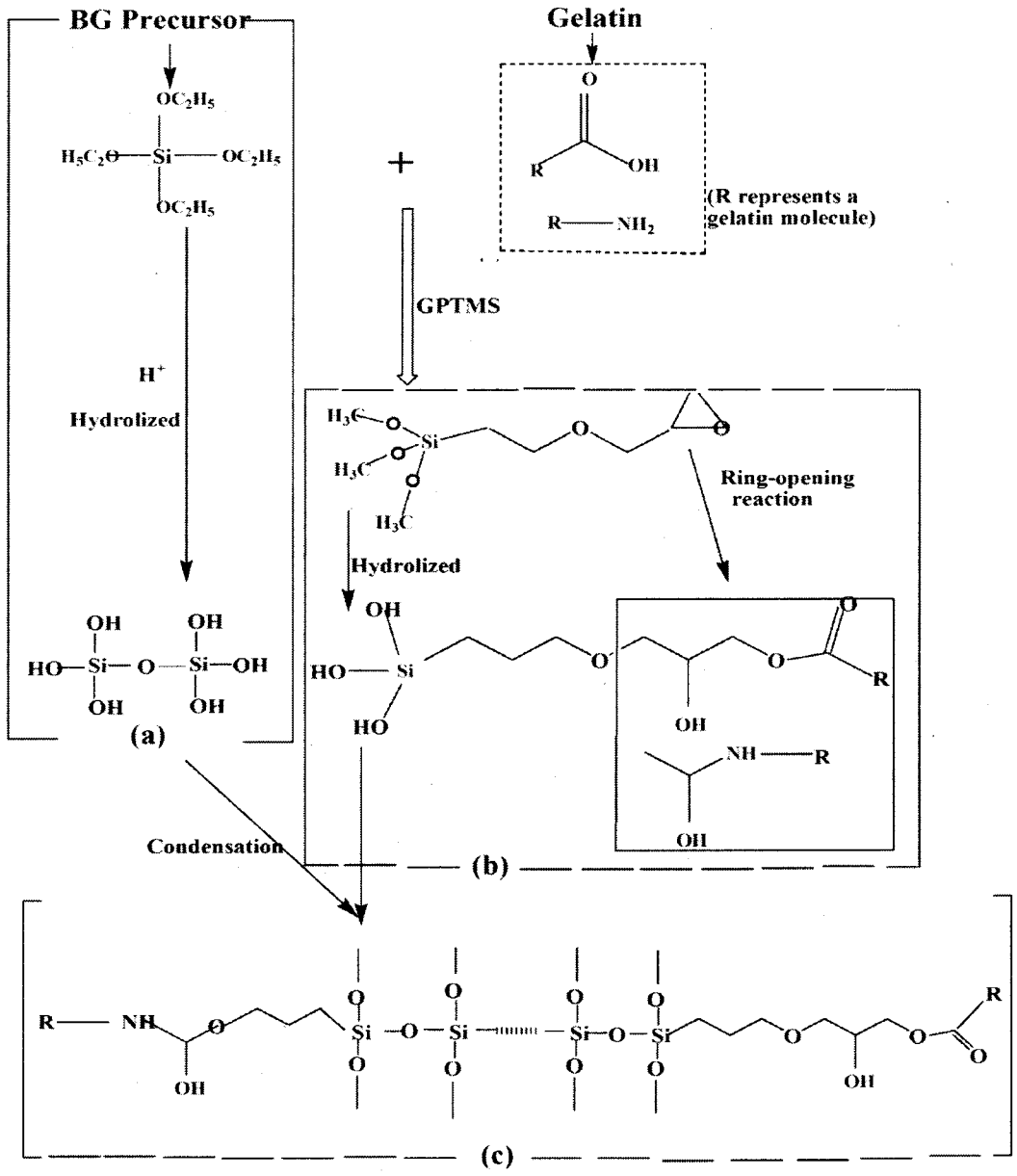

Figure 5-9. Schematic representation of the formation of electrospun gelatin–BG hybrids composed of gelatin molecules bonded to siloxane chains of sol–gel derived BG using a crosslinking agent (GPTMS).

An interesting feature of the results is the rapid formation of HA-like precipitates within 12 h of immersion in SBF; these precipitates formed an HA-like layer on the gelatin–BG scaffolds

after 5 days (Figs. 5-4 – 5-6). The formation of an HA-like layer on the surface of a scaffold is desirable for bone repair because it has been shown to be responsible for producing a firm bond between the scaffold and bone as well as soft tissues *in vivo* [26]. In comparison, the formation of an HA-like layer was observed after 21 days for gelatin-apatite composite [42] and after 7 days for gelatin–siloxane fibrous mats [23]. The rapid formation of an HA-like material on the gelatin–BG scaffolds prepared in this work presumably resulted from (1) rapid degradation of the scaffolds resulting from the fine diameter of the electrospun fibers, and (2) the uniform mixing of the gelatin and siloxane network. The rate of dissolution of a material depends inversely as the radius. Consequently, these electrospun gelatin–BG scaffolds should have a high dissolution rate, leading to rapid release of calcium ions and precipitation of an HA-like material. The uniform mixing of the gelatin and siloxane network can lead to numerous nucleation sites for the HA-like material to nucleate and grow. In an aqueous phosphate solution, such as an SBF, silicon ions can form silanol groups on the surface of the gelatin–BG fibers which are believed to act as nucleation sites for the formation of HA crystals [43].

In addition to enhancing the bioactivity, the incorporation of BG into the gelatin system also enhanced the mechanical response. Both the tensile strength and elongation to failure of the gelatin–BG hybrids were superior to those of the gelatin material with a similar architecture. Presumably, the homogeneously distributed inorganic siloxane network covalently bonded to the gelatin enabled the hybrid nanofibers to better resist extension in response to an applied load. In addition to the higher tensile strength, the ability to maintain a high ductility (elongation to failure) should be beneficial for the potential use of these gelatin–BG hybrids as a membrane or

scaffold for bone regeneration.

In vitro cell culture studies confirmed that the gelatin–BG hybrid scaffolds prepared in this work were biocompatible. The scaffolds supported the attachment and proliferation of osteogenic MC3T3-E1 cells (Fig. 5-7) and mineralization of the cell-seeded scaffolds (Fig. 5-7, inset). In addition, the cell-seeded scaffolds showed a greater capacity to support ALP activity when compared to control substrates (cell-seeded gelatin scaffold and TCP) (Fig. 5-8). Research is presently underway to evaluate the ability of these gelatin–BG scaffolds to support bone regeneration *in vivo*.

5.6 Summary

A process that combined sol–gel and electrospinning techniques was used to prepare gelatin–bioactive glass (BG) hybrid scaffolds with a fibrous architecture that mimicked the extracellular matrix (ECM). The scaffolds consisted of an amorphous homogenous phase consisting of gelatin covalently bonded to a siloxane network. Immersion of the scaffolds in a simulated body fluid (SBF) resulted in the formation of HA-like crystals on the surface of the fibers within 12 hours, showing the excellent bioactivity of the scaffolds. The external surface of the scaffolds was almost completely covered with an HA-like layer within 5 days. The gelatin–BG hybrid scaffolds supported the proliferation of osteoblastic MC3T3-E1 cells, alkaline phosphatase activity, and mineralization during *in vitro* culture, showing their biocompatibility. When compared to electrospun gelatin scaffolds with the same nanofibrous architecture, the gelatin–BG hybrid scaffolds showed approximately an order of magnitude increase in tensile strength (from 0.5 ± 0.2 MPa to 4.3 ± 1.2 MPa) and a large improvement in the elongation to

failure (from 63 ± 2 % to 168 ± 14 %). The results indicate that these gelatin–BG hybrids have potential for application as scaffolds in bone regeneration.

References

[1] Hutmacher DW. Scaffolds in tissue engineering bone and cartilage. Biomaterials. 2000;21: 2529-43.

[2] Alves NM, Leonor IB, Azevedo HS, Reis RL, Mano JF. Designing biomaterials based on biomineralization of bone. J Mater Chem. 2010; 20:2911-21.

[3] Tanase CE, Popa MI, Verestiuc L. Biomimetic bone scaffolds based on chitosan and calcium phosphates. Mater Lett. 2011; 65:1681–3.

[4] Mata A, Geng Y, Henrikson KJ, Aparicio C,.Stock SR,Satcher RL, Stupp S. Bone regeneration mediated by biomimetic mineralization of a nanofiber matrix. Biomaterials. 2010; 31:6004-12.

[5] Venugopal J, Low S, Choon AT,Kumar TSS, Ramakrishna S. Mineralization of osteoblasts with electrospun collagen/hydroxyapatite nanofibers. J Mater Sci: Mater Med. 2008; 19:2039–46.

[6] Tilocca A. Molecular dynamics simulations of a bioactive glass nanoparticle. J Mater Chem. 2011; 21: 12660–7.

[7] Holzwarth JM, Ma PX. Biomimetic nanofibrous scaffolds for bone tissue engineering. Biomaterials.2011; 32: 9622-9.

[8] Calandrelli L, Annunziata M, Ragione FD, Laurienzo P, Malinconico M, Oliva A. Development and performance analysis of PCL/silica nanocomposites for bone regeneration. J Mater Sci: Mater Med. 2010;21:2923–36.

[9] Wei GB, Ma PX. Nanostructures biomaterials for regeneration. Adv Func Mater. 2008; 18:3568-82.

[10] Teo WE, Ramakrishna S. Electrospun nanofibers as a platform for multifunctional, hierarchically organized nanocomposite. Compos Sci Technol. 2009;69:1804-17.

[11] Jang JH, Castano O, Kim HW. Electrospun materilas as potential platforms for bone tissue

engineering. Adv Drug Deliv Rev. 2009;61:1065-83.

[12] Mozafari M, Rabiee M, Azami M, Maleknia S. Biomimetic formation of apatite on the surface of porous gelatin/bioactive glass nanocomposite scaffolds. Appl Surf Sci. 2010; 257:1740–9.

[13] Liu XH, Smith LA, Hu J, Ma PX. Biomimetic nanofibrous gelatin/apatite composite scaffolds for bone tissue engineering. Biomaterials. 2009; 30:2252–8.

[14] Murphyt SBR. Structure and rheology of gelatin gels: recent progress. Polymer 1992;33(12): 2622-7.

[15] Choktaweesap N, Arayanarakul K, Aht-ong D, Meechaisue C, Supaphol P. Electrospun gelatin fibers: effect of solvent system on morphology and fiber diameters. Polym J. 2007; 39: 622–31.

[16] Chen HC, Jao WC, Yang MC. Characterization of gelatin nano-fibers electrospun using ethanol/formic acid/water as a solvent. Polym. Adv. Technol. 2009; 20: 98–103.

[17] Zhang YZ, Venugopal J, Huang ZM, Lim CT, Ramakrishna S. Crosslinking of the electrospun gelatin nano-fibers. Polym. 2006 ; 47: 2911–7.

[18] Ko JH, Yin HY, An J, Chung DJ. Characterization of cross-linked gelatin nanofibers through electrospinning. Macromol Res. 2010;18: 137-43.

[19] Panzavolta S, Gioffre M, Focarete ML, Gualandi C, Foroni L. Electrospun gelatin nanofibers : optimization of genipin cross-linking to preserve fiber morphology after exposure to water. Acta Biomater. 2011;7:1702-9.

[20] Mahony O, Tsigkou O, Ionescu C, Minelli C, Ling L. Silica-gelatin hybrids with tailorable degradation and mechanical properties for tissue regeneration. Adv Func Mater. 2010; 20:3835-45.

[21] Ren L, Tsuru K,Hayakawa S, Osaka A. *In Vitro* Evaluation of Osteoblast Response to Sol-Gel Derived Gelatin-Siloxane Hybrids. J Sol-Gel Sci Techn. 2003;26, 1137-40.

[22] Hench LL. Bioceramics. J Am Ceram Soc. 1998; 81:1705-28.

[23] Rahaman MN, Day DE, Bal BS, Fu Q, Jung SB, Bonewald LF. Bioactive glass in tissue

engineering. Acta Biomater. 2011;7: 2355-73.

[24] Fujihara K, Kotaki M, Ramakrishna S. Guided bone regeneration membrane made of polycaprolactone/calcium carbonate composite nano-fibers. Biomaterials. 2005; 26: 4139–47.

[25] Sheikh FA, Barakat NAM, Kanjwal MA, Park SJ, Park DK, Kim HY. Synthesis of poly(vinyl alcohol) (PVA) nanofibers incorporating hydroxyapatite nanoparticles as future implant materials. Macromol Res. 2010; 18: 59-66.

[26] Choi JY, Lee HH, Kim HW. Bioactive sol–gel glass added ionomer cement for the regeneration of tooth structure. J Mater Sci: Mater Med. 2008; 19:3287–94.

[27] Kokubo T, Takadama H. How useful is SBF in predicting *in vivo* bone bioactivity? Biomaterials. 2006; 27: 2907–15.

[28] Gregory CA, Gunn WG, Peister A, Prockop DJ. An Alizarin red-based assay of mineralization by adherent cells inculture: comparison with cetylpyridinium chloride extraction. Anal Biochem. 2004, 329: 77–84.

[29] Song JH, Yoon BH, Kim HE, Kim HW. Bioactive and degradable hybridized nanofibers of gelatin-siloxane for bone regeneration. J Biomed Mater Res. 2008; 84A:875-84.

[30] Duran A, Serna C, Fornes V, Navarro JMF. Structural considerations about SiO_2 glasses prepared by Sol-Gel. J Non-Cryst Solids. 1986; 82: 69-77.

[31] Tonda-Turo C, Gentile P, Saracino S, Chiono V, Nandagiri VK, Muzio G, Canuto RA, Ciardelli G. Comparative analysis of gelatin scaffolds crosslinked by genipin and silane coupling agent. Int J Biol Macromol. 2011;49:700-6.

[32] Chernev GE, Borisova BV, Kabaivanova LV, Salvado IM. Silica hybrid biomaterials containing gelatin synthesized by sol-gel method. Cent. Eur. J. Chem. 2010; 8: 870–6.

[33] Liu YL, Su YH, Lai JY. In stiu crosslinking of chitosan and formation of chitosan-silica hybrid membranes with using γ-glycidoxypropyltrimethoxysilane as a cross-linking agent. Polymer.2004;45:6831-7.

[34] Towprfe GK, Composto RJ, Shapiro IM, Ducheyne P. Nucleation and growth of calcium phosphate on amine-, carboxyl- and hydroxyl-silane self-assembled monolayers. Biomaterials.

2006; 27:631-42.

[35] Ren L, Tsuru K, Hayakawa S, Osaka A. Novel approach to fabricate porous gelatin-siloxane hybrids for bone tissue engineering. Biomaterials. 2002; 23:4765-73.

[36] Ren L, Tsuru K, Hayakawa S, Osaka A. Synthesis and characterization of gelatin-siloxane hybrids derived through sol-gel procedure. J Sol-Gel Sci Technol. 2001; 2:115-21.

[37] Schottner G .Hybrid Sol-gel-derived polymers: applications of multifunctional materials. Chem Mater. 2001; 13: 3422-35.

[38] Liu X, Smith LA, Hu J, Ma PX. Biomimetic nanofibrous gelatin/apatite composite scaffolds for bone tissue engineering. Biomaterials. 2009; 30:2252-8.

[39] Ren L, Wang J, Yang FY, Wang L, Wang D, Wang TX, Tian MM. Fabrication of gelatin-siloxane fibrous fibrous mats via sol-gel and electrospinning procedure and its application for bone tissue engineering. Mater Sci Eng. 2010, 30: 437-44.

[40] Cui W, Li X, Xie C, Zhuang H, Zhou S,Weng J. Hydroxyapatite nucleation and growth mechanism on electrospun fibers functionalized with different chemical groups and their combinations. Biomaterials. 2010; 31:4620-9.

CHAPTER 6 Conclusions and Recommendation for Future Research

6.1 Conclusions

In this study, one of the most important objectives is to design and develop an true organic/inorganic hybrid with highly tailorable properties which can achieved through careful control of their nanoscale interactions. Combining tough biodegradable polymer with brittle bioglass can produce composite with improved mechanical properties. Two different biodegradable polymers contain synthetic PVA and natural Gelatin have been introduced into the silicate-based bioglass system by the sol-gel process. To mimic the structure of the nature bone, electrospinning and robocasting techniques have been employed to fabricate the fibrous scaffolds.

Chapter 3 described a novel hierarchical nanofibrous bioglass mats has been fabricated by electrospinning and using polymer/Pluronic F127 as co-templates. Compared with other bioglasses, these mesoporous bioglass nanofibers exhibited a larger specific surface area and pore volume, which enhanced the deposition rate of a HAp layer in SBF. Although the unique nanoscale mesoporous structure can greatly improve the bioactivity, their brittleness is still a defect which limited their further applications in bone tissue engineering. An effective strategy is to introduce a polymer to improve their toughness.

Chapter 4 described a facile method for creating a fibrous composite scaffold that would combine the bioactivity of bioglass desirable structure and properties of a nanofibrous

biodegradable polymer. Our approach was to deposit a sol–gel derived BG coating on cross-linked electrospun PVA fibers. PVA was selected as a model polymer because it can be electrospun from aqueous solutions, in addition to its acceptable biomechanical properties, biocompatibility, and chemical stability. The results showed that a sol–gel method provided a facile process for coating electrospun PVA fibers (diameter = 286 ± 14 nm) with a layer of bioglass. The biogIss coating resulted in mineralization of the fiber surface within 3 days in a simulated body fluid (SBF). When compared to PVA scaffolds (no BG coating), the bioglass-coated PVA scaffolds showed a higher elastic modulus, no difference in tensile strength, and a reduction in elongation to failure. Immersion of the bioglass-coated PVA scaffolds in SBF for 5 days resulted in an increase in the elastic modulus and elongation to failure when compared to the as-fabricated PVA scaffolds. *In vitro*, the bioglass-coated PVA scaffolds showed a better capacity to support the proliferation of osteogenic MC3T3-E1 cells, alkaline phosphatase activity, and mineralization when compared to the uncoated PVA scaffolds. Although these bioglass-coated PVA fibrous scaffolds showed excellent bioactivity and good tensile mechanical, a drawback with this bioglass-coated PVA scaffolds is that the constituent phases have different dissolution rate which can often be unpredicate, leading to unhomogenous depredate.

Therefore, chapter 5 described a homogeneous solution, composed of gelatin, the BG precursor, and GPTMS as a coupling agent, was used in the electrospinning process to enhance the mixing of the gelatin and BG phases and to covalently link the gelatin and BG at the nanoscale level. A process that combined sol–gel and electrospinning techniques was used to prepare gelatin–bioglass hybrid scaffolds with a fibrous architecture that mimicked the

extracellular matrix (ECM). The scaffolds consisted of an amorphous homogenous phase consisting of gelatin covalently bonded to a siloxane network. Immersion of the scaffolds in a simulated body fluid (SBF) resulted in the formation of HA-like crystals on the surface of the fibers within 12 hours, showing the excellent bioactivity of the scaffolds. The external surface of the scaffolds was almost completely covered with an HA-like layer within 5 days. The gelatin–bioglass hybrid scaffolds supported the proliferation of osteoblastic MC3T3-E1 cells, alkaline phosphatase activity, and mineralization during *in vitro* culture, showing their biocompatibility. When compared to electrospun gelatin scaffolds with the same nanofibrous architecture, the gelatin–bioglass hybrid scaffolds showed approximately an order of magnitude increase in tensile strength (from 0.5 ± 0.2 MPa to 4.3 ± 1.2 MPa) and a large improvement in the elongation to failure (from 63 ± 2 % to 168 ± 14 %). These results suggest that the fabricated gelatin-BG composite scaffolds could be applied as biological scaffolds for sponge bone repair and regeneration.

6.2 Future work

1. Experimental results indicated the gelatin/bioglass hybrid scaffolds can act as an effective bone grafts, but there still need to do some experiments to make sure the reactive mechanisms between the gelatin and bioglass.
2. These bioglass-based composites fabricated in this research only focus on combination the features of organic and inorganic biomaterials, leading these scaffolds possess bioactivity, degradability, and biocompatibility. Growth factor is important for regulating a variety of cellular processes. It can stimulate the cellular growth, proliferation, and differentiation.

Therefore, the fabrication process should be low temperature, non-toxic solvents to provide the possibility to incorporate growth factor.

3. Overall, the findings presented in this work provided a great deal of insight on development of organic/inorganic hybrids for use in bone tissue regeneration. Although great strides have been made, this work should lead to more in-depth biological studies to ensure that these scaffolds function as expected *in vivo*.

List of Publications

1. **C.X. Gao***, Q. Gao, X. Bao, Y. Li, A. Teramoto, K. Abe. Preparation and *in vitro* bioactivity of novel mesoporous borosilicate bioactive glass nanofibers. *Journal of the American Ceramic Society*. 2011; 94(9): 2841-45.

2. **C.X. Gao***, Q. Gao, Y. Li, M. N. Rahaman, A. Teramoto, K. Abe. Preparation and *in vitro* characterization of electrospun PVA scaffolds coated with bioactive glass for bone regeneration. *Journal of Biomedical Materials Research Part A*.2012; 100A (5): 1324-34.

3. **C.X. Gao***, Q. Gao, Y. Li, M. N. Rahaman, A. Teramoto, K. Abe. *In vitro* evaluation of electrospun gelatin–bioactive glass hybrid scaffolds for bone regeneration. *Journal of Applied Polymer Science*. 2012; (DOI: 10.1002/app.37946).

International Conferences

1. **C.X. Gao**, Teramoto A, Abe K*. Preparation of Mesoporous Borosilicate Bioactive Glass Fibers for Bone Eissue Engineering. International Conference of Future Textile 2010, July 15-17, 2010, P97 (Shinshu university, Ueda, Japan) **(Poster, Excellent Poster Award)**

2. **C.X. Gao**, Teramoto A, Abe K*.The Preparation and Characterization of Hierarchical Borosilicate Glass Nanofibers. The 5th Nagoya Univeristy-UCLA International Symposium, August26-28, 2010, August26-28, 2010, P42, (Shinshu university, Ueda, Japan). (Poster)

3. **C.X. Gao**, Teramoto A, Abe K*.Preparation and Characterization of Nanofibrous Bioactive Glass Scaffolds. The Second International Conference on Advanced Textile Materials & Manufacturing Technology. October 20-24, 2010, P8, (Zhejiang Sci-Tech University, Hangzhou, China). (Oral)

4. **C.X. Gao**, Teramoto A, Abe K*. *In vitro* Evaluation of Electrospun Gelatin–Bioglass Hybrid Scaffolds for Bone Regeneration. The 6th International Conference on Advanced Fiber / Textile Materials. Dec 7-9, 2011. P13 (Shinshu university, Ueda, Japan). (Poster).

5. **C.X. Gao**, Teramoto A, Abe K*. Synthesis, Characterization and *in vitro* Cellular Performance of Bioglass-coated-PVA Nanofibrous Scaffolds for Bone Regeneration. The 2011 International Symposium on Molecular Systerms~Global COE Symposium for Young Reserachers. May 9-11, 2011. P12 (The Luigans, Fukuoka, Japan). (Oral)